The Dissertation Committee for Janine Mauzeroll Certifies that this is the approved version of the following dissertation:

Scanning Electrochemical Microscopy Studies Applied to Biological Systems

Committee:

Allen J. Bard, Supervisor

Richard A. Morrisett

Paul F. Barbara

James A. Holcombe

Keith J. Stevenson

Scanning Electrochemical Microscopy Studies Applied to Biological Systems

by

Janine Mauzeroll, B.S.

Dissertation

Presented to the Faculty of the Graduate School of

The University of Texas at Austin

in Partial Fulfillment

of the Requirements

for the Degree of

Doctor of Philosophy

The University of Texas at Austin

May, 2004

Dedication

Á toute ma famille: Guy, Hélene, Guy-Olivier, Hector, Claudette, Luc, Claudine, Luc-André, Alex, Juliette, Jeannine, Grégoire, Louise, Gérald, André et Maurice. Au-delà des distances et à travers les années vous êtes la source dans laquelle s'abreuvent mes racines.

Acknowledgements

Personal Acknowledgments

I would like to acknowledge Allen J. Bard for his supervision. It is a rare gift to have been able to benefit from the knowledge and guidance of such a great mentor.

I am grateful for the opportunity to have worked with all the wonderful scientists that I have met through the Bard group over the years. It is absolutely impossible for me not to mention Frank Fan. The discussions, advice and support provided with such consistancy have been of prime importance. I would also like to thank: Dr. Mihai Buda for the help with theoretical treatments, discussions and his invaluable friendship; Zhifeng Ding for helpful discussions and technical support in developing the laser pulled tips; Angie Nelson for all of the administrative help with the fellowship demands, insurance red tape and for her constant proof reading of my documents; Gregory Kalyushny for his friendship and help with the yeast fluorescence experiments, and Bob LeSuer for help with Mathematica.

During this thesis, many collaborators expedited the work and provided invaluable expertise. Prof. Appling and Sherwin Chan of the University of Texas, Chemistry and Biochemistry Department are gratefully acknowledged for their gift of the DAY4 yeast cells and discussions. Prof. Terrence Monks and Omeed Owhadian of the Pharmacy Department of the University of Arizona in Tucson are acknowledged for the Hep G2 liver cell cultures, cytotoxicity studies and helpful discussions in our

collaboration. Prof. Manuela Rueda and Dr. Paco Prieto are acknowledged for helpful discussions and for their expertise in making DOPC self-assembled monolayers on mercury.

On a personal note, I must give credit to my friends: Claudine d'Annunzio, Nina Antikinen and Adrian Goodey for their support and friendship. It is an absolute certainty that without the sports, food and good wine, I would have been a much sadder person.

Last but not least, this adventure would have been a lot less fun without the love, support, discussions and culinary skills of Steen B. Schougaard.

Acknowledgments Chapter 1

This work has been supported by the National Science Foundation (CHE 0109587) and the Robert A. Welch Foundation. Dr. M. Buda, Dr. Y. Lee and Dr. F.-R. F. Fan are acknowledged for their help and useful discussions.

Acknowledgments Chapter 2

This work was funded by the National Science Foundation (CHE 0109587) (UT) the Ministry of Science and Technology (Madrid) for BQU2001-3197 project and a Grant from the Andalusian Research Plan (Seville). We appreciate the help and advice of Dr. Z. Ding and Dr. F.-R. F. Fan.

Acknowledgments Chapter 3

This work was funded by the Edward G. Weston Summer Research Fellowship of the Electrochemical Society and by the National Science Foundation (CHE 0109587) (UT). The yeast cells DAY4 and DAY4vac were graciously donated by Prof. D. Appling

of the Chemistry and Biochemistry Department (UT). We appreciate the help and advice of Dr. S. Chang.

Acknowledgments Chapter 4

This work was funded by the University of Texas Continuing Fellowship, the Edward G. Weston Summer Research Fellowship of the Electrochemical Society and by the National Science Foundation (CHE 0109587) (UT). The authors are grateful to Prof. Terrence Monks, of the Pharmacy Department of the University of Arizona in Tucson and Omeed Owhadian for the culturing of the Hep G2 cells and helpful discussions.

Scanning Electrochemical Microscopy Studies Applied to Biological Systems

Publication No._____

Janine Mauzeroll, PhD

The University of Texas at Austin, 2004

Supervisor: Allen J. Bard

This dissertation specifically deals with scanning electrochemical microscopy (SECM) studies of cellular transport processes that involve ion channels or activated transport proteins. To study biological systems, the substrate generation-tip collection (SG-TC) mode of SECM is used. Because of the inherent difficulty in quantifying such measurements, a two electrode system is first used to understand the general behavior of SG-TC transients. Numerical simulations confirm that the transient currents measured in SG-TC mode of SECM agree with the experimental behavior of simple electroactive compounds. The influence of the ultramicroelectrode (UME) geometry on recorded and simulated transient response is discussed. Finally, significant experimental and theoretical differences in the feedback mode of SECM for hemispherical and disk UMEs are presented.

This knowledge is subsequently applied to a biomimmetic system where an ion channel is inserted in a self-assembled monolayer. The transport of thallium ions across gramicidin ion channels is detected at a nearby hemispherical mercury UME. This

transport system is a model system for real biological systems. Nevertheless, important kinetic information about differences in the transport energy barrier between the two ends of the gramicidin half-channel can be obtained. The small level current measured in the above work confirmed that the SG-TC mode of SECM had the sensitivity to measure the efflux of electroactive biological material from cells.

As such, the uptake of menadione and subsequent release of an electroactive biological metabolite from yeast cells is also reported. The synthesis, electrochemical characterization and detection of the menadione glutathione conjugate export from yeast cells are discussed. Kinetic treatment of the collection currents from yeast aggregates revealed that the uptake of menadione is the slow dominant step in the experiment.

Finally, single human liver cells are studied using SECM measurements while exposed to cytotoxic concentrations of menadione. A determined cytotoxic dose of menadione imposes a chemical stress on hepatocytes and leads to the export of the menadione-glutathione conjugate via an ATP-dependent pump. The process is observed and imaged for both isolated and differentiated cells and has some interesting biological relevance.

Table of Contents

List of Tables xiv

List of Figures xv

INTRODUCTION **1**

Main Themes of the Dissertation 1

Scanning Electrochemical Microscopy (SECM) 2

Ultramicroelectrodes as SECM Probes 2

SECM Modes of Operation 6

SECM and Biological Applications 9

Collection Mode Versus Feedback Mode 9

Biological Systems Previously Studied 10

SECM studies on living cells and organisms 12

Dissertation outline 13

References 15

CHAPTER 1: SCANNING ELECTROCHEMICAL MICROSCOPY. HG/PT HEMISPHERICAL ULTRAMICROELECTRODES - FABRICATION AND CHARACTERIZATION **17**

Introduction 17

Experimental Section 19

Electrodes 19

Materials and Solutions 21

SECM Apparatus 22

SG-TC Experiments 22

Results and Discussion 24

Numerical Simulation of SG-TC Mode for Disk and Hemispherical UME 24

SG/TC Experiments at a Disk UME 27

Formation and Characterization of a Hg/Pt UME 34
Mercury Deposition 34
Voltammetry 35
SECM Experiments with the Hg/Pt Tip in the Feedback Mode 37
SG-TC Experiments at a Hemispherical UME 38

Conclusions 41

References 43

CHAPTER 2: DETECTION OF TL(I) TRANSPORT THROUGH A GRAMICIDIN-DIOLEOYLPHOSPHATIDYLCHOLINE MONOLAYER USING THE SUBSTRATE GENERATION-TIP COLLECTION MODE OF SCANNING ELECTROCHEMICAL MICROSCOPY 46

Introduction 46

Experimental Section 49
Solution Preparation 49
SECM Apparatus 50
Electrodes 51
Procedure 52

Results and Discussion 54
Substrate Generation-Tip Collection (SG/TC) Experiments 54
Formation of Hg/Pt Submarine Electrodes 54
Tip Transient Response in Collection Experiments 58
Tip to Substrate Distance Evaluation 60
Monolayer Formation and Characterization 63
SG-TC of Thallium(I) in Gramicidin Channels 66

Conclusions....72

Supporting Information....72

References....75

CHAPTER 3: SCANNING ELECTROCHEMICAL MICROSCOPY OF MENADIONE-GLUTATHIONE CONJUGATE EXPORT FROM YEAST CELLS 78

Introduction....78

Materials and Methods....80

2-Methyl- 3-Glutathionyl-1,4-Naphthoquinone Synthesis....80

Chemicals and Solutions....81

Cell Growth and Sample Preparation....81

Electrode Fabrication....83

Electrochemistry....86

Results and Discussion....88

Thiodione Electrochemistry....88

Bulk Yeast Cell Experiments....90

Yeast Cell Aggregate Experiment....94

Theoretical Model....96

Conclusions....102

References....103

CHAPTER 4: MENADIONE TOXICITY STUDY ON HEPATOBLASTOMA HEP G2 CELLS USING SCANNING ELECTROCHEMICAL MICROSCOPY 105

Introduction....105

Menadione: A Model system for Adriamycin®....105

Relationship Between Multidrug Resistance and Glutathione Conjugate Transport....106

Studied System: Hepatoblastoma Hep G2 Cell Line....108

Objectives....110

Materials and Methods....110
Chemicals and Solutions....110
Cell Growth and Sample Preparation....111
Neutral Red Cytotoxicity Assay....111
Electrode Fabrication....113
Electrochemistry....114
SECM Cyclic Voltammetry Experiments....114
SECM Imaging Experiments....115
Results and Discussion....116
Cytotoxicity Experiments....116
Collection Experiments on Differentiated Cells....117
Single Cell Imaging of Thiodione Export....119
Time Profile of Thiodione Export from Single Human Liver Cells....124
Biological Relevance....127
Conclusions....129
References....131
CONCLUSION **134**
Chapter Highlights....134
Dissertation Highlights and Outlook....135
Theoretical Treatment of Transients....135
Ultramicroelectrode Design....136
SECM and Biological Applications....136
BIBLIOGRAPHY **138**
VITA **151**

List of Tables

Table 1.1: Tip to substrate distance evaluation using an error function complement approximation. From the error function complement argument, the tip to substrate distance (X) is extracted and compared to the distance obtained by the experimental approach curve fitting to hemispherical SECM theory. 33

Table 2.1: Tip to substrate distance evaluation using an error function complement approximation. From the error function complement argument, the tip to substrate distance (X)is extracted and compared to the distance obtained by the experimental approach curve fitted to hemispherical SECM theory. 62

TABLE 4.1: The human multidrug resistance protein (MRP) family and other reported nomenclature for individual members. 108

TABLE 4.2**:** List of incubation times in 80 μM menadione for all liver cell figures displayed. 126

List of Figures

Figure I.1: SECM Experimental Setup. The ultramicroelectrode is moved in three directions by the piezo-electric inchworms fixed to a translation stage. The electrochemical current is measured through the ultramicroelectrode and the auxiliary electrode. The potential applied at the ultramicroelectrode is measured versus the potential of a stable reference electrode. The application and acquisition of potential and electrochemical currents are controlled by a biopotentiostat and data acquisition system that is connected to a computer. 3

Figure I.2: Diagram depicting the possible geometries and the components of an UME. The ratio between the radius of the insulating glass sheet and that of the metal wire is defined as RG. To use UMEs in SECM applications, the RG must be minimized to a value of 10 or less. 4

Figure I.3: Diagram of the different possible SECM modes. 7

Figure 1.1: Experimental set-up for the formation of Hg/Pt UME by electrodeposition from a $Hg_2(NO_3)_2$ solution with 0.1 M KNO_3 acidified to 0.5% with HNO_3 as supporting electrolyte. This glass cell was joined at the base with a microscope slide. The underwater objective was lowered into solution and the deposition curve recorded during a 300 s potential step of -0.1 V vs. Ag/AgCl. 20

Figure 1.3: Fitting of the numerical simulation results for a large amplitude potential step at a 25 μm UME to the equation of Shoup & Szabo.[37] This fitting was done for a tip in a 1 mM $Ru(NH_3)_6Cl_3$ solution with a diffusion coefficient of 6.7×10^{-6} cm^2/s. 28

Figure 1.4: a) SG-TC simulation at a finite disk for different tip to substrate separations for a 25 μm UME tip in a 1 mM $Ru(NH_3)_6Cl_3$ solution with an assumed diffusion coefficient of 6.7×10^{-6} cm^2/s. (o) Diffusion time calculated from the diffusion layer thickness approximation:$\delta=\sqrt{2}Dt$. b) Fitting of the simulated steady-current for different tip to substrate separations and positive feedback SECM theory for a finite disk. ...29

Figure 1.5: 1 parameter fit of the simulated and experimental results for the SG-TC of 1 mM $Ru(NH_3)_6Cl_3$ solution at a 25 μm Pt finite disk UME for different tip to substrate distances and a diffusion coefficient of 6.7×10^{-6} cm^2/s.....31

Figure1.7: a) Voltammetric behavior of the 25 μm (--) Pt and (solid line) Hg/Pt UMEs in 1 mM $Ru(NH_3)_6Cl_3$, cobalt sepulchrate trichloride and methyl viologen in 0.1 M KNO_3. b) Positive feedback SECM fitting of the (□) finite disk theory, (♦)hemispherical disk theory and (line) experimental results for the 1 mM $Ru(NH_3)_6Cl_3$. c) Positive feedback SECM fitting of the (□) finite disk theory, (♦)hemispherical disk theory and (line) experimental results for the 1 mM cobalt sepulchrate trichloride in 0.1 M KNO_3. d) Positive feedback SECM fitting of the (□) finite disk theory, (♦)hemispherical disk theory and (line) experimental results for the 1 mM methyl viologen.....36

Figure 1.8: 1 parameter fit of the simulated and experimental results for the SG-TC of $TlNO_3$ at a hemispherical Hg/Pt UME for different tip to substrate distances. For a 25 μm Hg/Pt UME tip in a 10^{-4}M $TlNO_3$ solution in 0.1 M phosphate buffer at pH 7 with an assumed diffusion coefficient of 1.85×10^{-5} cm^2/s. 40

Figure 2.1: Full channel image of gramicidin A outlining the position of the four tryptophan groups at each extremity of the dimmer. The reported structure was reproduced based on solid NMR studies.'.....49

Figure 2.2: Experimental setup for the SG-TC experiments. A 750 ml cut beaker contains 250 mL of phosphate buffer and 250 μL of $TlNO_3$ stock solution, sealed with a Teflon cap that accommodates the HMDE, Hg/Pt submarine UME, Hg/Hg_2SO_4 reference, Pt auxiliary electrode and a gas inlet for Ar. 35 μL of the DOPC stock solution was added drop wise to form the monolayer at the Ar/solution interface. 15 μL of gramicidin stock solution was added and stirred. Each new mercury drop had an area, A= 0.0139 ± 0.0003 cm^2. A battery operated potentiostat and SECM setup were used respectively to control the substrate and tip potential.....51

Figure 2.3: Formation and characterization of the Hg/Pt submarine electrode. a) The Pt submarine electrode in phosphate buffer (pH=7) as it approached the HMDE while poised at –1.1 V vs. Hg/Hg_2SO_4. Upon contact with the HMDE, a hemispherical mercury layer is deposited onto the Pt UME. b) Hydrogen evolution at Pt and Hg/Pt submarine UME in phosphate buffer. c) Voltammogram of the 10^{-4} M Tl(I) at the Hg/Pt submarine electrode in phosphate buffer.....55

Figure 2.4: Positive feedback SECM curve fitting of (line) Hg/Pt submarine electrode approach curve to (♦) hemispherical SECM theory and (□) disk SECM theory for a 2 mM hexammineruthenium chloride solution in phosphate buffer (pH=7). The Hg/Pt UME approached the HMDE. 58

Figure 2.5: (line) Tip transient response for the collection of generated Tl(I) for different tip to substrate separations. The distances were evaluated by curve fitting the final approach curve in 10^{-4} M $TlNO_3$ to the negative feedback hemispherical SECM theory. The ( ) represents the error function complement fits performed from a non-linear least square fitting based on LV algorithm. The ( ) represents the time extracted from the diffusion layer thickness equation:$\Delta = \sqrt{(2Dt)}$.....60

Figure 2.6: The voltammetric response of (a) bare HMDE, (b) DOPC modified HMDE and (c) gramicidin-DOPC modified HMDE in 10^{-4} M $TlNO_3$ in phosphate buffer for a 50 mV/s scan rate. (d) The voltammetric response of the DOPC-modified HMDE system outlining the reversible first and second monolayer transitions in 10^{-4} M $TlNO_3$ in phosphate buffer for a 50 mV/s scan rate.....65

Figure 2.7: SG-TC tip transient response for the a) bare Tl/HMDE, b) DOPC modified Tl/HMDE and c) gramicidin-DOPC modified Tl/HMDE with a tip to substrate distance of 87 μm. The Tl/Hg amalgam was formed for 30 s and the measurements were performed in 10^{-4} M $TlNO_3$ in phosphate buffer. These results were obtained with a different Hg/Pt UME than the results presented in Figure 5.....67

Figure 2.8: Fitting of the rising part of the gramicidin-DOPC modified transient response to equation 8. The non-linear fitting used the LM algorithm to extract P1 = $k_{het}/\sqrt{D}$ = 0.06347 ± 0.00153. The reduced Chi square (1.3268E-22) was minimized. The fit yielded k_{het} = 2.8 (±0.1) x 10^{-4} cm/s for x= 87μm, D= 2 x 10^{-5} cm^2/s.....70

Figure 3.1: The smallest scale division represents 10 μm. (A) Side view of a sharpened laser pulled Pt UME. (B) Top view of an exposed and polished laser pulled Pt UME. (C), (D), (E) Voltammograms of 0.59, 1 and 3.5 μm, respectively, Pt diameter laser pulled UME in 1 mM ferrocene methanol solution in 0.1 M KCl electrolyte. The potential was measured versus a Hg/Hg_2SO_4 reference electrode and a 0.5 mm Pt wire was used as an auxiliary electrode. Argon was bubbled through the solution prior to the experiments. 85

Figure 3.2: Experimental setup for the electrochemical detection of the export of thiodione from immobilized yeast aggregates using laser pulled Pt UMEs. 87

Figure 3.3: (A) Voltammetric response of (A) 0.5 mM menadione, (B) 0.5 mM synthesized thiodione and (C) 0.5 mM reduced GSH. (B) Oxidation wave for the formation of thiodione with time. Equal molar amounts of menadione (0.25 mM) and reduced GSH (0.25 mM) spontaneously react to form thiodione. The limiting current of the oxidation wave becomes larger with time until the reaction is complete. (C) Calibration curve for the synthesized thiodione; oxidation current vs. concentration of thiodione. The responses (A,B,C) were obtained in PBS pH=7, the potential was measured with respect to Hg/Hg_2SO_4 and the scan rate was 50 mV/s. Argon was bubbled through all solutions for 30 min and a 0.5 mm Pt auxiliary electrode was used. (D) Appearance of a broad shoulder at 425 nm during thiodione formation. Equimolar amounts of menadione (0.125mM) and reduced GSH (0.125mM) in PBS pH=7 electrolyte spontaneously reacted to form thiodione. As thiodione is formed, the absorbance at 425 nm increased. Inset, the calculated concentration of thiodione increase with time. 89

Figure 3.4: (A) Electrochemical detection of thiodione exported from bulk DAY4 yeast cells at a 25 μm Pt electrode. Approximately 10^9 cells were treated with 0.5 mM menadione in PBS pH=7 electrolyte. The potential was cycled between -0.95 and 0.5 V at 10 mV/s. The wave height increased with time until it reached a steady-state value. (B) Comparison of the oxidation response at a 25 μm Pt electrode for PBS pH=7 buffer (a) to that of the synthesized thiodione (b) and that recorded from the bulk DAY4 yeast cells. (C) Electrochemical detection of the formation of thiodione at a 4 μm Pt UME from the spontaneous reaction of menadione (0.25 mM) and reduced GSH (0.25 mM) in PBS pH=7.4 solution. The red line represents the expected steady-state current value for 100% completion reaction. The potential was cycled between -0.95 and 0.5 V at 50 mV/s. All potentials (A,B,C) were measured with respect to a Hg/Hg_2SO_4 electrode, and a 0.5 mm Pt auxiliary electrode was used. All solutions were degassed with Ar for 30 min. 92

Figure 3.5: Electrochemical detection of reduced GSH at a HMDE (area, A= 0.0139 ± 0.0003 cm^2). Voltammograms of the HMDE for (A) PBS pH=6.97 electrolyte (B) over DAY4 yeast cells left soaking in the PBS for 1 h in a 2 mL volume and (C) in a 0.5 mM reduced GSH solution. The response was obtained between -1.8 and -0.4 V at 50 mV/s. The solutions were previously bubbled with Ar for 30 min. The potentials are reported versus Hg/Hg_2SO_4 electrode and a 0.5 mm Pt wire was used as an auxiliary electrode.....93

Figure 3.6: (A) Positive control of living immobilized DAY4 yeast cells on glass. The cells were treated with 10 mM FUN1 dye for 1 h incubation time. The living cells metabolize the dye, to produce diffuse green fluorescence in the cytosol and red cylindrical features. (B) Negative control of living immobilized DAY4 yeast cells on glass. The immobilized cells were incubated in the UV reactor for 1 h. The dead cells do not metabolize the dye and produce diffuse red fluorescence with no features. (C) Optical micrograph of the 4 μm Pt wire from the tip (bright spot) over the immobilized aggregate of cells prior to the start of the collection experiment. The tip was10 μm away from the glass surface. (D) Collection of exported thiodione from the immobilized aggregate of DAY4 yeast cells following the imposition of oxidative stress by 50 μL of 0.1 mM menadione. The response was collected between -0.5 to 0.5 V at a 20 mV/s. The potential was recorded with respect to a Ag/AgCl electrode coil in a two electrode configuration.95

Figure 3.7: (A) Schematic representation of the theoretical model used to treat the immobilized aggregate collection experiments. The model was applied to a 4 μm Pt UME, 10 μm away from the glass surface and in presence of 0.1 mM bulk concentration of menadione (M_o*). The menadione (M_o) diffuses through the cell wall and membrane with time at the assumed first order rate k_i (s^{-1}). Once inside, the menadione (M_i) rapidly conjugates with intracellular reduced glutathione (G =2.5 mM). The intracellular thiodione (MG_i) is then pumped out of the cell via the GS-X analog pump at an assumed first order rate k_o (s^{-1}). The expelled thiodione (MG_o) is then detected at the UME with time. The diffusion time from the cells to the tip is neglected. (B) Uptake of menadione with time. The concentration was calculated from the menadione current at -0.5 V vs. Ag/AgCl. This is a two electron process at a 2 μm radius Pt UME and a diffusion coefficient of 4 x 10^{-6} cm^2/s was used. An apparent rate of uptake of menadione of 5 (±0.6) x 10^{-3} s^{-1} was obtained.(C) Fit of the appearance of menadione with time for the immobilized aggregate experiments. The concentration was obtained from the steady-state current at 0.35 V vs. Ag/AgCl and used a diffusion coefficient of 8 x 10^{-6} cm^2/s. The concentration profiles with time were fit to eq. 7. From the fit, the apparent rate of uptake of menadione is in the range 0.6 x 10^{-3} to 30 x 10^{-3} s^{-1}. The uptake of menadione is the rate-determining step in this experiment and the rate of export through the pump was too fast to be measured. 99

Figure 4.1: Experimental setup used in the SECM measurements of human liver cells. The SECM head is attached to the inverted microscope. The top illumination column could not be used and a side lamp was added to the setup to assist in the acquisition of clear optical images of the liver cells. 115

Figure 4.2: Neutral Red assay results for cells of 75% or more confluency. (A) Viability of Hep G2 cells with varying menadione concentration applied to the cells for a 30 min incubation time. The values represent three independent measurements where three replicates of each concentration studied were taken. (B) Histogram of the effect of exposure time of 80 μM menadione on the viability of the Hep G2 cells. The values are representative of three replicates. 117

Figure 4.3: Electrochemical detection of thiodione from differentiated Hep G2 cells. (A) Voltammogram of thiodione detection with time. The potential was scanned from -0.8 to 0.65 V vs. Hg/Hg_2SO_4 at a scan rate of 100 mV/s in degassed 37.5°C PBS buffer. The signal was recorded at a 10 μm Pt UME. (B) The steady-state current of the voltammogram in A plotted versus the calculated time. The tip to substrate distance in this measurement was large and can be assumed to be representative of a bulk solution measurement. 119

Figure 4.4: Insulating SECM approach curve to the Petri dish using menadione reduction as redox species. The theoretical behavior for a totally insulating approach curve for a 10 μm Pt UME with an RG of 2 is represented by the solid line. The experimental points follow the theory and predict that the electrode was placed 4.3 μm from the substrate.120

Figure 4.5: SECM imaging of the export of thiodione from Hep G2 cells as detected by a 10 μm Pt UME with an RG of 2. (A) SECM image of Hep G2 cells. The tip potential was held at 0.55 V vs. Hg/Hg_2SO_4 and scanned at 300 μm/s over an area of 300 x 300 μm in the positive x direction. It took 5 min to acquire this image. A 2 s quiet time was applied. (B) Simultaneous optical micrograph of the Hep G2 cells being imaged. The black spot on the micrograph is the Pt UME. One large division corresponds to 50 μm. (C) Superimposed transparent optical micrograph on the SECM image. This image was acquired following 15 min of incubation in the 80 μm menadione solution.....122

Figure 4.6: SECM imaging of the export of thiodione from two neighboring human liver cells as detected using a 10 μm Pt UME with an RG of 2. (A) SECM image of Hep G2 cells. The tip potential was held at 0.55 V vs. Hg/Hg_2SO_4 and scanned at 150 μm/s over an area of 400 x 200 μm in the positive x direction. The total time to acquire the image was 17 min. A 2 s quiet time was applied. (B) Simultaneous optical micrograph of the Hep G2 cells being imaged. The black disk on the micrograph is the Pt UME. One division corresponds to 10 μm. (C) Superimposed transparent optical micrograph on the SECM image. This image was acquired following 26 min of incubation in the 80 μm menadione solution.....123

Figure 4.7: Time dependent profile of the export of thiodione from a single human liver cell as detected by SECM imaging. (A-D) SECM image of Hep G2 cell. The tip potential was held at 0.55 V vs. Hg/Hg_2SO_4 and scanned at 150 μm/s in the positive x direction. A 2 s quiet time was applied. (E, F) Simultaneous optical micrograph of the Hep G2 cell being imaged. The black spot on the micrograph is the Pt UME. From (E) and (F) it is clear that the tip is being scanned over this single cell. One division corresponds to 10 μm. (G-J) Superimposed transparent optical micrograph on the SECM image. These images were acquired following 43 min of incubation in the 80 μm menadione solution. All images were formatted such that the same scale is being used for all. 125

INTRODUCTION

Main Themes of the Dissertation

Living organisms are the most elegant and complicated electrochemical cells. They are guarded by a selective membrane that defines the cell's periphery and regulates transport in and out of cells. Cellular membranes are lipophilic domains across which a potential drop exists based on an established ion gradient. Transport in and out of a cell is governed either by passive diffusion of ambiphilic compounds or assisted by channels and transport proteins. Within this restricted volume, the synergistic action of an impressive number of redox couples is maintained. The concentration of these couples is not fixed since it is affected by environmental and developmental pressures that lead to the synthesis of new electroactive material.

Electrochemical reactions of cellular redox couples occur as a result of energy consumption, respiration and enzymatic activity that are intrinsic to cells. As such, the cell must have an overall redox capability that is affected by all the individual couples. This, in turn, leads to a number of fundamental questions. How can one define this redox potential and how does it change with time or environmental conditions? For example, would it be possible to titrate a cell and quantify the cellular redox potential? What happens to cells when they are exposed to such chemical stress? By changing the delicate equilibrium of cellular redox agents, changes in the membrane permeability occur via the activation of selective transport pumps. Can these transport events be monitored and quantified?

It is probably unlikely that a single experiment can answer all of the above questions. One must therefore rely on a number of different techniques which,

individually, only provide part of the complete picture. In our case, we are interested in the information provided by the study of scanning electrochemical microscopy (SECM) on cells. Our philosophy is simple: slowly kill cells by chemical stress and measure the electroactive species that are effluxed. Some quantitative information concerning ion and molecular transport across the cell membrane might then be available.

The ultimate goal would be to monitor and image the transport process at a single channel. As far as we know, only patch clamp has succeeded in recording single channel events. Compared to patch clamp experiments that measure the overall conductance of single channel, SECM experiments hold the promise of quantification of the transport process and direct detection of the concentration of ions or molecules exported out of the cell. SECM is a completely non-invasive technique since the probe electrode approaches the biological substrate without touching it, as opposed to patch clamp where the pipette adheres to the cell membrane.

Scanning Electrochemical Microscopy (SECM)

ULTRAMICROELECTRODES AS SECM PROBES

SECM was developed by Prof. A. J. Bard's group in the late eighties and much of the information related to this technique has been reported elsewhere.[1]

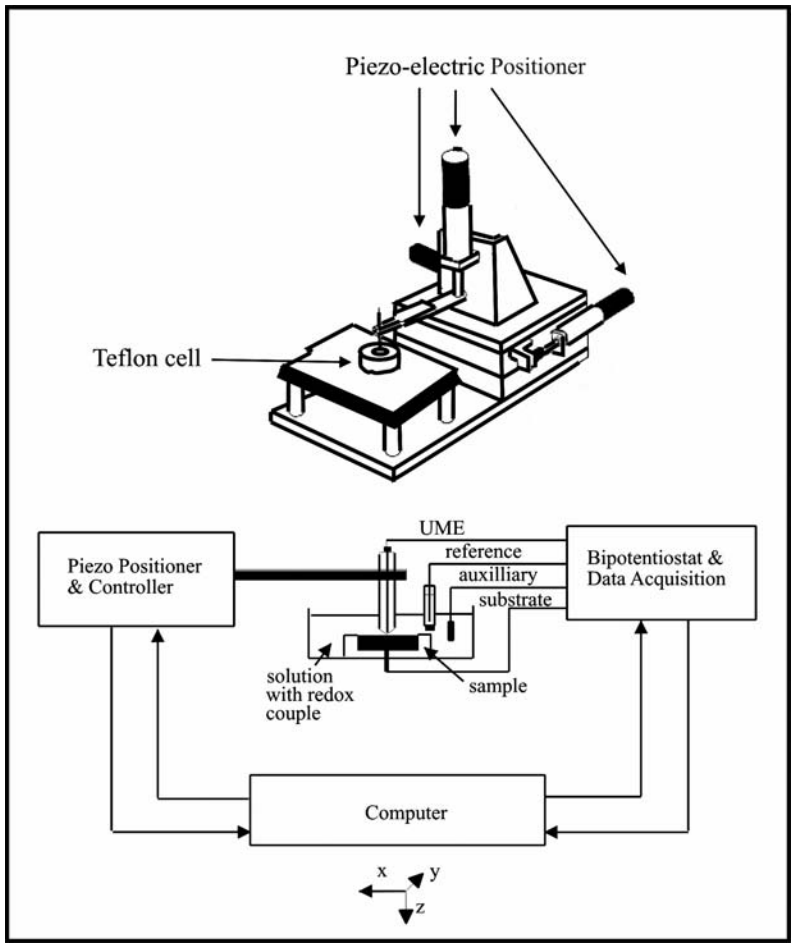

Figure I.1: SECM Experimental Setup. The ultramicroelectrode is moved in three directions by the piezo-electric inchworms fixed to a translation stage. The electrochemical current is measured through the ultramicroelectrode and the auxiliary electrode. The potential applied at the ultramicroelectrode is measured versus the potential of a stable reference electrode. The application and acquisition of potential and electrochemical currents are controlled by a biopotentiostat and data acquisition system that is connected to a computer.

Much like other scanning probe techniques, SECM was developed to study surfaces. SECM, like atomic force microscopy (AFM), can measure the topography of a surface, but has limited lateral resolution as a result of the large probe electrode. This is

why some efforts have been made to combine AFM and SECM techniques.[2] Also, there is a constant quest for ways of manufacturing smaller tips with well-defined geometries to increase lateral resolution. SECM is useful because it probes the chemical or biochemical activity of a surface. It does so by recording the electrochemical response of an ultramicroelectrode (UME) as it is moved towards or over a substrate by piezo-electric motors (Figure 1). An UME simply consists of a metal wire, typically gold, platinum or carbon, embedded in a glass tube at one end and electrically connected to a cupper lead at the other (Figure 2). The UME can have different geometries, but the most commonly used one is the planar disk UME.

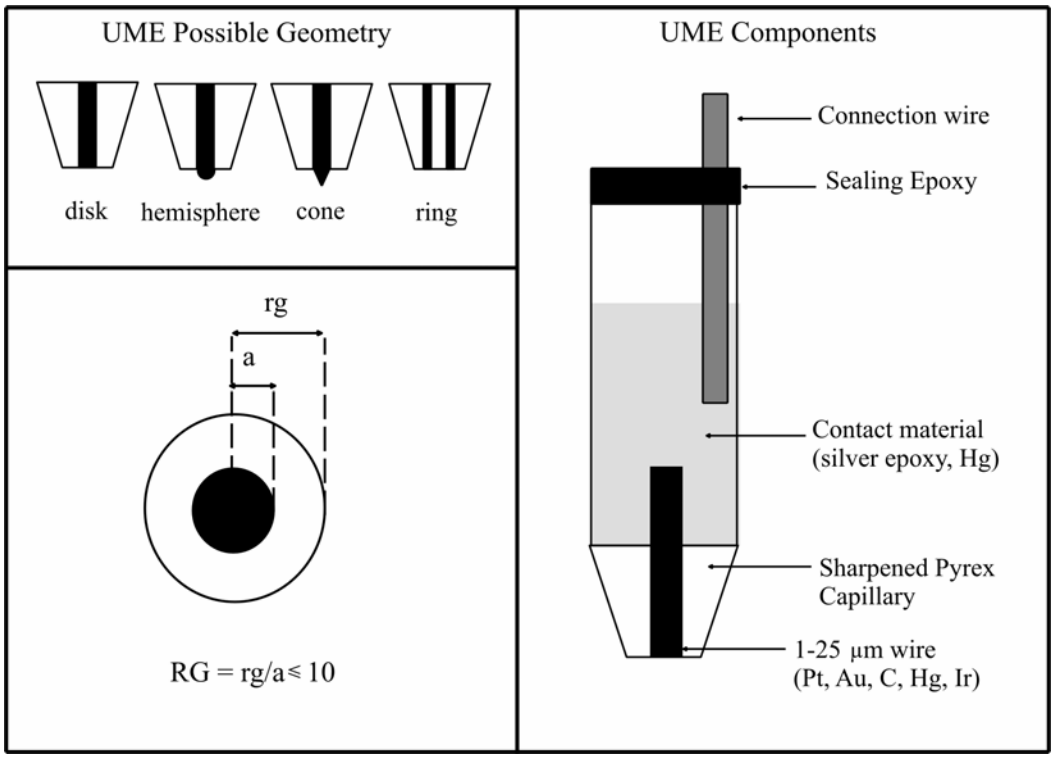

Figure I.2: Diagram depicting the possible geometries and the components of an UME. The ratio between the radius of the insulating glass sheet and that of the metal wire is defined as RG. To use UMEs in SECM applications, the RG must be minimized to a value of 10 or less.

The recorded signal is usually a current coming from an electron transfer reaction at the UME but it can also be applied to potentiometric studies.[3] Heterogeneous reactions at UMEs depend on the diffusion of a chemical species, O, from solution to the surface of the electrode and the subsequent transfer of an electron from that specie to the metal or vice versa. The transfer of electrons to the UME is recorded as a current and this current is expressed for a disk shape UME in bulk solution as:

$$I_{tip} = 4nFDCa \qquad (1)$$

Where n is the number of electrons that one specie can transfer to the electrode, F is the Faraday constant (96485.4 C/mol). The diffusion coefficient of species O, D (cm^2/s), is a measure of how fast species O can move through the solution, C is the initial concentration of O in solution (mol/cm^3), a is the radius of the encapsulated metal wire (cm) and I_{tip} is the current measured at the UME (A=C/s).

By virtue of equation 1, small concentrations can be detected at UMEs since they readily measure currents on the order of pA. Unlike macroelectrodes, UMEs are insensitive to convection and also reach steady-state quickly (μs-ms) from the application of a potential step. They can therefore be considered as steady-state systems when moving through the solution. When an UME reaches a steady-state current, it implies that the current measured is governed by the diffusion of species O to the electrode.

Under bulk conditions, when the tip is far from the surface, the hemispherical diffusion of an electroactive species O to the tip is unaffected by the size of the insulating sheet surrounding the active electrode area. The size of the insulating layer is, however, very important when UMEs are used in SECM applications. To approach the substrate

within a tip radius, the glass insulating sheet needs to be sharpened down to a pencil like shape (Figure 2). The smaller the insulating layer, the easier it is to approach the UME within a few microns of the substrate and the more sensitivity is gained. When a UME is approached to a substrate, it becomes increasingly sensitive to changes in concentration profile. This means that blocking of the species diffusion to the active area of the UME by the glass sheet becomes increasingly important with shorter distances. The ratio of the radius of the glass sheet to that of the metal wire is always minimized to a value that is below 10. This is referred to as the RG value of a UME. This allows for a close approach of the tip to the substrate and limits hampering of the approach by the glass sheet in the case where the tip is not completely perpendicular to the substrate.

SECM MODES OF OPERATION

Conventional SECM has several modes: feedback, tip generation-substrate collection (TG-SC) and substrate generation-tip collection (SG-TC) as presented in Figure 3. The feedback mode is the most commonly used since it is often needed for the proper determination of tip to substrate distance and evaluation of kinetic parameters. This is mainly because many theories have been developed for different probe geometries and for many experimental situations.

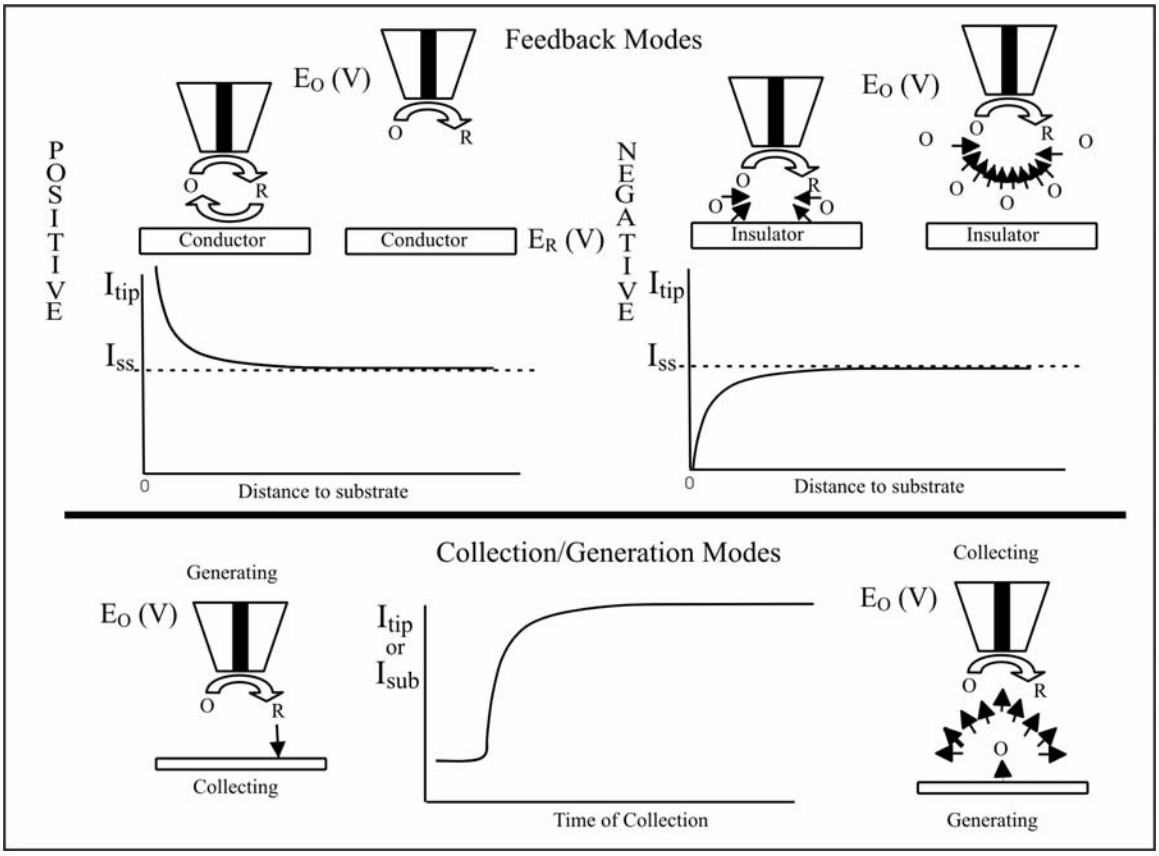

Figure I.3: Diagram of the different possible SECM modes.

To understand the principles behind the feedback modes, let's assume that the UME is poised at a potential (E_o) where the reduction reaction of O + ne → R is mass transfer limited. When the UME is far away from the substrate, the current measured at the tip corresponds to the hemispherical steady-state diffusion controlled reaction. As the UME is approached to the substrate by the piezo-motors, the concentration of O diffusing to the UME can be altered by the substrate in two ways. If the substrate is an insulator, like a piece of glass, no R – ne → O oxidation reaction will occur and the approach to the substrate will result in a negative feedback response. This implies that as the tip is approached to the glass, the hemispherical diffusion of O to the UME will progressively

be blocked by the substrate and will result in a decrease in the tip current relative to the steady-state current. The tip current dependence on the tip to substrate distance is called an approach curve.

If the substrate is conductive and poised at the potential (E_R) where the reverse oxidation reaction occurs, the UME will record an increasing concentration of O as it approaches the substrate. The UME current, with decreasing distance to the substrate, will therefore increase relative to the current measured when the UME was in the bulk of the solution. The increase of UME current with decreasing distance to a conductor is called positive feedback. Note that in the positive feedback approach, the blocking of the hemispherical diffusion by the substrate still takes place but is outweighed by the regeneration reaction of O.

The TG-SC mode of SECM is often used in the study of homogenous reaction kinetics. This mode can be used in decomposition studies, for example. Assume the tip is reducing species O at the mass transfer rate at a given distance from the substrate. Meanwhile, the substrate electrode is poised at the reverse oxidation reaction (E_R) where it is regenerating O. In the case where R decomposes or reacts with a passive compound in solution, the tip current approach curve will be influenced by the positive feedback signal from the regeneration reaction at the substrate and the finite rate at which R decomposes or reacts with solution species. The homogenous kinetics are determined by comparing experimental approach curves to theoretical ones where kinetic contributions are accounted for.

Finally, SG-TC mode of SECM is the mode that is less often used because of its inherent transient component. In this mode, the substrate generates a species that diffuses across the substrate and tip gap and is detected electrochemically at the UME. The theoretical treatment of this mode is complicated by the variable time. As will be

discussed in the following chapters, two options exist for quantification in this mode: numerical simulations and development of study specific models with analytical approximations.

SECM and Biological Applications

COLLECTION MODE VERSUS FEEDBACK MODE

When studying biological systems, one can choose between feedback or generation collection (GC) mode. In general, the negative feedback mode can be used to evaluate the tip to substrate distance and localize biological samples based on changes in topography or blocking of a conductive layer by biofilms. Such measurements yield little information concerning the biological activity of the substrate. Although recently, negative feedback imaging has been used to image new emerging micron size topography from PC12, dopamine releasing immortal rat cells.[4]

The choice is mostly between positive feedback and GC measurements. GC experiments use the probe electrode as a passive sensor that does not significantly perturb the local concentrations. This differs from feedback experiments where the tip generated species is actively involved in a surface reaction. Since the GC mode is independent of the substrate process, it is very flexible and can use different selective probes, such as amperometric, enzyme-modified or ion-selective. The quantitative characterization of this mode is often done using numerical simulations or through the development of experiment specific models that do not reach the level of generality or easy access that the feedback treatments have attained. In fact, GC experiments often rely on independent feedback measurements for the evaluation of distances by using passive mediators or dual-barrel electrodes.[5]

GC experiments are governed by the uncontrolled mass transport of the biological specimen because, unlike the feedback experiment, they do not localize the reaction under the electrode. This implies that feedback experiments benefit from better lateral resolution and are more suited for imaging experiments. However, the GC mode can detect lower analyte concentrations than the feedback mode because it does not have a significant background current coming from the dissolved mediator in solution. If, for example, the minimum catalytic rate, k_{cat}, of immobilized enzymes measured in the GC mode was compared to that of the feedback mode, the GC experiments could measure a k_{cat} 3 orders of magnitude faster than that obtained via the feedback study.[6] When deciding on which SECM mode to use in a biological experiment, the importance of imaging resolution over detection limits should be weighed.

BIOLOGICAL SYSTEMS PREVIOUSLY STUDIED

There is considerable literature where the use of SECM has been valuable in enzymatic studies.[6] Table 1 outlines the enzymes studied, the SECM mode used and provides references for the interested reader.

These studies showed that enzyme activity could be studied using SECM and often, catalytic rates could be extracted. In the case of glucose oxidase, for example, they showed that under conditions of high glucose concentration (substrate saturation), the feedback current depended on the enzyme turnover rate of glucose, the kinetics of the sacrificial electroactive mediator (or enzyme co-factor) and the flux of the mediator to the enzyme. Patterning of enzymes on surfaces and the long scanning distances of SECM make this an attractive option for enzyme activity assays.

Table I.1: Examples of Enzyme Activity Studies Using SECM.

Feedback Mode Studies		Collection Generation Mode Studies	
Enzyme	**Reference**	**Enzyme**	**Reference**
Glucose Oxidase	7, 8, 9, 10	Glucose Oxidase	11, 12
NADH-cytochrome *c* reductase	8	Urease	13, 14
Diaphorase	15	NADPH-dependent oxidase	16
Horseradish Peroxidase	17	Horseradish Peroxidase	18
Nitrate Reductase	19	Alkaline Phosphotase	20
		NAD+-dependent alcohol dehydrogenase	21

The advantage of studying enzymes is that they can be regenerated by known substrate. Although they might be influenced by the enzyme turn over rate, the enzymatic substrate can sustain a level of activity that is harder to find in other interesting biological systems. In antibody[17] or DNA hybridization studies there are a finite number of events that can be detected. SECM therefore, must turn to tagging strategies to enhance the detected signal. Recent DNA hybridization studies, for example, employed a silver staining technique to increase sensitivity that allowed them to detect 30 amol of material per analyzed spot.[22] This is a spectacular, unique example that is not representative of common electroactive tagging methods. Although common tagging is successful in enhancing the SECM response, it cannot compete with the expertise and sensitivity of the current fluorescent tagging methods. There is, however, great promise in combining the SECM measurements with selective fluorescent tags in biological studies.

SECM STUDIES ON LIVING CELLS AND ORGANISMS

Until very recently, little work has been done on complete full live cells. There was the study of photosynthesis on the leaves of *Tradescantia fluminensis* based on oxygen reduction profiles[23] and the study resorption of osteoclasts on bone slices using a Ca^{2+} potentiometric sensor.[24] Since then, a significant body of work by Matsue et al. and Mirkin et al. has allowed SECM to graduate to full cellular studies.

In the former case, live cell studies monitored respiration rate changes using oxygen reduction profiles for different cell types.[5,25,26,27,28] In these experiments, oxygen is present in solution and is consumed by the living organism. Close to the cells, more oxygen is consumed and a lower oxygen reduction current is measured. The differences in oxygen reduction currents are in the ranges of 10 pA to nA. There are many interesting studies performed by this group, we will describe one particularly applicable study of the respiration rate of in-vitro bovine embryos. The study showed that the respiration rate of the embryos in the morula developmental stage was related to their quality and viability. Embryos having a higher respiration rate in the morula stage were shown to grow into larger and healthier embryos at subsequent developmental stages. Such information could definitely be useful in supplementing the morphological data used to assess which embryos are to be used in bovine insemination.

In the latter group, most of the work was done on human breast cells[29] and *Rhodobacter sphaeroides*.[30] In these studies, the feedback mode of SECM was used to look at the regeneration reaction of different mediators when exposed to cells. These studies provide useful information about the permeability of the membrane to a wide variety of redox couples. It developed a theoretical treatment that could extract kinetic information about these processes.[31] Recently, it was reported that SECM could

distinguish between normal and malignant cells.[32] These SECM results were corroborated by optical and fluorescence microscopy measurements.

Dissertation outline

The former and latter studies both use experimental situations where the observed mediator is in high concentration in the bulk solution. This work is concerned with SECM experiments where a small analyte concentration is released from the biological system. This dissertation specifically deals with SECM studies of cellular transport processes that involve ion channels or activated transport proteins. To study biological systems, SG-TC mode of SECM is used. Because of the inherent difficulty in quantifying such measurements a two-electrode system is first used to understand the general behavior of SG-TC transients. In Chapter 1, numerical simulations confirm that the transient currents measured in SG-TC mode of SECM agree with the experimental behavior of simple electroactive compounds.[33] The influence of the UME geometry on recorded and simulated transient response is discussed. Finally, significant experimental and theoretical differences in the feedback mode of SECM for hemispherical and disk UMEs are presented.

The knowledge gained in Chapter 1 is subsequently applied to a biomimmetic system where an ion channel is inserted in a self-assembled monolayer. Thallium transport from a Tl/Hg amalgamated substrate across a gramicidin half-channel imbedded in a phospholipids self-assembled monolayer is studied.[34] The transport of thallium ions across gramicidin is detected at a nearby hemispherical mercury UME. The study in Chapter 2 is a model system for real biological systems and extracts important kinetic information about differences in the transport energy barrier between the two ends of the

gramicidin half-channel. The small current transients measured confirm that the SG-TC mode of SECM has the sensitivity to measure the efflux of electroactive biological material from cells.

A study is therefore reported in Chapter 3 that deals with the uptake of menadione and subsequent release of an electroactive biological metabolite from yeast cells. Most of the work is dedicated to synthesizing, electrochemical characterizing and detecting from live yeast cells the menadione glutathione conjugate export that is associated with oxidative stress conditions.[35] Kinetic treatment of the collection currents reveal that the uptake of menadione is the slow dominant step in the experiment.

The study in Chapter 3 is limited to the detection of the conjugate over aggregates of yeast, cells but Chapter 4 reports single human liver cell SECM measurements made during a similar menadione cytotoxicity study. A determined cytotoxic dose of menadione imposes a chemical stress on hepatocytes and leads to the export of the menadione-glutathione conjugate via an ATP-dependent pump. The process is observed and imaged for both isolated and differentiated cells and has some interesting biological relevance.[36]

References

[1] Bard, A. J.; Mirkin, M. V.; Eds.; *Scanning Electrochemical Microscopy*, Marcel Dekker, Inc.; New York, **2001**, 1-200.

[2] Kueng, A.; Kranz, C.; Lugstein, A.; Bertagnolli, E.; Mizaikoff, B. *Angew. Chem. Int.* **2003**, *42*, 3237.

[3] Horrocks, B. R.; Mirkin, M. V.; Pierce, D. T.; Bard, A. J.; Nagy, G.; Toth, K. *Anal. Chem.* **1993**, *65*, 1213.

[4] Liebetrau, J. M.; Miller, H. M.; Baur, J. E.; Takacs, S. A.; Anupunpisit, V.; Garris, P. A.; Wipf, D. O. *Anal. Chem.* **2003**, *75*, 563.

[5] Yasukawa, T.; Kaya, T.; Matsue, T. *Anal. Chem.* **1999**, *71*, 4637.

[6] Bard, A. J.; Mirkin, M. V.; Eds.; *Scanning Electrochemical Microscopy*, Marcel Dekker, Inc.; New York, **2001**, 445-519.

[7] Pierce, D. T.; Unwin, P. R.; Bard, A. J. *Anal. Chem.* **1992**, *64*, 1795.

[8] Pierce, D. T.; Bard, A. J. *Anal. Chem.* **1993**, *65*, 3598.

[9] Kranz, C.; Wittstock, G.; Wohlschläger, H.; Schuhmann, W. *Electrochim. Acta* **1997**, *42*, 3105.

[10] Wijayawardhana, C. A.; Wittstock, G.; Halsall, H. B.; Heineman, W. R. *Anal. Chem.* **2000**, *72*, 333.

[11] Wittstock, G.; Schuhmann, W. *Anal. Chem.* **1997**, *69*, 5059.

[12] Horrocks, B. R.; Schmidtke, D.; Heller, A.; Bard, A. J. *Anal. Chem.* **1993**, *65*, 3605.

[13] Horrocks, B. R.; Mirkin, M. V.; Pierce, D. T.; Bard, A. J. *Anal. Chem.* **1993**, *65*, 1213.

[14] Horrocks, B. R.; Mirkin, M. V. *J. Chem. Soc. Faraday Trans.* **1998**, *94*, 1115.

[15] Shiku, H.; Takeda, T.; Yamada, H.; Matsue, T.; Uchida, I. *Anal. Chem.* **1995**, *67*, 312.

[16] Berger, C. E. M.; Horrocks, B. R.; Datta, H. K. *J. Endocrin.* **1998**, *158*, 311.

[17] Shiku, H.; Matsue, T.; Uchida, I. *Anal. Chem.* **1996**, *68*, 1276.

[18] Shiku, H.; Hara, Y.; Matsue, T.; Uchida, I. *J. Electroanal. Chem.* **1997**, *438*, 187.

[19] Zaumseil, J.; Wittstock, G.; Bahrs, S.; Steinrücke, P. *Fresenius J. Anal. Chem.* **2000**, *367*, 352.

[20] Wittstock, G.; Yu, K. J.; Halsall, H. B.; Ridgway, T. H.; Heineman, W. R. *Anal. Chem.* **1995**, *67*, 3578.

[21] Antonenko, Y. N.; Pohl, P.; Rosenfeld, E. *Arch. Biochem. Biophys.* **1996**, *333*, 225.

[22] Wang, J.; Song, F.; Zhou, F. *Langmuir* **2002**, *18*, 6653.

[23] Tsionsky, M.; Cardon, Z. G.; Bard, A. J.; Jackson, R. B. *Plant Physiol.* **1997**, *113*, 895.

[24] Berger, C. E. M.; Rathod, H.; Gillespie, J. I.; Horrocks, B. R.; Datta, H. *J. Bone and Min. Res.* **2001**, *16*, 2092.

[25] Nishizawa, M.; Takoh, K.; Matsue, T. *Langmuir* **2002**, *18*, 3645.

[26] Takii, Y.; Takoh, K.; Nishizawa, M.; Matsue, T. *Electrochim. Acta* **2003**, *48*, 3381.

[27] Kaya, T.; Nishizawa, M.; Yasukawa, T.; Nishiguchi, M.; Onouchi, T.; Matsue, T. *Biotech. Bioeng.* **2001**, *76*, 391.

[28] Shiku, H.; Shiraishi, T.; Ohya, H.; Matsue, T.; Abe, H.; Hoshi, H.; Kobayashi, M. *Anal. Chem.* **2001**, *73*, 3751.

[29] Liu, B.; Rotenberg, S. A.; Mirkin, M. V. *PNAS USA* **2000**, *97*, 9855.

[30] Cai, C.; Liu, B.; Mirkin, M. V.; Frank, H. A.; Rusling, J. F. *Anal. Chem.* **2002**, *74*, 114.

[31] Biao, L.; Rotenberg, S. A.; Mirkin, M. V. *Anal. Chem.* **2002**, *74*, 6340.

[32] Feng, W.; Rotenberg, S. A.; Mirkin, M. V. *Anal. Chem.* **2003**, *75*, 4148.

[33]Mauzeroll, J.; Hueske, E. A.; Bard, A. J. *Anal. Chem*. **2003**, *75*, 3880.

[34]Mauzeroll, J.; Buda, M.; Bard, A. J.; Prieto, F.; Rueda, M. *Langmuir* **2002**, *18*, 9453.

[35] Mauzeroll, J.; Bard, A. J. **2003**, manuscript in preparation.

[36] Mauzeroll, J.; Monks, T.; Bard, A. J. **2003**, manuscript in preparation.

CHAPTER 1: SCANNING ELECTROCHEMICAL MICROSCOPY. HG/PT HEMISPHERICAL ULTRAMICROELECTRODES - FABRICATION AND CHARACTERIZATION*

Introduction

We report the fabrication of Hg on Pt hemispherical SECM tips and their characterization. We also include experimental and theoretical comparison between SG-TC experiments at a Pt disk and Hg/Pt UME. Effects of tip to substrate separation were studied and numerical analysis for both geometries correlated well with experimental results and allowed the extraction of diffusion coefficients. This study confirms the enhanced sensitivity of hemispherical tips to radial diffusion in SG-TC measurements and discusses the potential advantages of using such tips.

SECM transient current measurements provide information about homogenous kinetics and time dependent systems. The SECM transient response has previously been simulated and experimentally studied for planar electrodes, microdisks and thin-layer cells over a wide time range.[2,3] Provided that the tip radius is known, transient current measurements allow for the determination of diffusion coefficients without knowledge of solution concentration and the number of electrons transferred.[4,5]

Most SECM investigations use Pt planar disk-shaped UMEs. However, for some studies it is desirable to work at tip potentials in negative potential regions where proton reduction occurs at Pt. An example is the monitoring of Tl(I) as a surrogate for K(I) in studies of ion transport through channels in membranes[6,7] or in studies of surface reactions where a very negative redox couple, like methyl viologen, is needed. Mandler

---

* *"Reproduced in part with permission from Analytical Chemistry 2003, vol 75, pp 3880-3889"*

and coworkers,[8] for example, demonstrated the use of an Hg-Au amalgam UME in SECM studies of surface reactions catalyzed by Pt.

There are a number of possible choices for the substrate for Hg UMEs. Ideally the substrate should be easily wet by mercury and yet have a low solubility in mercury. In the case of glassy carbon, the substrate surface shows poor wetting leading to the formation of inhomogeneous scattered mercury droplets.[9] For metals like platinum, silver and gold, the formation of intermetallic compounds at the base metal can occur. Thermal evaporation experiments have shown that the formation of intermetallic species leads to a potential window that extends to less negative potentials than that of the hanging mercury drop electrode (HMDE).[10] However, the dissolution of platinum is hindered by the presence of surface oxides and can often be neglected in voltammetric studies following the deposition of a sufficiently thick mercury layer.[11] Another possible substrate material is iridium. Osteryoung and coworkers fabricated and studied Ir[12] and Ir/Pt[13] alloy based mercury UMEs. However, the difficulty in obtaining Ir/Pt alloy wires in sufficiently small sizes and the brittleness of Ir wires make them less attractive as SECM probes. In this work, Pt was selected as the substrate.

Hg/Pt UMEs have a hemispherical shape. Conical, hemispherical and spherical shaped UMEs have been used in steady-state SECM studies, but little work has been done on the transient response of such tips.[14-19] Nonplanar UMEs are often easier to construct in small dimensions[20-23] and suffer less from problems with the insulating shielding hitting the substrate because of inexact alignment. This paper deals with the fabrication of hemispherical tips, their characterization, and their application in substrate generation tip collection (SG-TC) SECM studies. In SG-TC SECM mode, the substrate electrogenerates a species that diffuses into the bulk. A UME positioned close to the substrate collects the generated species. The tip is at least an order of magnitude smaller

than the substrate and has a thinner diffusion layer than the substrate. The tip reaction, therefore, does not significantly affect the substrate current except at very small separations.

Historically, SG-TC experiments with an amperometric tip were pioneered by Engstrom et al.[24-26] Using small carbon UMEs, they collected and studied species generated at a close macroscopic electrode. They addressed the theoretical behavior of the tip transient response using potential step functions and impulse response functions. Other mathematical approaches have been applied to the theory of a disk-shaped tip and flat substrate, including finite element,[27] boundary element[28] and alternating direction implicit finite difference methods (ADIFDM).[29] Mandler et al.,[18] have recently treated the theoretical behavior of a hemispherical UME used in feedback SECM studies by ADIFDM and compared these simulations to those previously obtained by the same method for a finite disk. Here, we follow this theoretical comparison with experimental characterization of a hemispherical mercury UME by SECM in the SG-TC mode and numerical simulations based on the finite element method (FEM).

Experimental Section

ELECTRODES

A 25 μm diameter Pt wire (Goodfellow, Cambridge, U.K.) was sealed into a 5 cm Pyrex glass capillary under vacuum as described previously.[2] The electrode was polished and shaped into a UME on a polishing wheel (Buehler, Lake Bluff, IL) with 180 grid Carbimet paper disks (Buehler, Lake Bluff, IL) and micro polishing cloth with 1.0, 0.3, and 0.05 μm alumina (Buehler, Lake Bluff, IL). The tip was sharpened to an RG of 2-3

where RG is the ratio of the diameter of the UME that includes the glass sheet and the diameter of the Pt wire.

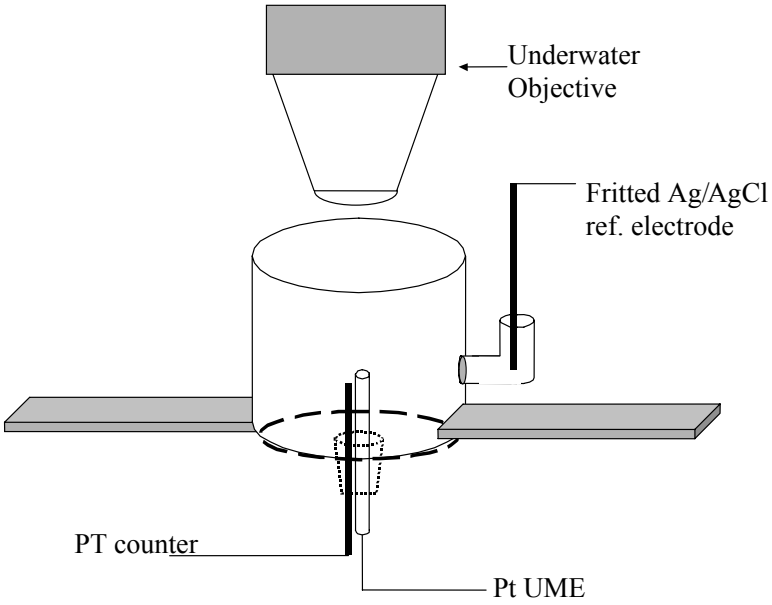

Figure 1.1: Experimental set-up for the formation of Hg/Pt UME by electrodeposition from a $Hg_2(NO_3)_2$ solution with 0.1 M KNO_3 acidified to 0.5% with HNO_3 as supporting electrolyte. This glass cell was joined at the base with a microscope slide. The underwater objective was lowered into solution and the deposition curve recorded during a 300 s potential step of -0.1 V vs. Ag/AgCl.

Hemispherical Hg/Pt UMEs were produced using two equivalent methods. Mercury was deposited onto the Pt UME from a 10 mM $Hg_2(NO_3)_2$ (J.T. Baker Chem. Co. Phillipsburg, NJ) in 0.1 M KNO_3 solution acidified to 0.5% with HNO_3 in a three-electrode setup and control by a Model 660 potentiostat (CH Instruments, Austin, TX). A 1 mm Pt wire served as a counter electrode, and a fritted Ag/AgCl electrode served as a reference electrode. The working Pt UME and counter electrode were inserted through a hole at the base of the cell while the reference was positioned in a side compartment as seen in Figure 1. The deposition curve was recorded during a 300 s potential step of -0.1

V vs. Ag/AgCl. The deposition was monitored in-situ with an optical microscope (Olympus model BH-2) equipped with a water immersion objective (Olympus FLxw40). A personal computer and Pixera camera (PVC 100c, Pixera Corp.) were used to record the images. The voltammetric characterization and feedback SECM studies of the Hg/Pt UME presented in this paper used this first method.

In a second method to produce the Hg/Pt UME the Pt UME was sealed into a J glass tube using Teflon tape to produce a submarine electrode.[30] The Hg/Pt UME was then formed by applying –1.1 (V vs. Hg/Hg_2SO_4 (Radiometer, Copenhagen, Denmark)) at the Pt UME and contacting it with the mercury (Bethlehem Instr. Hellertown, PA) of a hanging mercury drop electrode (Metrohm Instr. Herisau, Switzerland) in phosphate buffer. Reproduction of the voltammetric and SECM characterization confirmed that the two methods used to form Hg/Pt electrodes were equivalent. The SG-TC experiments were performed with UME produced by this second method.

MATERIALS AND SOLUTIONS

Cyclic voltammetry and SECM characterization experiments used 1 mM in cobalt sepulchrate trichloride (Aldrich), hexammineruthenium (III) chloride (Strem Chem. Newbury Port, MA), methyl viologen (Aldrich) redox couples. The supporting electrolyte used for the SG-TC experiments is formed by 0.1 M KCl solutions buffered by a 1:1 molar ratio of NaH_2PO_4/Na_2HPO_4 of total concentration of 0.01 M at pH 7. The redox couples employed are 1 mM hexammineruthenium (III) chloride (Strem Chem., Newburyport, MA) and thallium(I) nitrate (Aldrich). The stock solution of 0.1 M thallium nitrate was made in water. The thallium concentration in the reaction cell was 10^{-4} M. All solutions were prepared with Milli-Q (Millipore Corp.) reagent water, and degassed with Ar for 30 min prior to all experiments.

SECM APPARATUS

A CHI Model 900 scanning electrochemical microscope (CH Instruments, Austin, TX) was used to control the tip potentials, obtain the approach curves and monitor the tip to substrate distance. A home built floating potentiostat was used to control the HMDE or Pt disk substrate potential. The use of this battery operated potentiostat as the potential control for the substrate prevented interferences observed with the CHI instrument during transient measurements when the tip was positioned in close proximity to the substrate.

The cell platform was modified to accommodate a chamber designed to allow measurements under oxygen-free conditions. In the case of the Tl collection experiment, the experimental setup has been described elsewhere.[7] As for the other SECM experiments, they were performed either with the SECM head in a glove bag under positive pressure or the SECM cell covered with Parafilm and in the presence of an argon blanket.

SG-TC EXPERIMENTS

The SG-TC experiments at a disk electrode were performed in a Teflon SECM cell that accommodated four electrodes. The Pt disk UME approached the Pt substrate in the feedback mode. The tip was positioned close to the substrate and the tip current transient response for different tip to substrate separations was measured. For each tip to substrate separation, a new solution containing redox species was added. At the end of the experiment an approach curve was measured to evaluate the true tip to substrate distance based on an SECM calibration.

The SG-TC experiments at the Hg/Pt UME were performed in a 750 mL cut beaker with a machined Teflon cap with an O-ring. The cap accommodated the HMDE, the submarine electrode, a reference electrode, an auxiliary electrode, a gas inlet and a microsyringe. An argon blanket was maintained over the solution at all times.

The reaction vessel was filled with 250 mL of phosphate buffer and closed with all electrodes in place. The solution was purged with argon for 30 min. The tip and HMDE (area, A= 0.0139 ± 0.0003 cm^2) were aligned during the formation of the Hg/Pt UME. The tip was then retracted from the HMDE to a known distance. The reaction vessel was deaerated for 30 min after which 250 μL of $TlNO_3$ stock solution was added. Voltammetric response of thallium ion was then recorded at both tip and substrate.

The distance dependence of the tip transient response was evaluated. The substrate and the tip were both poised at –1.1 V for 30 s to respectively form the substrate amalgam and stabilize the tip current. The substrate potential was then switched to –0.75 V to oxidize the thallium amalgam. The tip collected the released thallium ions from the substrate for 100 s and remained poised at –1.1 V. The tip was then moved 25 μm further away from the substrate and the experiment was repeated for several tip to substrate distances. A new amalgamated HMDE was used for each distance. Upon completion, an approach curve was recorded to assess the true tip to substrate distance.

Results and Discussion

NUMERICAL SIMULATION OF SG-TC MODE FOR DISK AND HEMISPHERICAL UME

In SG-TC experiments, the substrate electrogenerates redox-active species, R, from an initial solution of species, O. The generated R diffuses away from the substrate and a fraction is collected at the nearby UME and undergoes the reverse reaction, oxidation to O. The tip response varies with time and depends on the tip geometry, the tip to substrate separation and the concentration profile generated at both the substrate and tip.

The concentration of a species, I, is denoted as $C_i(r,z,t)$ and the diffusion equation for that species in cylindrical coordinates is:

$$\frac{\partial C_i}{\partial t} = D_i \left(\frac{\partial^2 C_i}{\partial r^2} + \frac{1}{r}\frac{\partial C_i}{\partial r} + \frac{\partial^2 C_i}{\partial z^2} \right) \qquad (1)$$

where r and z are radial and normal directions from the tip surface, D_i is the diffusion coefficient of i, C_i is the concentration of the species (O or R) and t is the time.

In the present experiments, the initial and boundary conditions for the planar disk and the hemispherical UME are different as a result of the redox couple used for each UME and the geometry of the tip. The planar disk SG-TC experiment involved both O and R soluble and, hence, concentration profiles of both the Ru(II) and Ru(III) species. Thus, two diffusion equations were solved simultaneously and the boundary conditions for both species were defined. The hemispherical UME SG-TC experiment involved only one electroactive species soluble in the aqueous medium, Tl(I), and required the solution of only one partial differential equation. The initial and mixed boundary conditions for both experiments were defined at every line of the domains in Figure 2.

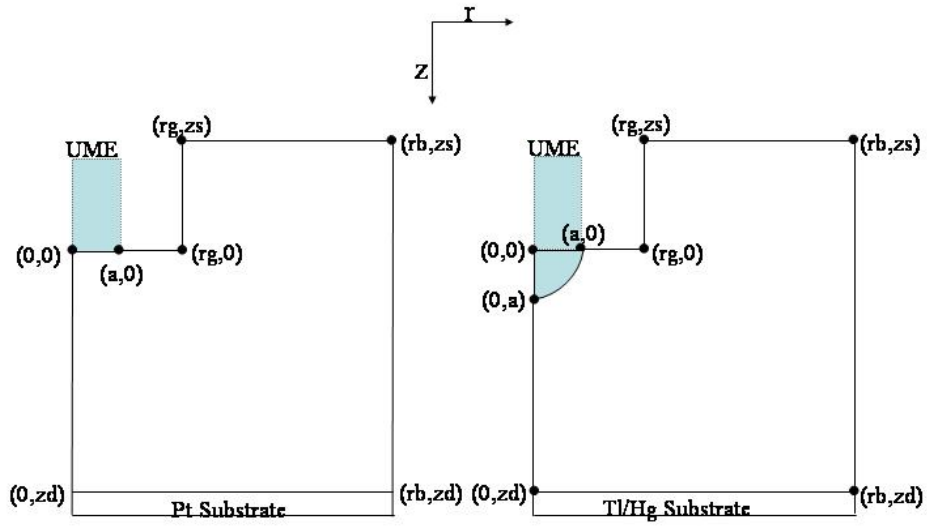

Figure 1.2: Defined space domain for the numerical analysis of (left) finite planar disk and (right) hemispherical UME.

For each tip geometry the initial and mixed boundary conditions are:

Planar disk:

$t = 0;$ $C_o = C_o^*; C_R = 0$ (2)

$t > 0; r = 0;$ $0 \le z \le zd;$ $\frac{\partial C_o}{\partial r} = \frac{\partial C_R}{\partial r} = 0$ (3)

$t > 0; 0 \le r \le rb;$ $z = zd;$ $C_o = 0; C_R = C_o^*$ (4)

$t > 0; r = rb;$ $zs \le z \le zd;$ $\frac{\partial C_o}{\partial r} = \frac{\partial C_R}{\partial r} = 0$ (5)

$t > 0; rg \le r \le rb;$ $z = zs;$ $C_o = C_o^*; C_R = 0$ (6)

$t > 0; r = rg;$ $zs \le z \le 0;$ $\frac{\partial C_o}{\partial r} = \frac{\partial C_R}{\partial r} = 0$ (7)

$t > 0; a \le r \le rg;$ $z = 0;$ $\frac{\partial C_o}{\partial z} = \frac{\partial C_R}{\partial z} = 0$ (8)

$t > 0; 0 \le r \le a;$ $z = 0;$ $C_o = C_o^*; C_R = 0$ (9)

Hemisphere:

$t = 0;$ $C_o = C_o^*$ (10)

$t > 0; r = 0; \quad a \le z \le zd;$ $\frac{\partial C_o}{\partial r} = 0$ (11)

$t > 0; 0 \le r \le rb; \quad z = zd;$ $C_o = C_{amal}^*$ (12)

$t > 0; r = rb; \quad zs \le z \le zd;$ $\frac{\partial C_o}{\partial r} = 0$ (13)

$t > 0; rg \le r \le rb; \quad z = zs;$ $C_o = C_o^*$ (14)

$t > 0; r = rg; \quad zs \le z \le 0;$ $\frac{\partial C_o}{\partial r} = 0$ (15)

$t > 0; a \le r \le rg; \quad z = 0;$ $\frac{\partial C_o}{\partial z} = 0$ (16)

$t > 0; 0 \le r \le a; \quad z = \left(a^2 - r^2\right)^{1/2}; \quad C_o = 0$ (17)

Where **t** is the time, **a** is the radius of the Pt wire, **rg** is the radius of the UME that includes the glass sheet, **zs** an arbitrary distance above the tip bottom that is large compared to the substrate diffusion layer, **rb** is the substrate radius and **zd** is the tip to substrate separation distance.

The tip transient response was simulated using a FEM. This method differs from difference methods because it is based on a discretized polynomial approach. It is useful because it can be applied to any geometrical shape and has been well-documented in previous electrochemical studies.[27,31-35] In the FEM, the concentration gradient of species is approximated using a sequentially continuous function. In our case, a 2D grid is defined with triangular elements. At each node, basis functions, usually linear and quadratic polynomials, are defined to insure continuity. Space and time matrices are then solved numerically. To calculate the tip current, the concentration gradient normal to the

tip surface is approximated. Taking advantage of the symmetry of the defined spaces in Figure 2(left), the tip current is then:

$$i_{tip} = nFD\left\{\int_{r=0}^{r=a} 2\pi r\left(\frac{\partial C_i}{\partial z}\right)_{z\cong 0} dr\right\} \qquad (18)$$

A similar integration was performed for the hemispherical geometry along the arc as defined in Figure 2(right). All these calculations were carried out with PDEase2D (Macsyma Inc., Arlington, MA), a commercial program that employs the FEM.[36]

SG/TC EXPERIMENTS AT A DISK UME

The numerical simulation for the disk UME response to a large amplitude potential step in bulk solution was examined to test the simulation when compared to known theory. Initially, the UME is at a potential where O is not reduced. The application of a potential step at t = 0 causes reduction of O at a diffusion-controlled rate. The diffusion to a planar disk UME occurs in two dimensions. This implies that the current density is not uniform across the disk and this was observed in the simulations. The simulated current response was compared to the expression given by Shoup and Szabo:[37]

$$i_{tip} = \frac{4nFAD_oC_o^*}{pa}\left\{0.7854 + 0.8862\tau^{-1/2} + 0.2146e^{-0.7823\tau^{-1/2}}\right\} \qquad (19)$$

where $\tau = 4D_ot/a^2$, F is Faraday's constant (96487 C/eq), n is the number of electrons (eq/mol), A is the area of the disk (cm^2), D_o is the diffusion coefficient (cm^2/s), C_o^* is the bulk concentration of O (mol/cm^3) and a is the radius of the disk UME (cm).

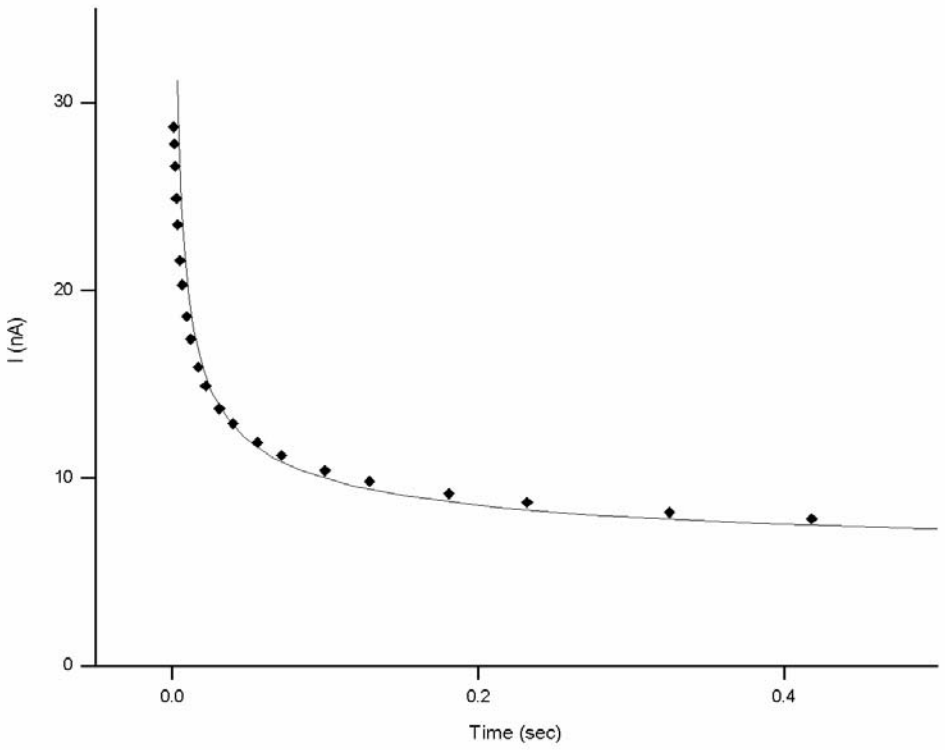

Figure 1.3: Fitting of the numerical simulation results for a large amplitude potential step at a 25 μm UME to the equation of Shoup & Szabo.[37] This fitting was done for a tip in a 1 mM $Ru(NH_3)_6Cl_3$ solution with a diffusion coefficient of 6.7×10^{-6} cm^2/s.

Equation (19) describes the chronoamperometric behavior of a finite disk electrode and improved on Osteryoung and Aoki's previous work that separated the response into two time ranges where different series were applicable.[39] Shoup and Szabo's relationship showed good correlation between experimental results and digital simulations that were based on an explicit hopscotch algorithm. The results of our numerical simulation in Figure 3 also produced a good correlation with Eq. (19). The

numerical simulation and theory were computed for the chronoamperometric behavior of a 25 μm Pt tip in a 1 mM $Ru(NH_3)_6^{3+}$ quiescent solution with a diffusion coefficient of 6.7×10^{-6} cm^2/s.

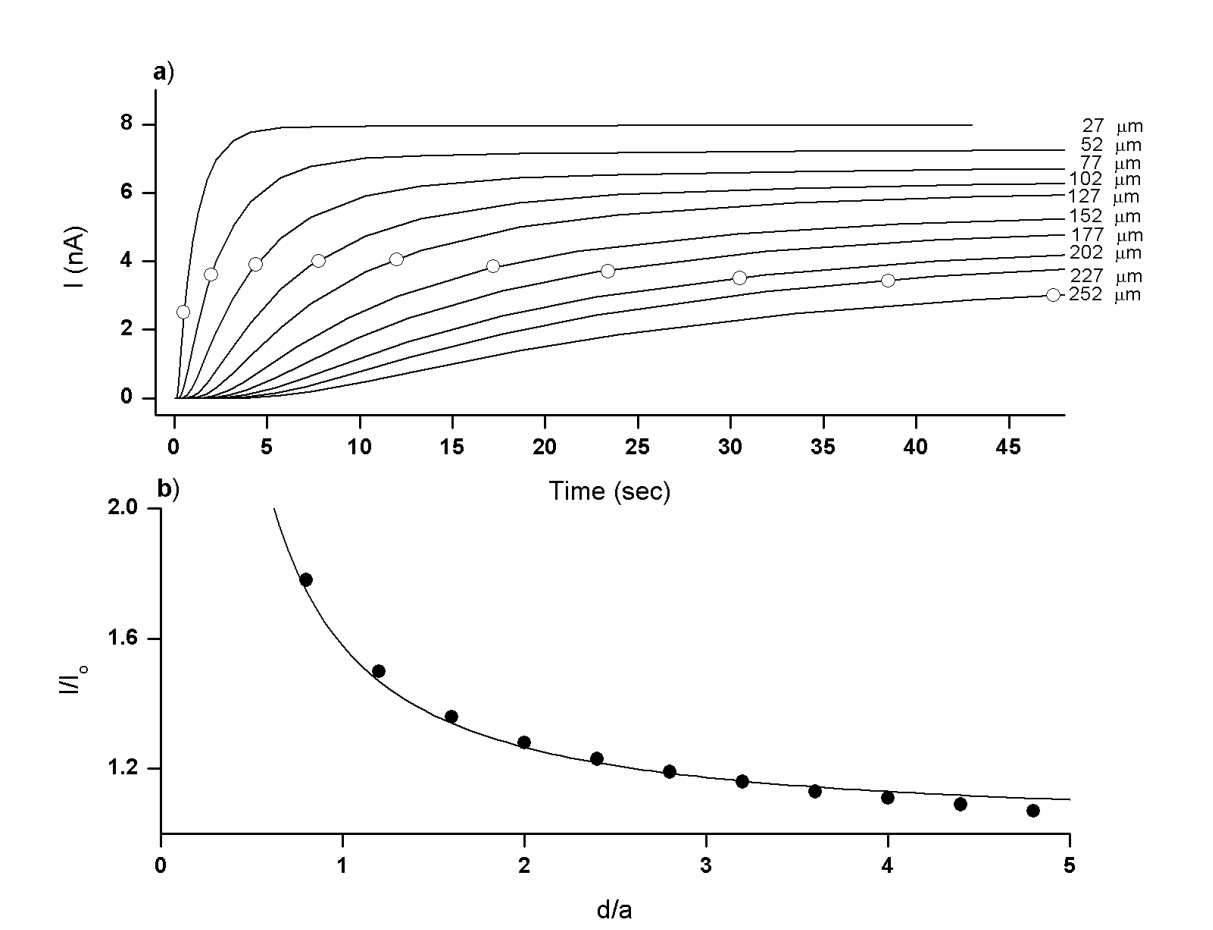

Figure 1.4: a) SG-TC simulation at a finite disk for different tip to substrate separations for a 25 μm UME tip in a 1 mM $Ru(NH_3)_6Cl_3$ solution with an assumed diffusion coefficient of 6.7×10^{-6} cm^2/s. (o) Diffusion time calculated from the diffusion layer thickness approximation:$\delta=\sqrt{2Dt}$. b) Fitting of the simulated steady-current for different tip to substrate separations and positive feedback SECM theory for a finite disk.

The same conditions were used in the SG-TC simulation at a finite planar disk for different tip to substrate separations as presented in Figure 4a. As the tip was moved further away from the generating substrate, the steady-state current decreased.

Previous simulations have used the decrease in steady-state current to test their simulations to SECM feedback theory.[5,40] The normalized steady-state current for a conductive approach curve is given by:

$$i_t / i_{t,\infty} = 0.68 + 0.7838/L + 0.3315 \exp\left[-1.0672/L\right] \qquad (20)$$

where i_t is the tip current, $i_{t,\infty}$ is the steady-state current when the tip is far from the substrate and L is the ratio of the tip to substrate spacing and the tip radius (12.5 μm). As seen from Figure 4b, the steady-state currents obtained from the simulation at different tip to substrate separations fit SECM theory well.

At small tip to substrate distances, the rising transient response has a steeper slope and a shorter diffusion time as shown in Figure 4a. As the separation increases, the slope of the transient decreases and the diffusion time increases. The diffusion layer thickness is often approximated by:

$$\delta = \sqrt{2Dt} \qquad (21)$$

where D is the diffusion coefficient (cm^2/s), t is the time (s) and δ is the thickness of the diffusion layer (cm). This approximation yields the diffusion times shown as circles in Figure 4a. From the simulation, one notes that the detection of current occurs sooner and suggests that in experimental measurements, eq. (21) is not a good approximation to estimate the tip to substrate separation.

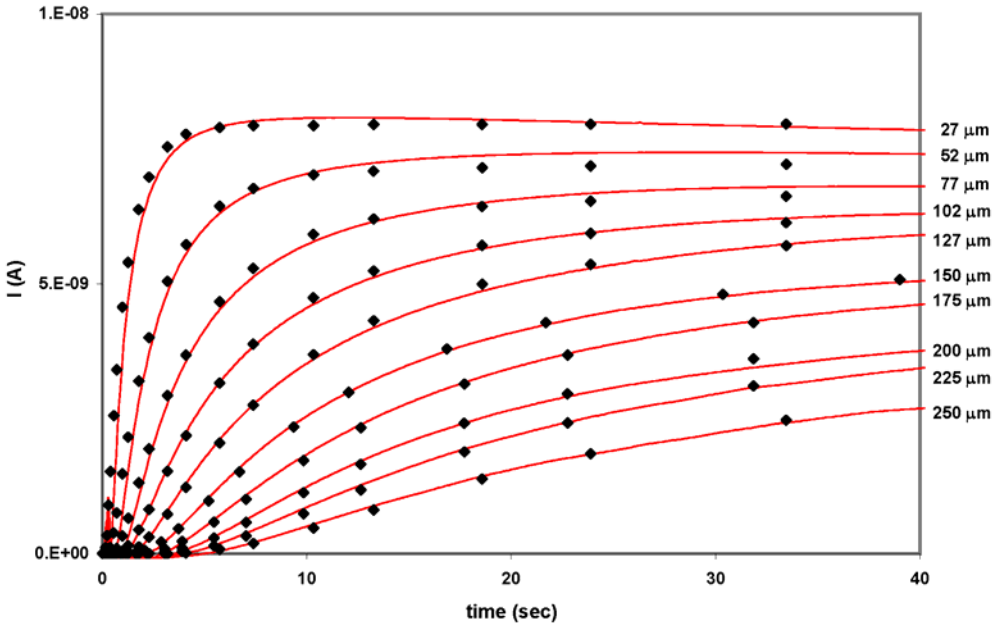

Figure 1.5: 1 parameter fit of the simulated and experimental results for the SG-TC of 1 mM $Ru(NH_3)_6Cl_3$ solution at a 25 µm Pt finite disk UME for different tip to substrate distances and a diffusion coefficient of 6.7×10^{-6} cm^2/s.

The results for the SG-TC experiments at a planar disk UME are presented in Figure 5. In this experiment, a large Pt substrate electrogenerated $Ru(NH_3)_6^{2+}$ from an initial solution containing $Ru(NH_3)_6^{3+}$. A fraction of the generated +2 species diffuses from the substrate and is then intercepted by the 25 µm Pt disk UME, causing an increase in tip current. The tip current eventually reaches a quasi steady-state when the concentration of +2 at the tip approaches the original bulk concentration of $Ru(NH_3)_6^{3+}$.

The tip to substrate separation affects the diffusion time, the fraction of $Ru(NH_3)_6^{2+}$ that is collected at the tip, and the magnitude of the steady-state tip current. The experiment was repeated for several tip to substrate separations, x, which were evaluated from an SECM calibration based on a feedback approach curve. From Figure 5, we see that the smaller was x, the steeper the slope of the transient response, the shorter the diffusion time, and the larger the final steady-state current. This behavior is consistent with that reported by Unwin et al. for smaller tip to substrate separations.[5] At longer times then those shown here, convection occurred and caused the current to decrease.

In fact, the simulated data, as shown in Figure 5, fits the experimental results quite well. In the simulation, the diffusion coefficients of reduced and oxidized species are assumed to be the same. The diffusion coefficient extracted from the simulation (D_s= 8.7×10^{-6} cm^2/s) is also in good agreement with the experimental one (D= $6.7\times10^{-6}cm^2/s$).

Engstrom et al. suggested using an error function complement approximation in earlier work.[24] They showed that the general shape, amplitude and time delay of the erfc predicted their experimental results for tip to substrate spacing greater than 10 μm. The concentration profile of the generated species, $C_o(x,t)$, was treated as a double potential step chronoamperometric problem.[7] The concentration profile generated at the substrate and detected by the tip is given by:[41]

$$C_o(x,t) = C_o^* erfc\left[\frac{x}{2(D_0 t)^{1/2}}\right] \qquad (22)$$

where C_o^* is the bulk concentration of the species in solution before electrolysis, x is the tip to substrate distance, and t is time. Equation (22) expresses the concentration as a

function of t at a given distance and can be substituted in eq. (23) to yield a tip current expression that also depends on time and tip separation.

$$i_T = 4nFDC_o(x,t)a \qquad (23)$$

Table 1.1: Tip to substrate distance evaluation using an error function complement approximation. From the error function complement argument, the tip to substrate distance (X) is extracted and compared to the distance obtained by the experimental approach curve fitting to hemispherical SECM theory.

ERFC Argument	X_{erfc} (μm)	X_{SECM} (μm)
0.643	33	27
1.005	52	52
1.795	92	77
2.129	110	102
2.546	131	127
2.991	154	152
3.362	174	177
3.770	195	202
4.192	217	227
4.648	240	252

The best fit value of x of the data in Figure 5, which is reported in Table 1, are then obtained by fitting eq. (23) to the data in Figure 5. These values are compared to the distances evaluated from the steady-state SECM feedback approach curves. At smaller distances, the approximation in eq. (22) does not hold as well because of feedback effects. At intermediate to long distances, however, a better agreement with the SECM-derived distances is observed

Formation and Characterization of a Hg/Pt UME

MERCURY DEPOSITION

We now discuss the fabrication of a Hg/Pt tip and its use in SECM. As discussed in the Experimental section, Hg is electrodeposited on the planar Pt UME disk. In the first stages of deposition, a very thin layer of inter-metallic species (Pt_2Hg) is formed.[10] This is followed by the spontaneous formation of mercury nuclei (Figure 6a) close to the edge of the platinum/glass interface where the current density is the highest.[42] With time, the nuclei coalesce until a full hemisphere is formed. This coalescence alters the surface area of the electrode and leads to indentations in the current deposition curves (Figure 6b). These results are consistent with previously reported work.[12] Once formed, the mercury hemisphere is firmly attached to the platinum substrate and could withstand washing; however, it could not be stored in air and left to dry. When dry, the hemisphere shrank and sometimes exposed platinum as a result of surface tension changes. Hg UMEs were therefore stored in a degassed potassium nitrate solution.

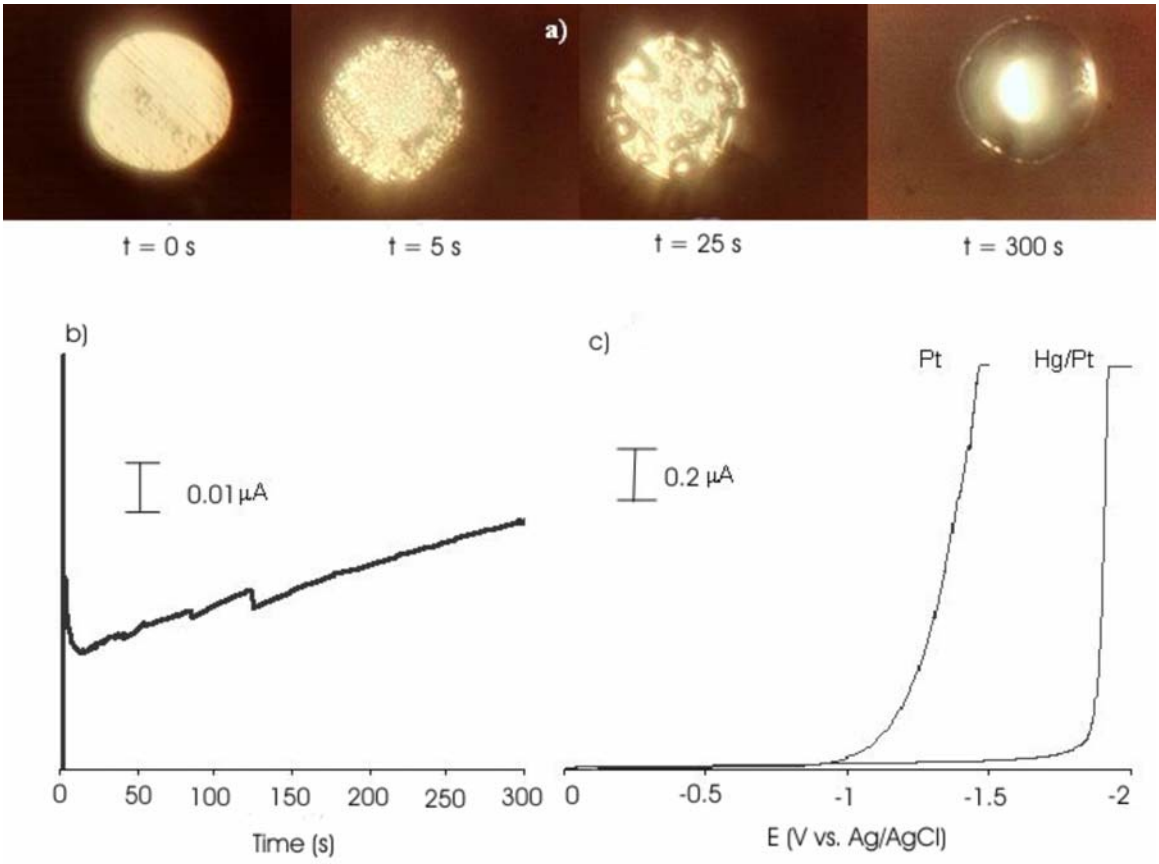

Figure 1.6: Characterization of the 25 μm Hg/Pt UME. a) In-situ micrographs of mercury deposition (0-300 s) from a 10 mM $Hg_2(NO_3)_2$ solution with 0.1 M KNO_3 supporting electrolyte acidified to 0.5% with HNO_3. b) The deposition curve recorded during a 300 s potential step of -0.1 V vs. Ag/AgCl. A 1 mm Pt wire served as counter electrode, and a fritted Ag/AgCl electrode served as reference electrode. c) Current-potential curves at Pt and Hg/Pt UMEs in 0.1 M KNO_3.

VOLTAMMETRY

The electrochemical behavior and stability of the Hg UME was evaluated using linear sweep voltammetry. After mercury deposition, the proton reduction overpotential shifted to more negative potentials from that seen at bare Pt by about 800 mV (Figure 6c). Dirty or damaged electrodes only shifted the overpotential by about 200 mV and

showed prewaves characteristic of platinum micro arrays. Clean UMEs with a thick mercury deposit, however, were well behaved.

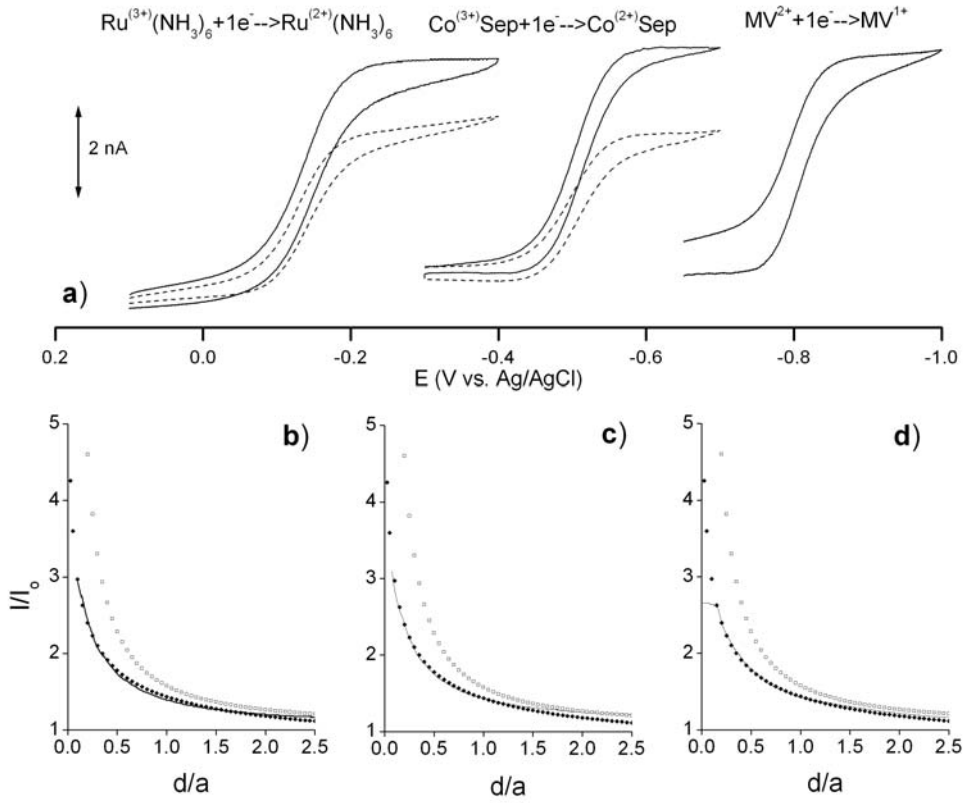

Figure1.7: a) Voltammetric behavior of the 25 μm (--) Pt and (solid line) Hg/Pt UMEs in 1 mM $Ru(NH_3)_6Cl_3$, cobalt sepulchrate trichloride and methyl viologen in 0.1 M KNO_3. b) Positive feedback SECM fitting of the ( ) finite disk theory, (♦)hemispherical disk theory and (line) experimental results for the 1 mM $Ru(NH_3)_6Cl_3$. c) Positive feedback SECM fitting of the ( ) finite disk theory, (♦)hemispherical disk theory and (line) experimental results for the 1 mM cobalt sepulchrate trichloride in 0.1 M KNO_3. d) Positive feedback SECM fitting of the ( ) finite disk theory, (♦)hemispherical disk theory and (line) experimental results for the 1 mM methyl viologen.

Proton reduction at Pt is catalyzed by methyl viologen. Electrochemical studies of this couple in aqueous media must, therefore, be performed at a mercury electrode. The methyl viologen voltammogram at the Hg UME was well behaved (Figure 7a), confirming good coverage of the Pt disk and demonstrating the use of Hg UMEs as probes in SECM in the negative potential regime.

The geometry of the Hg tip was confirmed by the change in limiting current in voltammograms of $Ru(NH_3)_6^{3+}$ (Figure 7a). The voltammograms showed a wave at the standard potential of the couple and a stable steady-state current. An increase in steady-state current was observed for the Hg UME relative to the Pt UME because of the change in geometry from disk to hemisphere. This follows the theoretical equations of the steady-state current at microelectrodes where the ratio of the limiting current of a disk UME[43] and that of a hemispherical UME is close to $\pi/2$. The observed change of steady-state current (i_h/i_d = 1.47) from the Pt UME to the Hg UME is close to this value for $Ru(NH_3)_6^{3+}$, confirming the near hemispherical geometry of the UME. The radius (r_{exp} = 12.6 μm), calculated from the voltammogram, is also equal to that of the mirodisk. A similar increase in the steady-state ratio (i_h/i_d = 1.57) was observed for cobalt sepulchrate trichloride (Figure 7a). Thus, both the optical and voltammetric analysis confirm the hemispherical geometry of the UME.

SECM EXPERIMENTS WITH THE HG/PT TIP IN THE FEEDBACK MODE

The theory[27,44,45] and applications of SECM have been discussed elsewhere.[36] Relevant to the present measurements is the effect of tip geometry on the SECM approach curves. An approximate approach to this question treated different tip shapes, e.g., cones, hemispheres, as variations on a collection of disks.[14] The shape of the hemispherical approach curve demonstrates the reduced sensitivity of the mercury

electrode to feedback relative to the Pt disk electrode (Figure 7b,c,d). This agrees with previously reported studies of gold spherical UMEs prepared by self-assembly of gold nanoparticles.[15] The diffusion of the electroactive species normal to the disk UME outweighs the radial diffusion component as the tip approaches a conductive substrate. The theoretical approach curve for a hemisphere, therefore, demonstrates the lower sensitivity inherent to the geometry of the tip. As the tip approaches the conductive substrate, the current measured will systematically be inferior to that measured at the disk electrode. Based on Figure 7b,c,d, all three tested redox couples present this behavior and are consistent with the theoretical current expression of Mandler et al.[8]

Experimentally, the close approach of the disk electrode is often hampered by the insulating sheath, which strikes the substrate prematurely due to misalignment of the tip. The protrusion of the active electrode area, like the mercury hemisphere, can allow for an uninhibited approach and a better estimation of the true zero distance. When SECM approach curves are fitted to theory, the zero tip to substrate distance, and the limiting current of the tip are variable parameters. We have tried to avoid variability in the limiting current by imposing a long equilibration time (minutes) prior to measuring the approach curves. The zero distance remains the main uncertainty in fitting the experimental curves to the theory but the adjustment parameter for a hemispherical tip is minimal.

SG-TC EXPERIMENTS AT A HEMISPHERICAL UME

The results for the SG-TC experiments at a hemispherical UME are presented in Figure 8. Unlike the disk experiments, these measurements were performed in presence of 10^{-4} M $TlNO_3$ in a phosphate buffer solution at pH=7, since this system was of particular interest in studying ionic diffusion through membrane channels,[7] and illustrates

another feature of the Hg/Pt tip, amalgam formation. Initially the Tl(I) was preconcentrated onto a HMDE by electrochemical formation of an amalgam. The Tl/Hg was then oxidized and the Tl(I) collected at a 25 μm submarine Hg/Pt UME. The tip current, initially at the Tl(I) background level, increases upon collection of the generated Tl(I) and reaches a quasi-steady-state current; it then decreases because of the exhaustion of the substrate (HMDE) amalgam. Figure 8 shows the background subtracted data and is restricted to the time domain where the amalgam exhaustion was not significant. This was done to simplify the numerical simulation by avoiding the description of the stripping behavior of the amalgamated HMDE. The experiment was repeated for several tip to substrate distances that were evaluated from a SECM calibration. From Figure 8, we see that the shorter the distances, the steeper the slope of the transient response, the shorter the diffusion time and the higher the final steady-state current. Qualitatively, the hemispherical transient response is similar to that presented in Figure 5 for the disk UME.

Quantitatively, the response is most sensitive to the tip geometry at small tip to substrate separations and short collection times. Indeed, the simulated data for the disk electrode is not a good approximation of the hemispherical response in this regime. The diffusion time is too short and causes an early increase in tip current. The enhanced lateral diffusion of the hemispherical tip reduces the sensitivity of the tip to concentration increases. The diffusion time observed at a hemispherical tip is therefore longer and the slope of the transient is smaller than that of the disk for a given tip to substrate separation. This observation concurs with the SECM feedback experiments of Figure 7b,c,d and the work reported by Mandler and coworkers.[8]

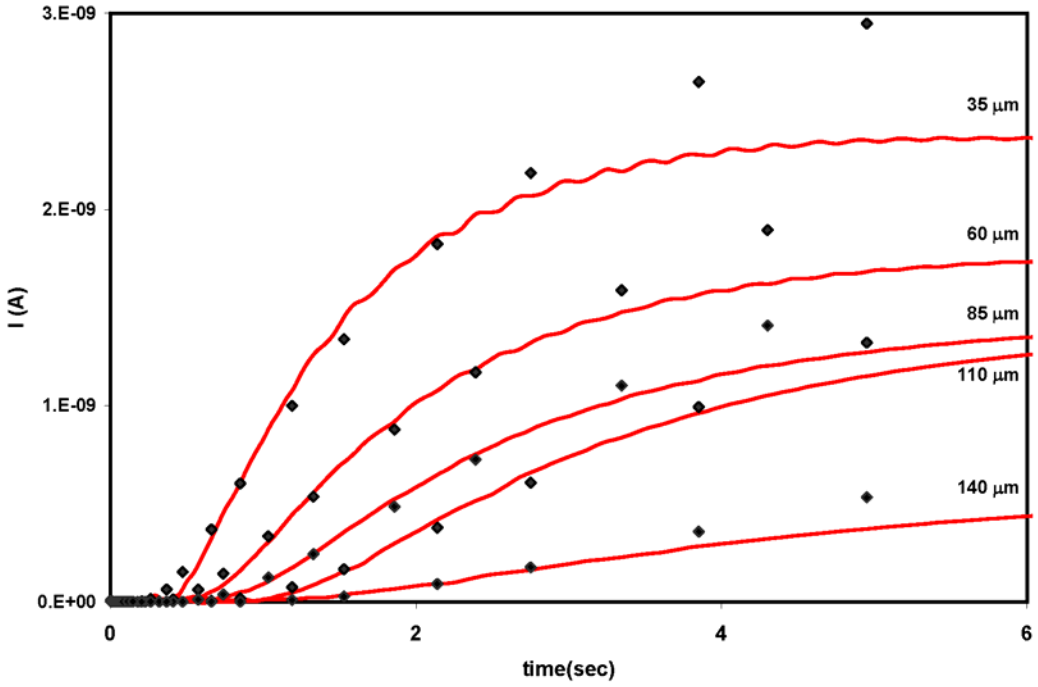

Figure 1.8: 1 parameter fit of the simulated and experimental results for the SG-TC of $TlNO_3$ at a hemispherical Hg/Pt UME for different tip to substrate distances. For a 25 µm Hg/Pt UME tip in a 10^{-4}M $TlNO_3$ solution in 0.1 M phosphate buffer at pH 7 with an assumed diffusion coefficient of 1.85×10^{-5} cm^2/s.

The results in Figure 8 show good agreement between experimental and simulated results at a hemispherical tip. The early collection time follows the simulated data very well. The deviation at longer time is explained by the gradual depletion of the Tl amalgam at the substrate. This deviation does not prevent us from extracting good values

for the diffusion coefficients for Tl(I) diffusion (D_s=1.88×10^{-5}cm^2/s). This value is almost identical to the one reported in the literature (1.85×10^{-5}cm^2/s).[46]

Conclusions

The Hg/Pt UME can be fabricated by two equivalent methods and characterized through optical and electrochemical means. Both techniques agree on the hemispherical nature of the UME and the total coverage of the platinum area by mercury. Voltammetric studies yield reversible results and confirm the extension of the potential window to more negative potentials for SECM in aqueous solutions, allowing mediators like methyl viologen to be employed. The conducting approach curves for methyl viologen, cobalt sepulchrate trichloride, and hexaminеruthenium (III) chloride show good agreement with the hemispherical theory of Mandler et al.[8] Another application of the Hg/Pt electrode is for species like S-containing peptides that give a good response on a Hg electrode, but not on Pt. Recent studies involving glutathione, the major non-protein sulfhydryl present in cells, have been carried out and will be reported elsewhere.[47]

The SECM tip transient in SG-TC mode for a disk and a hemispherical UME were calculated by numerical analysis using PDEase2D, a software program using FEM. The tip transient responses for both geometries were calculated at various tip to substrate distances. When the distance is small, the diffusion time is short, the slope of the transient response is large and the quasi, steady-state current is high. The diffusion times at particular separations were easily approximated by an error function complement relationship. Validation of the numerical analysis was obtained from a comparison of the disk UME response to a large amplitude potential step in a quiescent solution to that from the expression derived by Shoup and Szabo.[37] The diffusion-limited steady-state current

at long collection times also agreed well with the positive feedback theory of SECM. Finally, the extraction of the diffusion coefficient from the numerical analysis correlated well with the experimentally reported values for both geometries.

The electrode geometry affects the transient current response measured in SG-TC experiments. This was confirmed by the numerical simulation and is in line with the feedback studies.[8] But the main advantages of the mercury tips are the enhancement of potential window in the negative potential region and also the protrusion of the hemisphere beyond the glass sheet. The protrusion of the active electrode area can allow for a close approach and actual touching of the metal to the substrate without problems of premature touching of the glass insulator, thus yielding a better estimation of the true zero distance. Such qualities are desirable in many SECM studies.[7]

References

[1]Bard, A. J.; Mirkin, M. V.; Eds, *Scanning Electrochemical Microscopy,* Marcel Dekker, New York, **2001**.

[2] Bard, A. J.; Denuault, G.; Friesner, R. A.; Dornblaser, B. C.; Tuckerman, L. S. *Anal. Chem.* **1991**, *63*, 1282.

[3] Denault, G.; Mirkin, M. V.; Bard, A. J. *J. Electroanal. Chem.* **1991,** *308***,** 27.

[5] Martin, R. D.; Unwin, P .R. *Anal. Chem.* **1998**, *70*, 276.

[6] Rueda, M.; Navarro, I.; Ramirez, G.; Prieto, F.; Prado, C.; Nelson, A. *Langmuir* **1999**, *15*, 3672.

[6] Mauzeroll, J.; Buda, M.; Bard, A. J.; Prieto, F.; Rueda, M. *Langmuir* **2002,** *18*, 9453.

[8] Selzer, Y.; Turyan, I.; Mandler, D. *J. Phys. Chem. B* **1999**, *103*, 1509.

[9] Wu. H. P. *Anal. Chem.* **1994**, *66*, 3151.

[10] Yoshima, Z. *Bull. Chem. Soc. Jpn.* **1981**, *54*, 556.

[11] Wehmeyer, K. R.; Wightman, R. M. *Anal. Chem*. **1985**, *57*, 1989.

[12] Golas, J.; Galus, Z.; Osteryoung, J. *Anal. Chem.* **1987**, *59*, 389.

[13] Wechter, C.; Osteryoung, J. *Anal. Chim. Acta* **1990,** *234*, 275.

[14] Mirkin, M. V.; Fan, F.-R. F.; Bard, A. J. *J. Electroanal. Chem.* **1992**, *328*, 47.

[15] Demaille, C.; Brust, M.; Tionsky, M.; Bard, A. J. *Anal. Chem.* **1997**, *69*, 2323.

[16] Fulian, Q.; Fisher, A. C.; Denuault, G. *J. Phys. Chem. B* **1999**, *103*, 4387.

[17] Fulian, Q.; Fisher, A. C.; Denuault, G. *J. Phys. Chem. B* **1999**, *103*, 4393.

[18] Selzer,Y.; Mandler, D. *Anal. Chem.* **2000**, *72*, 2383.

[18] Zoski, C. G.; Mirkin, M. V. *Anal. Chem*. **2002**, *74*, 1986.

[20] Fan, F.-R. F.; Bard, A. J. *Science* **1995**, *267*, 871.

[21] Fan, F.-R. F.; Bard, A. J. *Science* **1995**, *270*, 1849.

[22] Fan, F.-R. F.; Bard, A. J. *Proc. Natl. Acad. Sci. U.S.A.* **1999**, *96*, 14222.

[23] Gray, N. J.; Unwin, P. R. *Analyst* **2000**, *125*, 889.

[24] Engstrom, R. C.; Weber, M.; Wunder, D. J.; Burgess, R.; Winquist, S. *Anal. Chem.* **1986,** *58*, 844.

[25] Engstrom, R. C.; Meaney, T.; Tople, R.; Wightman, R. M. *Anal. Chem.* **1987**, *59*, 2005.

[26] Engstrom, R. C.; Wightman, R. M.; Kristensen, E. W. *Anal. Chem.* **1988**, *60*, 652.

[27] Kwak, J.; Bard, A. J. *Anal.Chem.* **1989**, *61*, 1221.

[28] Fulian, Q.; Fisher, A. C.; Dennuault, G. *J. Phys. Chem. B* **1999**, *103*, 4393.

[29] Unwin, P. R. *J. Chem. Soc. Faraday Trans.* **1998**, *94*, 3183.

[30] Slevin, C. J.; Umbers, J. A.; Atherton, J. H.; Unwin, P. R. *J. Chem. Soc. Faraday Trans.* **1996**, *92*, 5177.

[31] Penczek, M.; Stojek, Z. *J. Electroanal. Chem.* **1984**, *170*, 99.

[32] Penczek, M.; Stojek, Z. *J.Electroanal. Chem.* **1984**, *181*, 83.

[33] Moorhead, E. D.; Stephens, M. M. *J. Electroanal. Chem.* **1990**, *282*, 1.

[34] Nann, T.; Heinze, J. *Electrochem. Comm.* **1999**, *1*, 289.

[35] Lee, Y.; Amemiya, S.; Bard, A. J. *Anal. Chem.* **2001**, *73*, 2261.

[36] Mirkin, M. V. In *Scanning Electrochemical Microscopy*, Bard, A. J.; Mirkin, M. V.; Eds.; Marcel Dekker, New York, **2001,** Chapter 4.

[37] Shoup, D.; Szabo, A. *J. Electroanal. Chem.* **1982**, *140*, 237.

[39] Aoki, K.; Osteryoung, J. *J. Electroanal. Chem.* **1981**, *122*, 19.

[40] Martin, R. D.; Unwin, P. R. *J. Electroanal. Chem.* **1997**, *439*, 123.

[41] Bard, A. J.; Faulkner, L. R. *Electrochemical Methods*, *1st ed.*, John Wiley & Sons, New York, **1980,** 180.

[42] Sharifer, B.; Hills, G. J. *J. Electroanal. Chem.* **1981**, *130*, 81.

[43] Wightman, R. M.; Wipf, D. O. *Electroanalytical Chemistry*, Bard, A. J.; Ed.; Marcel Dekker, New York, **1989,** *Volume 15*, 267.

[44] Bard, A. J.; Fan, F.-R. F.; Kwak, J.; Lev, O. *Anal. Chem.* **1989**, *61*, 132.

[45] Davis, J. M.; Fan, F.-R. F.; Bard, A. J. *J. Electroanal. Chem. Interfacial Electrochem.* **1987**, *238*, 9.

[46] Kolthoff, M.; Lingane, J. J. *Polarography*, Interscience Publishers, New York, **1952**, 52.

[47] Mauzeroll, J.; Bard, A. J. unpublished experiments.

CHAPTER 2: DETECTION OF TL(I) TRANSPORT THROUGH A GRAMICIDIN-DIOLEOYLPHOSPHATIDYLCHOLINE MONOLAYER USING THE SUBSTRATE GENERATION-TIP COLLECTION MODE OF SCANNING ELECTROCHEMICAL MICROSCOPY*

Introduction

We report the use of scanning electrochemical microscopy (SECM) to control the generation of Tl(I) at a mercury substrate and detect this species at a mercury-coated tip to study the transport of these ions through ion channels. The transport of Tl(I) across gramicidin D half channels imbedded in a dioleoylphosphatidylcholine (DOPC) monolayer supported on a Tl-amalgam hanging mercury drop electrode (HMDE) was studied using the substrate generation-tip collection (SG-TC) mode of SECM. A Hg/Pt "submarine" electrode, used as the SECM tip, was made through simple contact of the Pt ultramicroelectrode with the HMDE. The tip transient response for the collection of generated Tl(I) at the amalgam HMDE was recorded for several tip to substrate distances. This collection-generation experiment was repeated with a DOPC-modified Tl/HMDE and a gramicidin-DOPC modified Tl/HMDE. An apparent heterogeneous rate constant (k_{het}= 2.8 (± 0.1) x 10^{-4} cm/s) for the transport of Tl(I) through the gramicidin to the tip was extracted.

The theory[1-3] and applications of the SECM have been discussed elsewhere.[4] Most SECM measurements involve steady-state current measurements. However, transient current measurements have also been performed and provide information about the kinetics of homogenous reactions and time dependent systems. SECM transient response has previously been simulated and experimentally observed for planar

* *"Reproduced in part with permission from Langmuir 2002, vol 18(24), pp 9453-9461"*

electrodes, microdisks and thin-layer cells over a wide time range.[5] When the tip radius is known, transient current measurements allow for the determination of diffusion coefficients without knowledge of solution concentration and the number of electrons transferred. This concept was also corroborated by later work.[6] In the SG-TC SECM mode, the substrate generates an electroactive specie that diffuses into the bulk. An ultramicroelectrode (UME) positioned close to the substrate collects the generated species. The tip is at least an order of magnitude smaller than the substrate and has a thinner diffusion layer than the substrate. The tip reaction, therefore, does not significantly affect the substrate current.

Generation-collection experiments with an amperometric tip were pioneered by Engstrom et al.,[7-9] where a small carbon UME was employed to collect and study species generated at a nearby macroscopic electrode. They addressed the theoretical behavior of the tip transient response using potential step functions and impulse response functions and showed how this collection mode could be used for the collection of short-lived species, such as nicotinamide adenine dinucleotide (NAD) and epinephrine. They also studied the response time of a Nafion-coated UME in generation-collection experiments. The imaging capabilities of SECM in a SG-TC mode have also been used to monitor the activity of enzyme-modified microstructures.[10,11]

The diversity of membrane structures and transport mechanisms studied by SECM demonstrates the utility of this technique for studies of membrane transport. Diffusion across porous mica,[12] dentine[13] and iontophoresis across skin[14] are all examples of SECM studies of molecular transport across membranes. Previous work by our group used ion selective micropipette electrodes in the SECM feedback and SG-TC modes to study K(I) transport through gramicidin D channels in a horizontal bilayer lipid membrane.[15,16] As we describe here, Tl(I) can be used as a surrogate for K(I), so that ion

transport across gramicidin channels can be monitored using an amperometric UME rather than an ion selective probe. It also allows one to control the release of the Tl(I) into the gramicidin channels by preconcentration of the Tl as an amalgam on the HMDE with controlled oxidation of the amalgam using a potential step. A Hg/Pt submarine UME positioned close to the HMDE collects the generated Tl(I) following its diffusion from the substrate to tip. The tip collection response for different tip to substrate separations was evaluated. The response for the bare HMDE at a known tip to substrate distance was then compared to that of a DOPC and gramicidin-DOPC amalgamated HMDE.

Phospholipid-coated mercury electrodes with incorporated gramicidin have previously been used as membrane models.[17] The phospholipids form an organized monolayer at the Hg surface, where the tail of the lipid faces the mercury and the polar head groups face the electrolyte solution.[18-20] When gramicidin channels are inserted into the DOPC monolayer, the conduction of Tl(I) ions is found over a potential region where the layer is usually ion-impermeable.[21] Gramicidin is a linear 15-amino acid peptide synthesized by *Bacillus brevis* that is often used as a model ion channel for monovalent cations (Figure 1). It is composed of alternating D and L amino acids. The primary sequence of gramicidin A starting from the N terminal is: HCO-val-gly-L-ala-D-leu-L-ala-D-val-L-val-D-val-L-trp-D-leu-L-*trp*-D-leu-L-trp-D-leu-L-trp-$NHCH_2CH_2OH$. The italicized amino acid accounts for the natural variants of gramicidin (gram A (trp), gram B (phe), gram C (tyr)[22]) that make up gramicidin D in a 80:15:5 ratio, respectively. A full gramicidin channel (2.6-3 nm diameter) is formed from a dimer composed of two $\beta^{6.3}$ helices. A full channel is probably not present in a DOPC monolayer since the thickness of the layer is only half that of a full channel. The Tl(I) conduction observed in the studied system is thus provided by a half-channel whose length is similar to that of the monolayer.[19,23] The effects of gramicidin concentration and choice of supporting

electrolyte on the conduction of these half-channels have also been reported for this system.[24]

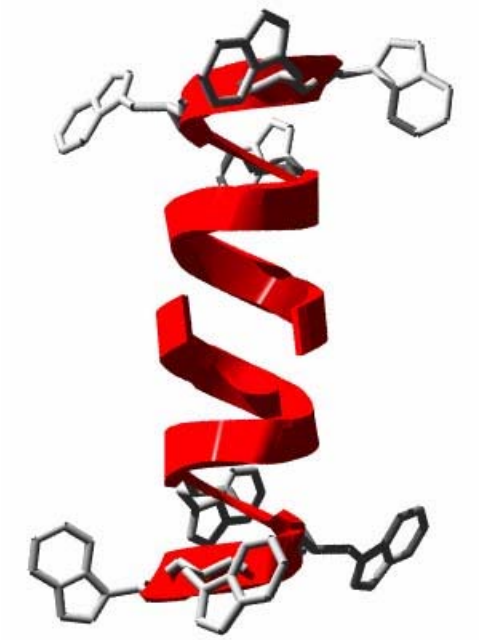

Figure 2.1: Full channel image of gramicidin A outlining the position of the four tryptophan groups at each extremity of the dimmer. The reported structure was reproduced based on solid NMR studies.[25,26]

Experimental Section

SOLUTION PREPARATION

All solutions and liquids were kept in glass containers previously washed overnight in saturated NaOH in EtOH and rinsed in water. The supporting electrolytes used were 0.1 M KCl solutions buffered with a 1:1 molar ratio of NaH_2PO_4/Na_2HPO_4 of total concentration 0.01M at pH 7 (Mallinckrodt AR, Paris, KY). The redox couples employed were 2 mM hexammineruthenium (III) chloride (Strem Chem., Newburyport, MA) and Tl(I) nitrate (Aldrich). The stock solution was 0.1 M Tl(I) nitrate with a Tl(I)

concentration in the reaction cell of 0.1 mM. All solutions were prepared with Milli-Q (Millipore Corp.) reagent water, and degassed with Ar for 30 min prior to all experiments.

A 0.1 % stock solution of dioleoylphosphatidylcholine (DOPC) (Lipid Products, Nutfield, UK) in pentane (EM Sciences, Gibbstown, NJ) was stored at temperatures below -20°C. A stock solution of 2.2 mM gramicidin D (Sigma) was prepared in methanol (EM Sciences, Gibbstown, NJ) and stored in the refrigerator. Both solutions were stored in brown glass bottles with a Teflon cap (VWR Sci. Prod., Siwanee, GA).

SECM APPARATUS

A CHI model 900 scanning electrochemical microscope (CH Instruments, Austin, TX) was used to control the tip potentials, obtain the approach curves and monitor the tip to substrate distance. A battery operated, home built, floating potentiostat was used for potential control of the HMDE to prevent electrical coupling with the SECM in generation-collection experiments. The commercial SECM experienced electrical coupling during SG-TC transient experiments at short tip to substrate distances. This led to the superimposition of long current transients onto the tip collection response. In addition, the cell stage was modified to accommodate a chamber designed to allow measurements under oxygen-free conditions.

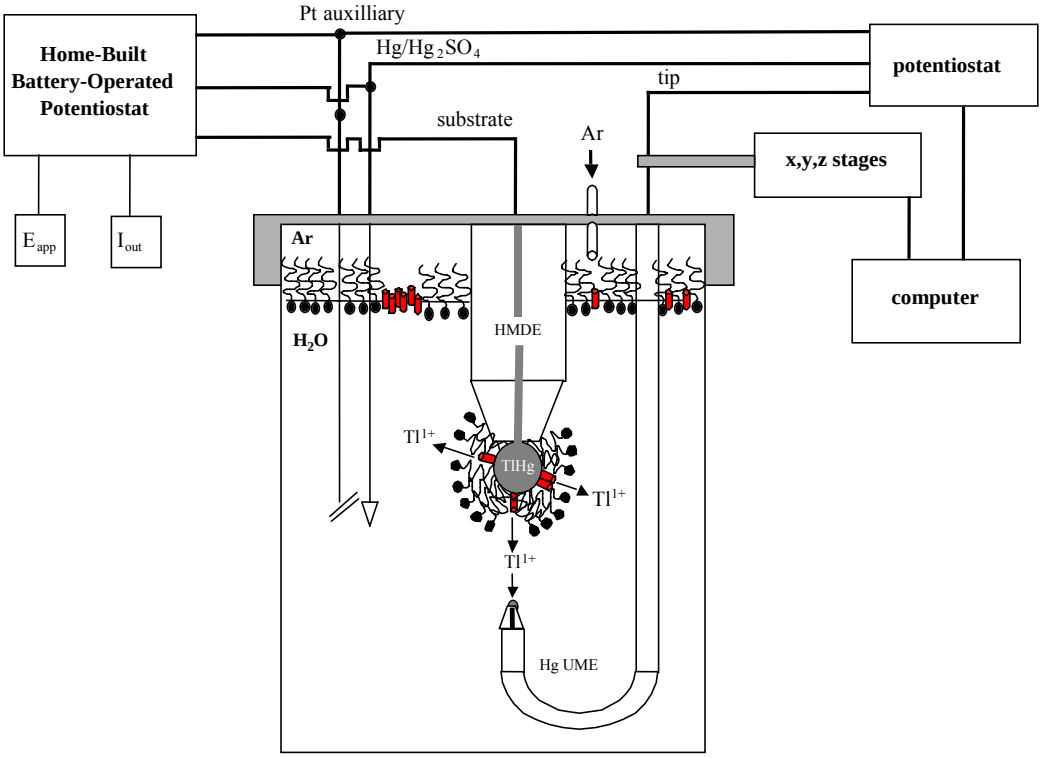

Figure 2.2: Experimental setup for the SG-TC experiments. A 750 ml cut beaker contains 250 mL of phosphate buffer and 250 μL of $TlNO_3$ stock solution, sealed with a Teflon cap that accommodates the HMDE, Hg/Pt submarine UME, Hg/Hg_2SO_4 reference, Pt auxiliary electrode and a gas inlet for Ar. 35 μL of the DOPC stock solution was added drop wise to form the monolayer at the Ar/solution interface. 15 μL of gramicidin stock solution was added and stirred. Each new mercury drop had an area, A= 0.0139 ± 0.0003 cm^2. A battery operated potentiostat and SECM setup were used respectively to control the substrate and tip potential.

ELECTRODES

A 25 μm diameter Pt wire (Goodfellow, Cambridge, UK) was sealed into a 5 cm Pyrex glass capillary under vacuum as described previously.[2] The electrode was polished

and shaped into a UME on a polishing wheel (Buehler, Lake Bluff, IL) with 180 grid Carbimet paper disks (Buehler, Lake Bluff, IL) and micro polishing cloth with 1.0, 0.3, and 0.05 μm alumina (Buehler, Lake Bluff, IL). The tip was sharpened to an RG of 3, where RG is the ratio of the diameter of the UME that includes the glass sheet and the diameter of the Pt wire. The UME was then sealed into a J glass tube using Teflon tape to form the submarine electrode shown in Figure 2. The Hg/Pt UME was formed by applying –1.1 V to the Pt UME and making contact with the mercury (Bethlehem Instr. Hellertown, PA) of the HMDE (Metrohm Instr. Herisau, Switzerland) in phosphate buffer.[28]

A 0.5 mm Pt wire (Goodfellow, Cambridge, UK) and Hg/Hg_2SO_4 (Radiometer, Copenhagen, Denmark) electrode were used as counter and reference electrodes respectively. All potentials are reported vs. Hg/Hg_2SO_4.

PROCEDURE

All experiments are performed sequentially in the same reaction vessel, a 750 mL cut beaker with a machined Teflon cap with an O-ring (Figure 2). The cap accommodated the HMDE, the submarine electrode, the reference and auxiliary electrodes, a gas inlet and a microsyringe. An argon blanket was maintained over the solution at all times. The reaction vessel was filled with 250 mL phosphate buffer and closed with all electrodes in place. The solution was purged with argon for 30 min. The tip and HMDE were aligned for the formation of the Hg/Pt UME. The tip was then retracted from the HMDE to a known distance. The reaction vessel was deaerated for 30 min, after which 250 μL of $TlNO_3$ stock solution was added. Voltammetric response of Tl(I) was then recorded at both tip and substrate.

The distance dependence of the tip transient response was evaluated by holding the substrate and tip at –1.1 V for 30 s to form the substrate amalgam and to stabilize the tip current. The substrate potential was then switched to –0.75 V to oxidize the Tl amalgam. The tip, at –1.1 V, collected the released Tl(I) from the substrate for 100 s. The tip was then moved 25 μm further away from the substrate and the experiment was repeated. This was carried out for several tip to substrate distances. A new amalgam HMDE was used for each distance but the same Hg/Pt tip was used for the entire experiment. This implies that the drop on the tip was incorporating thallium but saturation of the drop was not observed. Upon completion, an approach curve was recorded to assess the true tip to substrate distance. The solution was then purged with argon for 45 min.

The tip transient response was recorded for several tip to substrate distances with the amalgamated HMDE and the gramicidin-DOPC and DOPC modified amalgamated HMDE. To form the DOPC monolayer at the air/solution interface, 35 μL of the DOPC stock solution was added dropwise with a microsyringe. Upon contact, the drops spread at the interface and solvent evaporation was noticeable at the walls of the reaction vessel. The layer was left to organize on the solution surface for 30 min under an argon blanket.

The HMDE was used as the support for the DOPC and gramicidin-DOPC adsorbed monolayers. The adsorbed monolayers were prepared as previously reported.[19,29] The film spread at the air/solution interface was transferred to the bare and Tl amalgam HMDE by slowly passing it through the film. The quality of the film was then examined by looking at the decreased Tl(I) electrochemical response for a potential range that did not reach the first phase transition peak of the lipid layer (-1.3 V). Within –0.6 to –1.1 V, the monolayer is ion impermeable and the Tl(I) reduction at the HMDE should be significantly decreased by the presence of the DOPC layer as a result of

blocking. At potentials more negative then –1.3 V, characteristic phase transition peaks appear and their voltammetric behavior has been studied.

The gramicidin half channels were inserted into the DOPC air/solution interface by adding 15 μL of a 2.2 mM gramicidin stock solution to the solution in the cell. The solution and interface were then gently stirred for 5 min to allow uniform distribution of the gramicidin within the DOPC layer. The gramicidin-DOPC modified film was transferred to the HMDE in a similar fashion as described above. The voltammetric behavior of the gramicidin-DOPC film was also recorded prior to the SG-TC experiments; these are presented in the results section.

In the SG-TC experiments using the DOPC and gramicidin-DOPC modified substrates, the Tl/Hg amalgam was first formed for 30 s at the substrate. The films were then transferred to the amalgamated drop, and the drop was repositioned exactly at the same distance from the tip using a micromanipulator. A 30 s quiet time was applied to the tip prior to the oxidation of the amalgam. The substrate was then oxidized and the tip transient response was measured. At the end of each experiment, an approach curve was recorded to insure that the tip to substrate distance was conserved during the experiment. Each experiment used a new mercury drop (area, A= 0.0139 ± 0.0003 cm^2).

Results and Discussion

SUBSTRATE GENERATION-TIP COLLECTION (SG/TC) EXPERIMENTS

Formation of Hg/Pt Submarine Electrodes

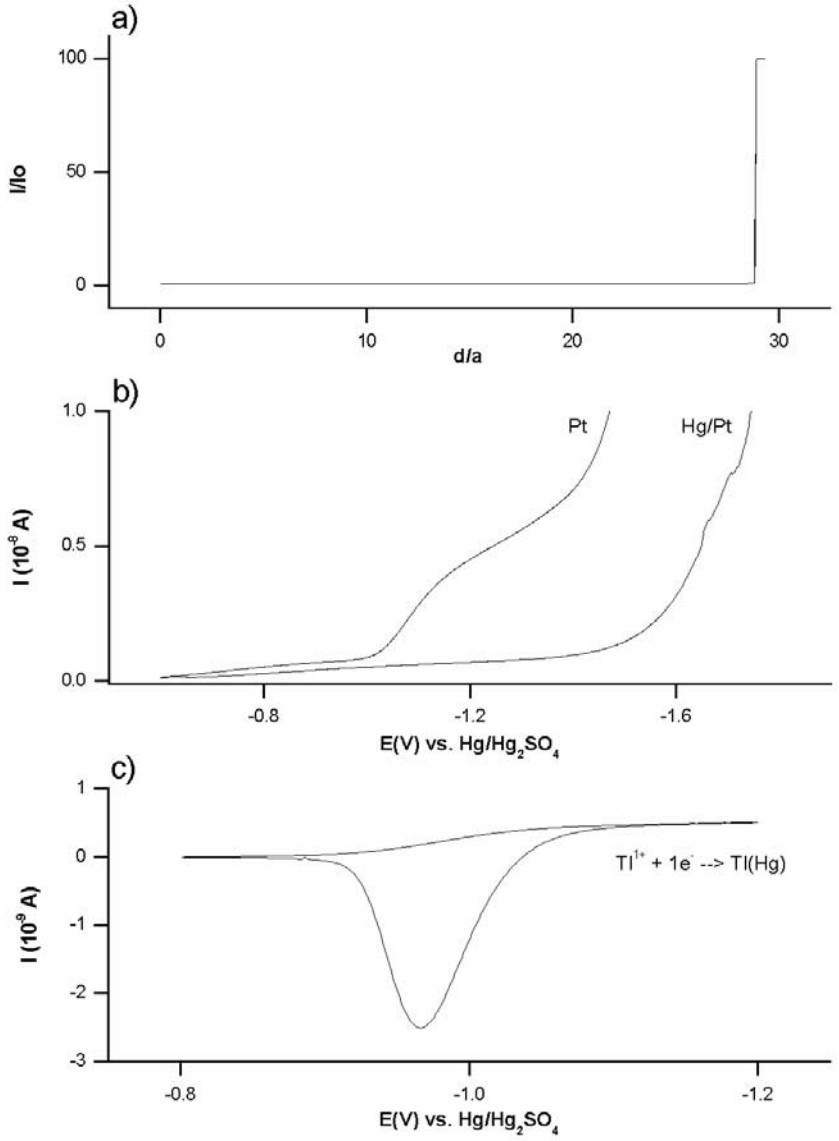

Figure 2.3: Formation and characterization of the Hg/Pt submarine electrode. a) The Pt submarine electrode in phosphate buffer (pH=7) as it approached the HMDE while poised at –1.1 V vs. Hg/Hg_2SO_4. Upon contact with the HMDE, a hemispherical mercury layer is deposited onto the Pt UME. b) Hydrogen evolution at Pt and Hg/Pt submarine UME in phosphate buffer. c) Voltammogram of the 10^{-4} M Tl(I) at the Hg/Pt submarine electrode in phosphate buffer.

A 25 μm Hg/Pt UME formed upon touching a Pt UME to Hg (Figure 3a). The 25 μm Pt "submarine" electrode was poised at –1.1 V and approached the HMDE in a deaerated phosphate buffer (pH=7) at 1 μm/s. This Hg/Pt UME was characterized by cyclic voltammetry and SECM feedback experiments. As shown in Figure 3b, a 0.5 V overpotential for hydrogen evolution was observed in deaerated phosphate buffer (pH=7) following the Hg deposition onto Pt. The response presented in Figure 3b suggests full coverage of the Pt by the Hg. The presence of uncovered Pt regions would have resulted in a microarray voltammetric response for hydrogen evolution on Pt. The extension of the potential window allowed the detection of Tl(I) electrochemistry at the SECM tip (Hg/Pt UME)(Figure 3c). The voltammogram presents a stable steady-state current for the Tl(I) reduction and a characteristic stripping peak for the oxidation of the Tl amalgam.

The Hg/Pt "submarine" UME showed good positive feedback with $Ru(NH_3)_6^{2+}$ when it approached a HMDE (Figure 4). The experimental approach curve fit the theory developed by Mandler et al.[30] for a hemispherical UME. The analytical approximation for the positive feedback equation (±1%) (normalized current vs. distance) of a hemispherical UME is:

$$i_t / i_{t,\infty} = 0.873 + \ln(1 + L^{-1}) - 0.20986 \exp\left[-(L - 0.1) / 0.55032 \right] \qquad (1)$$

where i_t is the tip current, $i_{t,\infty}$ is the steady-state current when the tip is far from the substrate and L is the ratio of the tip to substrate spacing and the active electrode radius (12.5 μm) (d/r_0).

The response is significantly different from that predicted for a disk.[31]

$$i_t / i_{t,\infty} = 0.68 + 0.7838/L + 0.3315 \exp\left[-1.0672/L\right] \quad (2)$$

The tip shape affects the approach curves because of proportional differences in lateral and normal diffusion to the tip. The normalized current for a hemispherical tip is smaller than that of the disk electrode at short distances (Figure 4). This agrees with previously reported studies of gold spherical UMEs prepared by self-assembly of gold nanoparticles.[32] For a disk UME, the diffusion of the electroactive species normal to the tip outweighs the radial diffusion component as the tip approaches a conductive substrate. The hemispherical UME protrudes from the glass sheet and is more sensitive to lateral diffusion. As the tip approaches the conductive substrate, the current measured will systematically be smaller than that at the disk UME.

The deposited Hg hemisphere was stable and did not change surface area upon subsequent contact with the HMDE because of liquid trapping between the two mercury surfaces.[27] This repulsion between two mercury surfaces has previously been reported and is said to depend on the symmetry of the two mercury surfaces, the charge, and the presence of adsorption processes.[36] The presence of a trapped layer was observed as a change of slope in the approach curves at very short distances in the SECM positive feedback experiments. In fact, a 25 μm size UME approaching a Hg pool could trap and push into the pool a 0.56 μm thick water layer.[37] Also, voltammograms recorded following successive contacts of the UME with the HMDE presented no significant change in the steady-state current, showing no appreciable change in the UME electrode area.

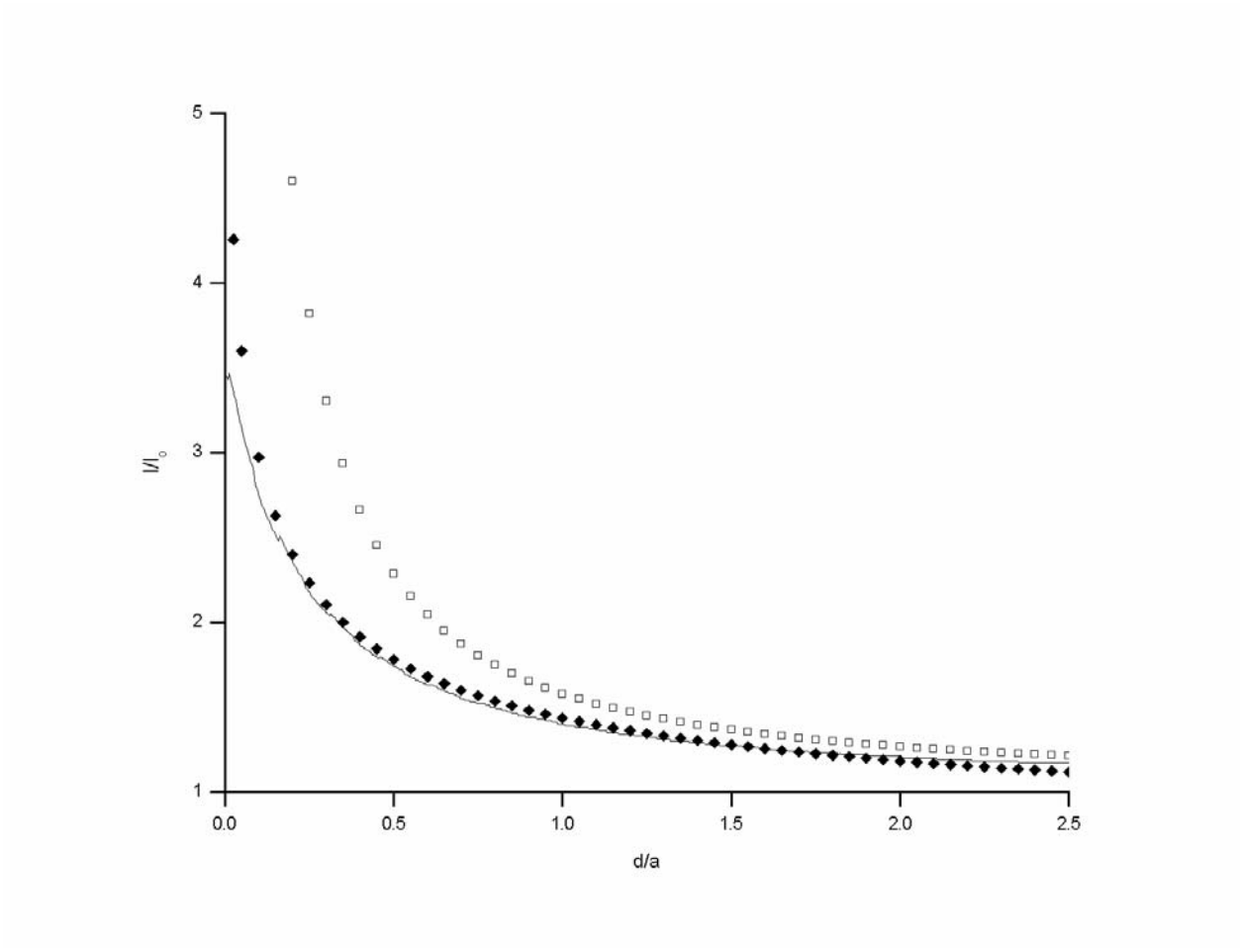

Figure 2.4: Positive feedback SECM curve fitting of (line) Hg/Pt submarine electrode approach curve to (♦) hemispherical SECM theory and (□) disk SECM theory for a 2 mM hexaminеruthenium chloride solution in phosphate buffer (pH=7). The Hg/Pt UME approached the HMDE.

Tip Transient Response in Collection Experiments

The tip transient response for the collection of the Tl(I) generated at a bare Tl(Hg) electrode is presented in Figure 5. The collection response depends on the Tl(I) concentration profile generated at the substrate. Since the substrate amalgam concentration, area and applied potential for oxidation remain constant for all

experiments, the generated concentration profile is entirely governed by the diffusion layer thickness. At short collection times, the tip current remains at baseline level until the generated Tl(I) has diffused from the substrate to the tip. For large tip to substrate separation, the diffusion time is long and the collection of Tl occurs later than for small separations. As discussed below, the tip collection current follows an error function complement relationship for the short time regime, and reaches a maximum because of depletion of Tl from the source amalgam. At small separations, the concentration profile is compact and the slope of the collection response is steeper than for larger separations. The transient peak maximum is smaller and generally tends to shift to longer times at larger tip to substrate distances.

The amalgam formation was limited to 30 s so that the surface properties of the Hg drop would not be altered significantly. The source amalgam is therefore exhausted rapidly during the transient collection at the tip. This leads to the formation of the peak maximum and the return of the tip current to the baseline value. The baseline current for the reduction of Tl(I) at the UME is non-zero due to the presence of some dissolved Tl(I) in the buffer solution. Because of the restrictions imposed by the gramicidin DOPC monolayer, it was impossible to conduct this experiment in the absence of background Tl(I).

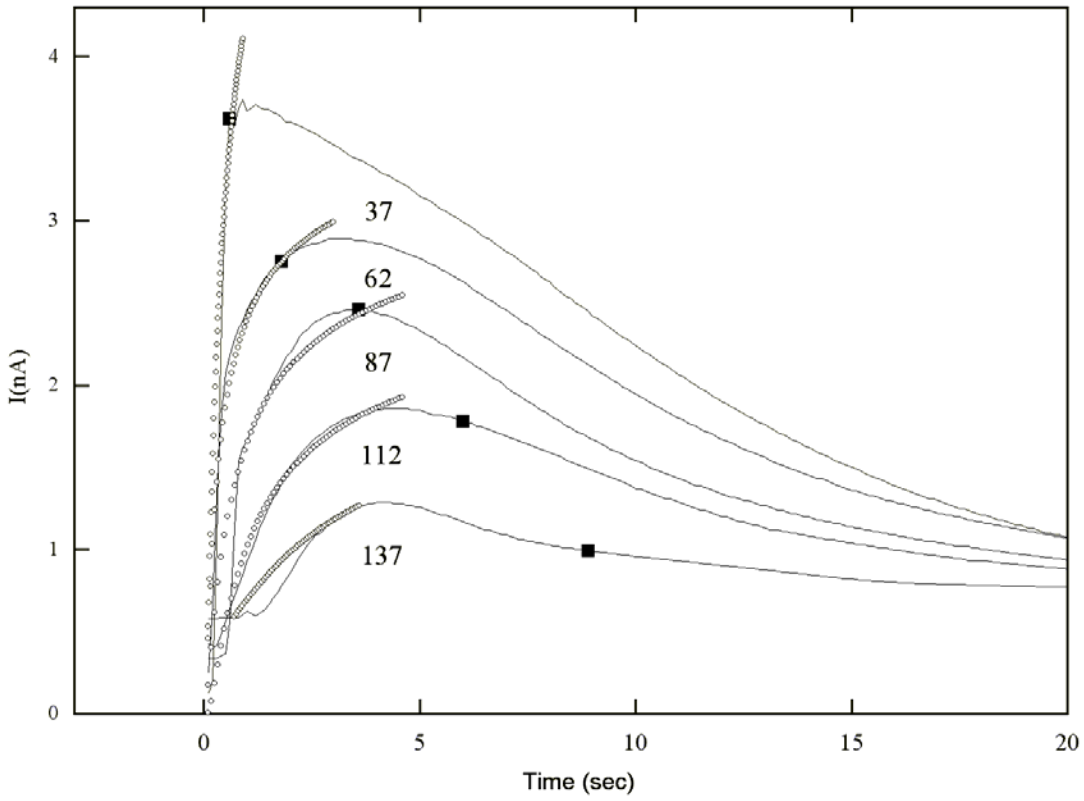

Figure 2.5: (line) Tip transient response for the collection of generated Tl(I) for different tip to substrate separations. The distances were evaluated by curve fitting the final approach curve in 10^{-4} M $TlNO_3$ to the negative feedback hemispherical SECM theory. The ( ) represents the error function complement fits performed from a non-linear least square fitting based on LV algorithm. The ( ) represents the time extracted from the diffusion layer thickness equation: $\Delta = \sqrt{(2Dt)}$.

Tip to Substrate Distance Evaluation

The tip to substrate distance dependence of SG-TC experiments for Tl(I) collection at the Tl/Hg HMDE is reported in Figure 5. A calibration curve for the distances reported in the figure were obtained from an SECM negative feedback

approach curve. To obtain this curve, the tip was poised at the potential for Tl(I) reduction in the electrolyte as it approached the HMDE (that was disconnected and so at open circuit). The SECM approach curve was fit to the negative feedback approximation equation for a hemispherical electrode:[33]

$$i_t / i_{t,\infty} = 0.39603 + 0.42412L + 0.09406L^2 \qquad (3)$$

The tip to substrate distance was evaluated from the fit. In the present case, the adjustment for zero distance is minimal because of the known position of initial contact of the tip to the HMDE during Hg/Pt UME formation. There is, however, some uncertainty in the determination of the contact distance and in the thickness of the Hg film that can account for some error in distance.

The tip to substrate distances extracted from SECM fits are presented in Table 1. These distances represent the thickness of solution layer that the Tl(I) generated at the HMDE must cross to reach the UME. The diffusion layer thickness, Δ, is usually given by an approximation such as $\Delta = \sqrt{2Dt}$, where D is the diffusion coefficient (cm^2/s) and t is the time (s). In the present collection experiments this approximation is not a good representation of the actual distance. The calculated diffusion time, t, from equation (4) use the tip to substrate distances presented in Table 1 and are plotted and represented by the squares in Figure 5. Experimentally, the initial collection of Tl(I) occurs much sooner than that predicted by the diffusion layer approximation.

Table 2.1: Tip to substrate distance evaluation using an error function complement approximation. From the error function complement argument, the tip to substrate distance (X)is extracted and compared to the distance obtained by the experimental approach curve fitted to hemispherical SECM theory.

ERFC Argument	$X_{erfc(x)}$ (μm)	X_{SECM} (μm)
0.431	27	37
1.103	70	62
1.384	88	87
1.765	112	112
2.282	144	137

The concentration profile, $C_o(x,t)$, of Tl(I) generated at the HMDE is governed by spherical diffusion. However, the close spacing of the tip to the much larger HMDE allows us to approximate the diffusion of the generated Tl(I) as linear. For the unmodified amalgam HMDE system, the generated concentration profile of Tl(I) from a preexisting Tl(Hg) amalgam is treated as a double potential step chronoamperometric problem (See supporting information). The concentration profile generated at the HMDE and detected by tip is given by:[38]

$$C_o(x,t) = C_o^* \, erfc\left[\frac{x}{2(D_0 t)^{1/2}}\right] \qquad (4)$$

where C_o^* is the bulk concentration of Tl(I) in solution before the amalgam formation, x is the tip to substrate distance and t is a time variable that considers the reversal time as the zero time. This approximation was also used by Engstrom et. al. in earlier work.[7] They showed that the general shape, amplitude and time delay of this equation predicted their experimental results for tip to substrate spacing greater than 10 μm. Here, the tip current is given by the usual UME equation with the concentration obtained from (4), i.e.,

$$i_T = 4nFD_O C_O(x,t) r_0 \qquad (5)$$

The tip to substrate distance was evaluated by fitting the rising portion of the curves in Figure 5; these are reported in Table 1 where they are compared to the distances evaluated from the SECM approach curves. The values obtained by this approximation are better than those derived from a simple diffusion layer approximation. At shorter distances, the approximation in eq. (4) does not hold as well because of feedback effects.

MONOLAYER FORMATION AND CHARACTERIZATION

Figure 6 presents the characterization of the DOPC films by voltammetry. Within the range of –0.6 V and –1.1 V, the DOPC monolayers adsorbed on mercury are generally ion impermeable. The Tl(I) voltammetric response for a DOPC modified HMDE is therefore significantly smaller compared to the bare HMDE signal (curves b

and a, respectively). DOPC monolayers adsorbed on mercury show a small density of defects that account for the residual Tl(I) signal observed in Figure 6b.[39] Beyond –1.1 V and up to the onset of the first phase transition peak (Figure 6d), the DOPC layer becomes more permeable to metal ions with applied potential. Beyond this first phase transition peak, the density of defects increases with potential. Molecularly, the lipid monolayer reverts to a two phase system of a thick and thin monolayer.[40] The second phase transition peak represents the growth and coalescence of defects formed in the first phase.[20] If the potential window is expanded further to more negative potentials, a third peak indicating the DOPC layer being displaced from the mercury surface appears. In this paper, the experiments were restricted to the potential window where the DOPC adsorbed layer was impermeable to metal ions.

The insertion of gramicidin in the DOPC monolayer increases the permeability of Tl(I) ions and this led to an increase in the voltammetric response (Figure 6c). The response resembles that of a process determined by a kinetically driven process. The orientation of the gramicidin-DOPC modified monolayer is governed by the hydrophobicity of the mercury.[40] The carbon tails of the DOPC face the metal surface while the head group is in solution. This orientation is supported by experimental results comparing the potential of zero charge of the DOPC layer on mercury to the surface potential of condensed phosphatidylcholine (PC) monolayers at the air-water interface.[39] Theoretical calculations also predict that within the potential range –0.6 to –1.1 V phospholipid molecules in a monolayer should have their tails facing the mercury and the head groups facing the electrolyte.[40] This arrangement prevents multilayer formation from repeated touches of the monolayer on the HMDE with the film at the air/water interface.

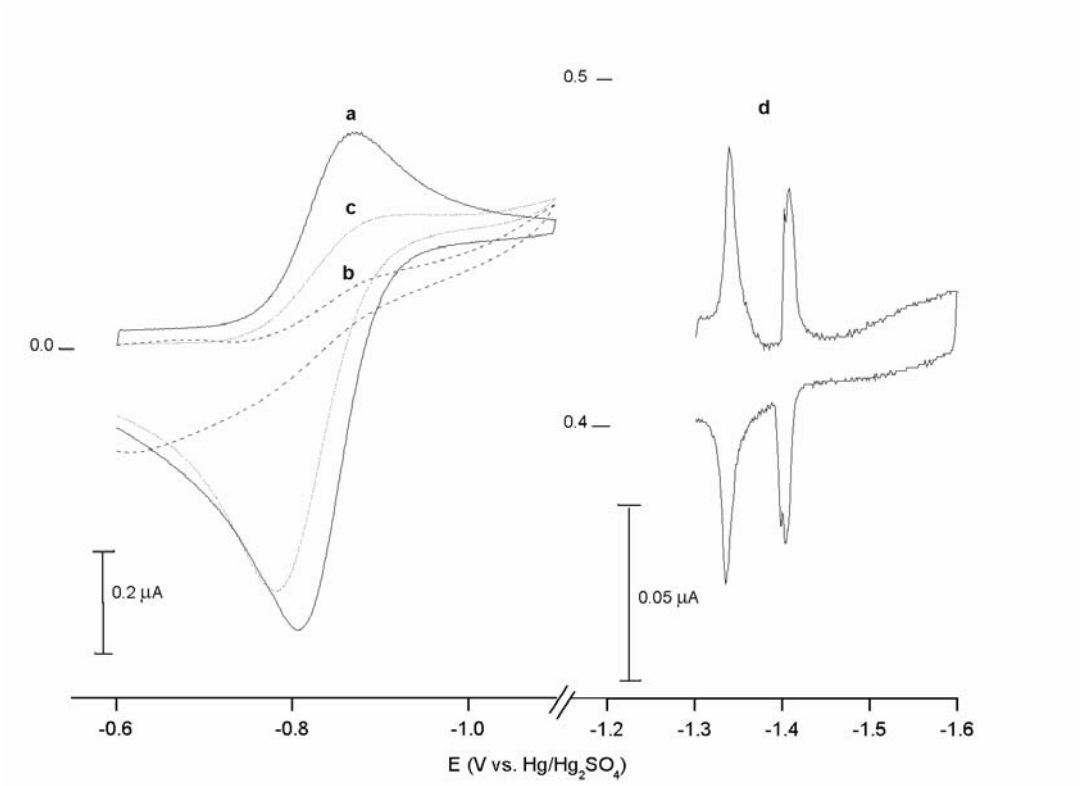

Figure 2.6: The voltammetric response of (a) bare HMDE, (b) DOPC modified HMDE and (c) gramicidin-DOPC modified HMDE in 10^{-4} M $TlNO_3$ in phosphate buffer for a 50 mV/s scan rate. (d) The voltammetric response of the DOPC-modified HMDE system outlining the reversible first and second monolayer transitions in 10^{-4} M $TlNO_3$ in phosphate buffer for a 50 mV/s scan rate.

The particular orientation of the DOPC layers influences the organization of the $\beta^{6.3}$ gramicidin helix in the layer. At the end of each gramicidin A there are four tryptophan residues as shown in Figure 1. These residues are polarizable and capable of hydrogen bonding to the polar head group of the lipid and with the water in solution.[41-44] The gramicidin half channels are therefore, probably closer to the electrolyte solution than the mercury. A similar arrangement is observed for gramicidin B and C that have one fewer tryptophan residue.

SG-TC OF THALLIUM(I) IN GRAMICIDIN CHANNELS

Collection experiments of Tl(I) at the Hg/Pt UME with generation at a Tl amalgam/HMDE, bare, DOPC-modified and gramicidin-DOPC-modified Tl/HMDE is reported in Figure 7. As mentioned earlier, the Tl amalgam is first formed on the HMDE prior to the adsorption of the DOPC and gramicidin-DOPC layers onto the substrate. Upon application of the potential capable of oxidizing Tl at the substrate, a switching transient is observed for a few 100 ms. The collection response was then recorded at a tip positioned 87 μm away from the substrate. All transient responses presented in Figure 7 were recorded with the same tip, (a different one than that used to collect the distance transients in Figure 5).

The trend recorded for the tip transient response for the bare, DOPC-modified and gramicidin-DOPC modified systems (Figure 7a,b,c respectively) is similar to that observed in the voltammetry experiments (Figure 6a,b,c). The bare electrode has the steeper slope and the highest maximum. The background current for the bare electrode is lower because this run was made just after degassing. The DOPC-modified and gramicidin-DOPC-modified results were recorded following monolayer formation and insertion of gramicidin into the layer. Although an Ar blanket was maintained for the entire experiment, some limited oxygen contamination could explain the small increase in background current for these systems.

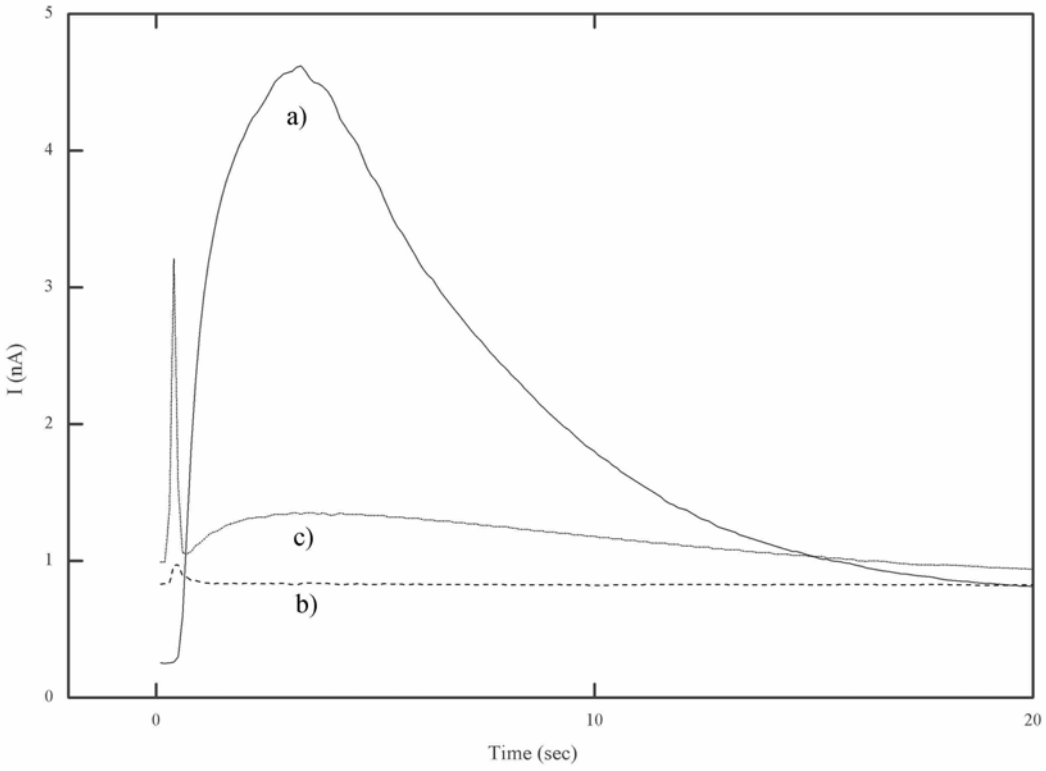

Figure 2.7: SG-TC tip transient response for the a) bare Tl/HMDE, b) DOPC modified Tl/HMDE and c) gramicidin-DOPC modified Tl/HMDE with a tip to substrate distance of 87 μm. The Tl/Hg amalgam was formed for 30 s and the measurements were performed in 10^{-4} M $TlNO_3$ in phosphate buffer. These results were obtained with a different Hg/Pt UME than the results presented in Figure 5.

The DOPC-modified system was totally blocking. This indicates that the defects observed in Figure 6b do not affect the response significantly and present a sensitivity limitation of the technique. The defects in Figure 6b were still present, but the Tl(I)

transport through them was undetectable by the Hg/Pt tip because it only addressed a small portion of the substrate and that there was a background current of Tl(I) in the solution. The introduction of gramicidin increased the passage of Tl(I) through the monolayer and this was detected. The Tl(I) released through the gramicidin channels (Figure 7c) showed a smaller slope and lower maximum. The response is broader and peaks at nearly the same time as compared to the bare Hg. The decay slope is also not as steep consistent with a slower release of the Tl into solution. These results were reproduced in two additional experiments at similar tip to substrates and showed good agreement with the results presented.

The generation of Tl(I), transport across gramicidin and subsequent collection at the tip from the solution can be viewed as a rate controlled by diffusion. The concentration profile is governed by mass transfer through the solution and the rate at which the generated Tl(I) is transported across the gramicidin channels (which we treat below as a heterogeneous kinetic process). We assume semi-infinite linear diffusion to calculate the concentration profile of the generated Tl(I). Linear diffusion is a reasonable model for this experiment because the tip to substrate distance is much larger than the spacing between two channels, but small with respect to the HMDE radius. To obtain the concentration profile[37] of the generated Tl(I), we use the diffusion equation, the initial, semi-infinite and flux balance conditions along with the heterogeneous rate constant as used in the irreversible potential step problem[45] to yield the following Laplace transformation:

$$\overline{C}_o(x,s) = \frac{k_{het} C_{Tl(I)}^{*}}{\sqrt{D}} \left\{ \frac{e^{-x\sqrt{\frac{s}{D}}}}{s\left(k_{het} / \sqrt{D} + \sqrt{s} \right)} \right\} \qquad (6)$$

with simple variable substitution and the inverse transformation of equation 6[46] we obtain:

$$C_o(b,t) = C_{Tl(I)}^{*}\left\{ erfc\left(\frac{b}{2\sqrt{t}}\right) - e^{ab}e^{a^2 t}erfc\left(a\sqrt{t}+\frac{b}{2\sqrt{t}}\right)\right\} \qquad (7)$$

where $a = k_{het}/D^{1/2}$, $b = x/D^{1/2}$, k_{het} is the apparent heterogeneous rate constant (cm/s) for the transport of Tl(I) through the channels, D is the diffusion coefficient of the generated species (cm^2/s) in solution, x is the tip to substrate separation (cm) and t is the diffusion time (s). $C_{Tl(I)}^{*}$ is the concentration of Tl(I) in the drop following the film formation. This concentration is assumed constant and is related to the amalgam formation time. From eqs. (5) and (7), the UME collection tip current for the Tl(I) generated at the HMDE that moves through the gramicidin channels and diffuses across the solution gap is:

$$i^t = 4nFr_o DC_{Tl(I)}^{*}\left\{ erfc\left(\frac{b}{2\sqrt{t}}\right) - e^{ab}e^{a^2 t}erfc\left(a\sqrt{t}+\frac{b}{2\sqrt{t}}\right)\right\} \qquad (8)$$

Equation (8) has two unknowns, the concentration of Tl(I) on the drop following film formation and the heterogeneous rate constant. The k_{het} was extracted based on a two parameter fit from the rising part of the SG-TC response of the gramicidin-DOPC modified system using a non-linear least square fitting based on the Levenberg-Marquardt (LM) algorithm. The background Tl(I) current was subtracted from the collection response, the switching transient and depletion region of the substrate were omitted from the fit. From the fitting results in Figure 8, k_{het} = 2.8 (±0.1) x 10^{-4} cm/s for

x= 87μm, D= 2 x 10^{-5} cm^2/s. The error function complement argument is very small in this fitting and so the expression is linear in this domain.

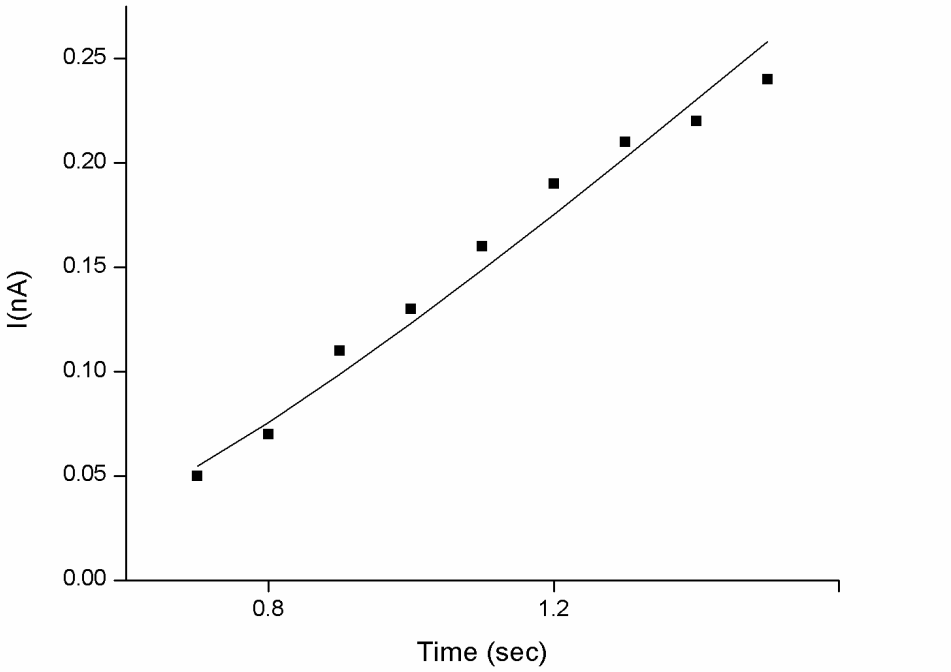

Figure 2.8: Fitting of the rising part of the gramicidin-DOPC modified transient response to equation 8. The non-linear fitting used the LM algorithm to extract P1 = $k_{het}/\sqrt{D}$ = 0.06347 ± 0.00153. The reduced Chi square (1.3268E-22) was minimized. The fit yielded k_{het} = 2.8 (±0.1) x 10^{-4} cm/s for x= 87μm, D= 2 x 10^{-5} cm^2/s.

There has been significant work and models put forth to elucidate the transport mechanism of monovalent cations from the bulk solution through gramicidin.[21,22,49] These are based on a porous layer model where the charge transfer takes place at microscopic inhomogeneities while the rest of the electrode surface is covered by a blocking film.[50] Molecularly, monovalent cations are partially dehydrated upon coordination with the carbonyls of the tryptophan residues at the mouth of the channel. They are then transported through the channel along with water molecules. The nature of our

experiments do not allow us to discuss the validity of these models. Our results do enable us to compare the heterogeneous rate constants extracted from our work with that of reported ones.

Most of the electrochemical methods used to study the transport process[17,21,42] looked at the reduction of Tl(I) for the transport of an ion from the bulk solution to the HMDE. The heterogeneous rate constant (k_{het}= 8 x 10^{-3}cm/s) derived from quasi steady-state chronoamperometric measurements is larger than the one reported here.[17] The transport process for the stripping experiment from Hg may well be different from that when the ion is transported from the bulk aqueous solution. Once oxidized from the substrate, the Tl(I) must be aquated and transported through the gramicidin. Once at the half-channel, the ion does not benefit from the carbonyl interactions at the mouth of the channel. The transport of Tl(I) from the HMDE to the bulk solution might therefore be more energetically costly and thus result in a smaller apparent heterogeneous rate constant. If there is asymmetry in the activation barrier of the half channels it would be interesting to compare the rates obtained for a similar system with a full channel (Figure 1) where the activation barrier should be more symmetric. Differences in rates in such experiments might then reveal some potential dependence of the rate constant for the Tl oxidation. A recent report by Guidelli,[47] however, suggests that the flux of Tl(I) from the gramicidin-DOPC modified Tl/HMDE to the solution is potential independent and mainly controlled by diffusion based on linear scan voltammetry performed on a similar system as used in the present work.

Conclusions

A Hg/Pt submarine UME tip was formed through simple contact of a Pt UME with a HMDE and used as a detector for Tl(I) (which serves as a surrogate for K^+) in SECM. The tip transient collection response for different tip to substrate distances was evaluated using Tl(I) generated at an amalgamated HMDE. Transfer of DOPC and gramicidin-DOPC monolayers onto the amalgamated HMDE from the air/solution interface was carried out and the collection of released Tl(I) across gramicidin at the Hg/Pt submarine electrode was achieved. Comparison of substrate (HMDE) generation – tip collection behavior of the bare amalgamated, DOPC and gramicidin-DOPC modified HMDE confirmed the selective transport of Tl(I) across gramicidin. Finally, an apparent heterogeneous rate constant for the transport of Tl(I) from the HMDE into the bulk was obtained.

To our knowledge, this is the first time that SECM has been used in an amperometric mode to control and monitor ion transport across ion channels. We plan to perform similar studies on living systems having complete phospholipid bilayers and biologically functional channels.

Supporting Information

The generation of Tl from a non-modified amalgam HMDE and collection experiments presented in Figure 5 are treated as a double potential step chronoamperometric problem. During the first potential step, a HgTl amalgam is formed by bulk electrolysis of a Tl(I) solution until the reversal time, τ, when the potential is

stepped to oxidize the amalgam back to Tl(I). The generated Tl(I) is then collected at the nearby UME.

The diffusion of Tl(0) in the mercury is identical to solution diffusion since the diffusion coefficients of both Tl(0) and Tl(I) are of the same order of magnitude. The concentration profile, $C_o(x,t)$, of Tl(I) generated at the HMDE is governed by spherical diffusion. However, the close spacing of the tip to the much larger HMDE and the time scale of the experiment allows an approximation of the diffusion of the generated Tl(I) as linear. From the theoretical treatment of the double potential step chronoamperometry problem, the concentration profile of the Tl(I) generated at the HMDE and subsequently collected at the UME is given by:[41]

$$\frac{C_o(x,t)}{C_o^*} = 1 - \left(\frac{1}{1+\xi\theta'}\right) erfc\left(\frac{x}{2\left[D_o t\right]^{1/2}}\right) + S_\tau(t)\left(\frac{\xi\theta''}{1+\varepsilon\theta''} + \frac{\xi\theta'}{1+\xi\theta'}\right) erfc\left(\frac{x}{2\left[D_o(t-\tau)\right]^{1/2}}\right) \quad \text{(A1)}$$

Where

D_o is the diffusion coefficient of Tl(I) in solution

x is the tip to substrate distance

t is the time at the start of the electrolysis step

$S_\tau(t)$ is a step function that is unity after reversal and zero before the reversal time

τ is the reversal time

$C_o^* = C_{Tl}(x,0)$, the bulk concentration of Tl(I) in solution before electrolysis

$\xi = \sqrt{(D_o/D_r)} \approx 1$

Since both diffusion coefficients are on the same order of magnitude

For $t < \tau$

$\theta' = C_{Tl}'(0,t)/C_{Tl,Hg}'(0,t)$, this ratio is very small

For $t > \tau$

θ"= C_{Tl}"(0,t)/ $C_{Tl,Hg}$"(0,t) , this ratio is very large

Based on the assumptions stated above, eq. A1 can then be reduced to

$$\frac{C_o(x,t)}{C_o^*} = erf\left(\frac{x}{2\left[D_o t\right]^{1/2}}\right) + erfc\left(\frac{x}{2\left[D_o(t-\tau)\right]^{1/2}}\right) \qquad \text{(A2)}$$

For the experimental times and distances studied in the generation-collection experiments, the error function argument in equation A2 is very small. The erf response represents only 5% of that of erfc and can be neglected, such that:

$$\frac{C_o(x,t)}{C_o^*} = erfc\left(\frac{x}{2\left[D_o(t-\tau)\right]^{1/2}}\right) \qquad \text{(A3)}$$

This yields eq. (4) in the text. The assumptions made do not hold strictly. At longer distance, as seen in Figure 5, the theoretical curve does not fit the experimental response well, although it does allow an adequate estimation of the tip to substrate distances in our experiments (Table 1). For experiments where the distances are larger, the erf term should be included.

References

[1] Kwak, J.; Bard, A. J. *Anal. Chem*. **1989**, *61*, 1221.

[2] Bard, A. J.; Fan, F.-R. F.; Kwak, J.; Lev, O. *Anal. Chem.* **1989**, *61*, 132.

[3] Davis, J. M.; Fan, F.-R. F.; Bard, A. J. *J. Electroanal. Chem. Interfacial Electrochem.* **1987**, *238*, 9.

[4] Bard, A. J.; Mirkin, M.V.; Eds.; *Scanning Electrochemical Microscopy*, Marcel Dekker Inc., New York, **2001**.

[5] Bard, A. J.; Denuault, G.; Friesner, R. A.; Dornblaser, B. C.; Tuckerman, L. S. *Anal. Chem.* **1991**, *63*, 282.

[6] Martin, R. D.; Unwin, P. R. *Anal. Chem.* **1998**, *70*, 276.

[7] Engstrom, R. C.; Weber, M.; Wunder, D. J.; Burgess, R.; Winquist, S. *Anal. Chem.* **1986,** *58*, 844.

[8] Engstrom, R. C.; Meaney, T.; Tople, R.; Wightman, R. M. *Anal. Chem.* **1987**, *59*, 2005.

[9] Engstrom, R. C.; Wightman, R. M.; Kristensen, E. W. *Anal. Chem.* **1988**, *60*, 652.

[10] Kranz, C.; Wittstock, G.; Wohlschläger, H.; Schuhmann,W. *Electrochim. Acta* **1997**, *42*, 3105.

[11] Wittstock, G.; Schuhmann, W. *Anal. Chem.* **1997**, *69*, 5059.

[12] Scott, E. R.; White, H. S.; Phipps, J. B. *J. Membrane Sci.* **1991,** *58*, 71.

[13] Macpherson, J. V.; Beeston, M. A.; Unwin, P. R.; Hughes, N. P.; Littlewood, D. *J. Chem. Soc. Faraday Trans*. **1995**, *91*, 1407.

[14] Scott, E. R.; Phipps, J. B.; White, H. S. *J. Invest. Derm.* **1995**, *104*, 142.

[15] Amemiya, S.; Bard, A. J. *Anal. Chem.* **2000**, *72*, 4940.

[16] Amemiya, S.; Ding, Z.; Zhou, J.; Bard, A. J. *Electro. Chem.*, **2000**, *483*, 7.

[17] Nelson, A. *Biophys. J.* **2001**, *80*, 2694.

[18] Miller, I. R.; Rishpon, J.; Tenenbaum, A. *Bioelectrochem. Bioenerg.* **1976**, *3*, 528.

[19] Nelson, A.; Auffret, N. *J. Electroanal. Chem.* **1988**, *244*, 99.

[20] Nelson, A.; Leermarkers, F. A. M. *J. Electroanal. Chem.* **1990**, *278*, 73.

[21] Nelson, A.; Bizzotto, D.; *Langmuir* **1999**, *15*, 7031.

[22] Woolley, G. A.; Wallace B. A. *J. Membrane Biol.* **1992**, *129*, 109.

[23] Hladky, S. B.; Haydon, D. A. *Curr. Topics Membr. Transport* **1984**, *21*, 327.

[24] Rueda, M.; Navarro, I.; Prado, C.; Silva, C. *J. Echem. Soc.* **2001**, *4*, E139.

[25] Ketchem, R. R.; Hu, W.; Cross, T. A.; *Science* **1993**, *261*, 1457.

[26] Ketchem, R. R.; Lee, K. C.; Huo, S.; Cross, T. A.; *J. Biomol. NMR* **1996**, *8*, 1.

[27] Mauzeroll, J.; Bard, A. J. in preparation.

[29] Nelson, A.; Benton, A. *J. Electroanal Chem.* **1986**, *202*, 253.

[30] Selzer, Y.; Mandler, D. *Anal. Chem.* **2000**, *72*, 2383.

[31] Arca, M.; Bard, A. J.; Horrocks, B. R.; Richards, T. C.; Treichel, D. A. *Analyst* **1994**, *119*, 719.

[32] Demaille, C.; Brust, M.; Tsionsky, M.; Bard, A. J. *Anal. Chem.* **1997**, *69*, 2323.

[36] Usui, S.; Yamasaki, T.; Simoiizaka, J. *J. Phys. Chem.* **1967**, *71(10)*, 3195.

[37] Mirkin, M.V.; Bard, A. J. *J. Electrochem. Soc.* **1992**, *139*, 3535.

[38] Bard, A. J.; Faulkner, L. R.; *Electrochemical Methods, 1st ed.*, John Wiley & Sons, New York, **1980**, 180.

[39] Bizzotto, D.; Nelson, A. *Langmuir* **1998**, *14*, 6269.

[40] Rueda, M.; Navarro, I.; Ramirez, G.; Prieto, F.; Prado, C.; Nelson, A. *Langmuir* **1999**, *15*, 3672.

[41] Wallace, B. A. *Annu. Rev. Biphys. Chem.* **1990**, *19*, 127.

[42] Killian, J. A.; *Biochim. Biphys. Acta* **1992**, *1113*, 391.

[43] Hu, W.; Lee, K. C.; Cross T. A. *Biochemistry* **1993**, *27*, 7035.

[44] Wallace, B. A. *Adv. Exp. Med. Biol.* **1996**, *398*, 607.

[45] Bard, A. J.; Faulkner, L. R.; *Electrochemical Methods, 2nd ed.*, John Wiley & Sons, New York, **2001**, 192.

[46] Carslaw, H. S.; Jaeger, J. C. *Conduction of Heat in Solids, 2nd ed.*, Clarendon Press, Oxford, **1959.**

[49] Becucci, L.; Moncelli, M. R.; Guidelli, R. *Biophys. J.* **2002**, *82*, 852.

[50] Amatore, C.; Savéant, J. M.; Tessier, D. *J. Elec. Anal.* **1983**, *147*, 39.

CHAPTER 3: SCANNING ELECTROCHEMICAL MICROSCOPY OF MENADIONE-GLUTATHIONE CONJUGATE EXPORT FROM YEAST CELLS

Introduction

The uptake of menadione (2-methylnaphthoquinone), which is toxic to yeast cells, and its expulsion as a glutathione complex was studied by scanning electrochemical microscopy (SECM). The menadione-glutathione conjugate was detected electrochemically following its synthesis and characterization. The progression of the reaction between menadione and glutathione, monitored by cyclic voltammetry electrochemically, correlated with the UV-Vis behavior. By incubating bulk yeast cells in menadione, the uptake of the menadione and the export of the conjugate from cells with time were measured. Similar experiments were performed on immobilized yeast cell aggregates stressed by a menadione solution. From the export of the menadione-glutathione conjugate detected at a ~1 μm diameter electrode held very near the cells, an apparent rate of uptake menadione by the cells was extracted and this event identified as the rate-determining process.

To probe the transport activity of cells, we use scanning electrochemical microscopy (SECM), a surface technique that allows one to detect electroactive ions or molecules that are transported from cells across membranes or ion channels into an outside solution. A complete description of the fundamental principles, theoretical treatment and applications of SECM has been reviewed elsewhere.[1] The transport rate for the detection of a detoxification product that is released from yeast cells, thiodione, when cells are stressed with menadione is studied.

Quinones are oxidants and electrophiles that are readily transported into cells where they retain their ability to redox cycle, impose oxidative stress and form covalent adducts with important cellular species. In vivo, quinone reduction to the semiquinone leads to the formation of reactive oxygen species (ROS) such as superoxide ion, peroxide, and hydroxyl radicals. The latter species is responsible for the quinone-related oxidative damage associated with DNA cleavage and cell growth arrest.[2] To cope with such stress, cells have enzymatic and non-enzymatic defenses. Glutathione (GSH) (L-γ-glutamyl-L-cysteinyl-glycine) is the major non-protein sulfhydryl compound present in cells.[3] It exhibits a protective role in cells via its antioxidant properties, by conjugation to harmful compounds and by chelation to heavy metals.[4] With quinones, GSH detoxifies cells by sacrificially undergoing nucleophilic addition to quinones to limit the irreversible modification of cellular macromolecules. The thioether conjugates (GS-X) can then be degraded to other substances[4] or actively removed from the intracellular media using an ATP-dependent GS-X pump. With thiodione, the GS-X remains intact and is transported into the extracellular media via the GS-X pump in cells[5,6] where it can be detected using SECM.

A detailed understanding of how oxidative stress affects organisms is also of interest because oxidative stress agents are used as drugs. For example, menadione is used as a component of drugs in the treatment of hypothrombinemia and as an anti-inflammatory agent.[7] Oxidative stress occurs because of (i) an increase in respiration, (ii) a transition from an anaerobic to aerobic growth environment, (iii) a decrease in antioxidant capacity or (iv) exposure to oxidants such as hydrogen peroxide or compounds (drugs or xenobiotics) that generate hydroxyl radicals.[8] Such events, increase ROS concentration in cells, alter the reduced to oxidized GSH ratio and cause the organism to defend itself. Some of the above examples are endogenous to cells and so all

organisms have developed mechanisms to protect their valuable cellular components against ROS. Thiolation has been proposed as one of these protective mechanisms to prevent irreversible modification of cysteine rich residues. A group of glutathione S-transferase (GSTs) enzymes use reduced GSH to generate large sets of thioether conjugates that are usually, but not always, used in the detoxification process.[9] In some instances, like that of menadione conjugation to GSH, the product is further activated by the conjugation and still capable of redox cycling.[10] Although the conjugation appears as a disadvantage, a priori, it is required for efficient excretion via GS-X pumps and in that respect is a detoxification pathway.[11]

The export of GSH conjugates from cells is ATP dependent and mediated by an integral membrane glycoprotein belonging to the multi-drug resistant protein (MRP) family. There are six isoforms of this pump in humans and numerous orthologs of it have been identified in other organisms such as yeast.[5] Such variety of MRPs in different systems prevents accumulation of GS-X in cells and shows the importance of these pumps in the final excretion of dangerous compounds. The main reason that studying the effect of oxidative stress on the organism and export processes via these GS-X pumps is interesting, is that resistance to the cytotoxic action of drugs have reported overexpression of both GSTs and the MRP proteins.[12,13]

Materials and Methods

2-METHYL- 3-GLUTATHIONYL-1,4-NAPHTHOQUINONE SYNTHESIS

2-methyl-3-glutathionyl-1,4-naphthoquinone (thiodione) was synthesized and recrystallized as previously reported.[14] Characterization of thiodione was achieved via elemental analysis and H-NMR. Characterization of thiodione was achieved via

elemental analysis (Exp: S, 7.12; C, 50.96; H, 5.55; N, 8.82; Calcd.: for $C_{21}H_{25}N_3O_9S$: S, 6.47; C, 50.90; H, 5.09; N, 8.48; Lit: S, 6.54; C, 51.32; H, 5.58; N, 8.50;) and H-NMR. The present elemental analysis deviated by 0.6% from the reported values that presented a 0.4% error to the theoretical prediction. From the H-NMR in deuterated water and dimethyl sulfoxide, formation of the conjugate and purification was confirmed by the disappearance of the δ(s, 6.881) peak assigned to the 3 position aromatic proton of the menadione parent constituent.

CHEMICALS AND SOLUTIONS

Menadione (Aldrich) was recrystallized from ethanol prior to use. Reduced GSH (Sigma) was used as received. 1 mM ferrocene methanol (Aldrich) in 0.1 M KCl was used to characterize the electrochemical behavior of electrodes prior to the experiments. All solutions were kept in glass containers previously washed overnight in saturated NaOH in EtOH, rinsed in water and air dried. The supporting electrolyte used in electrochemical experiments was a 0.01 M phosphate buffer, pH 7 containing 0.1 M KCl (Mallinckrodt AR, Paris, KY), which was sterilized in a UV reactor (Southern New England UV cie., Hamden, CT) for an hour and prior to all experiments. All solutions were prepared with Milli-Q (Millipore Corp., Bedford, MA) reagent water and degassed with Ar for 30 min prior to experiments.

CELL GROWTH AND SAMPLE PREPARATION

Saccharomyces Cerevisiae (strain day4, day4vac) were grown on rich media plates (10 g of Yeast extract (Fischer), 20 g of peptone (Fluka), 20g of dextrose (Fluka)

filtered after autoclaving, 20 g of agar (Fluka), 1 pellet of NaO H in an incubator at 37.5°C for three days.

To carry out the bulk yeast cell experiments, approximately 10^9 cells were transferred to an electrochemical cell containing degassed 0.5 mM menadione. This concentration was determined from successive dilution measurements on agar plates. A solution containing an unknown amount of yeast cells was used in the bulk experiments. To evaluate the concentration of living cells that contributed to the electrochemical signal, 50 μL aliquots of this solution were successively diluted in 10 mL of PBS buffer four times. Rich media plates were made and then plated with 200 μL aliquot of the different diluted solutions. Three sets of 5 plates were incubated for three days at 37.5°C and the number of colonies was counted. Only the plates with large number of isolated colonies were used for the concentration determination. The plates had to have well separated colonies that did not show any signs of discoloration. Since a colony comes from a single cell, the original concentration of cells in the solution used in the electrochemical experiments could be back-calculated. On average, 10^9 living cells contributed to the electrochemical current measured in the bulk cell experiments. Turbidity measurements were not used to determine concentrations because they are based on scattering of the cell wall and this does not differentiate between living and dead cells. The fact that such a large number of cells led to relatively small oxidation current implied that aggregate experiments would have to be made in small volumes to have any chance of detecting the thiodione export.

To attach the yeast cells to glass, the glass surface was cleaned overnight in 1% HCl, 70% ethanol and 29% water and then rinsed with water. The glass slides were dried in an oven at 110^{o}C while the glass bottom petri dishes (Delta T dishes, Bioptechs Inc. Butler, PA) were left to air dry. The glass surfaces were coated with a 10% poly-l-

lysine (Sigma Diagnostics, Inc., St. Louis, MO) solution for 5 min, after which they were thoroughly rinsed and dried in the oven at 60°C for 1 h. The 10% poly-l-lysine solution can be made in advance in all plastic containers, but must be stored in the refrigerator (up to three months) and allowed to warm up to room temperature prior to use. Yeast cells were then transferred to the phosphate buffer, stirred and poured over the poly-l-lysine treated glass petri dish or slides. The cell solution contacted the treated glass for 20 min and was drained, rinsed and dried. Fluorescence cytotoxicity experiments with 10 mM FUN1 fluorescent dye (Molecular Probes Inc., Eugene, OR) incubated 1 h in the dark confirmed that the immobilized cells were alive for several hours. FUN1 fluorescent dye was stored at -20°C. To observe fluorescence with FUN1 dye, a fluorescein filter set at 480 nm excitation was used and emission was observed above 530 nm. All pictures presented in this work used the same exposition time where the red and green channels had equal exposure time, no blue exposure time was necessary.

ELECTRODE FABRICATION

Ultramicroelectrodes (UMEs) (25 μm Pt) were used in the bulk yeast cell experiments. A detailed description of their fabrication and characterization is given elsewhere.[1] The yeast aggregate experiments used laser-pulled Pt UMEs as reported by Schuhmann et al.[15] The present work used Pt tips of 1 to 4 μm diameter, which were characterized by cyclic voltammetry and SECM. A 2 cm piece of annealed 25 μm Pt wire is placed at the center of a open ended quartz tube (inner diameter: 0.3 mm; outer diameter: 1.0 mm; length: 7.5 mm; Sutter Instrument, Co., Novato, CA) and positioned in a laser puller (P-2000 Sutter Instrument, Co., Novato, CA). To seal the quartz onto the Pt wire and pull it down, both a sealing and pulling program must be sequentially applied. Prior to sealing, two stoppers are positioned on the slays of the pusher to prevent any

application of tension on the quartz tube. The ends of the tube are connected to a pump and vacuum is maintained for 15-30 minutes prior to the sealing step. The quartz is melted onto the Pt wire by running the sealing program (*Heat*: 900; *Filament*: 5; *Velocity*: 100; *Delay*: 120; *Pull*: 1) five times for 50 s with 25 s rest periods in between each program run. During the last rest period, the vacuum is turned off, the pair of stoppers are removed and the pulling program (*Heat*: 875; *Filament*: 2; *Velocity*: 130; *Delay*: 150; *Pull*: 200) is run once. This pulls down the sealed Pt and quartz into two separated symmetric tips. The values for the heating/pulling program here are different from the ones published by Schuhmann et al. and are probably highly dependent on the age and condition of the laser puller used.

Good sealing and continuity of the Pt wire is observed under the microscope prior to making contact with small cupper wire and mercury. To deliver the mercury at the bottom of the seal tip, a custom made HPLC needle (SGE, Inc., Austin, TX) was required. The connected tip was then inserted into a larger glass tube (inner diameter: 1.5 mm; outer diameter: 3 mm; length: 35mm) to strengthen the tip and was sealed using 5 minute epoxy. The inner quartz tube should be parallel to the support tube. To expose the end of the tip and obtain the disk geometry, the fortified tip is wrapped in Teflon tape, placed in a rotating disk electrode set-up (Pine Instrument, Co., Grove City, PA) and rotated at 5000 rpm. A hard-drive, on which wet sand paper is taped, is then approached from below until it touches the tip (Figure 1b). Touching of the tip to the wet sand paper can be observed as an oscillation of the long quartz end. To obtain sub-micron tips, the touching step is critical and all following polishing attempts will slightly increase the diameter of the exposed Pt. On average, the RG obtained for these tips is between [10-20]. By rotating the hard drive, the glass sheet of the tip can be sharpened to reduce the RG value as seen in Figure 1a. Further polishing to improve electrochemical response can

be done using the same setup and micropolishing cloths or by hand. Using this protocol, 500 nm to 10 μm Pt tips can routinely be made (Figure 1c,d,e). Smaller tips have also been obtained but they are much more manipulator sensitive and it is difficult to rule out a recess geometry. Most tips (500 nm and above) are characterized by cyclic voltammetry and optical inspection but for precise shape characterization of smaller tips, theoretical fitting of the SECM feedback responses is necessary. For the purpose of the present work, tips on the order of a yeast cell (1-4 μm) were used.

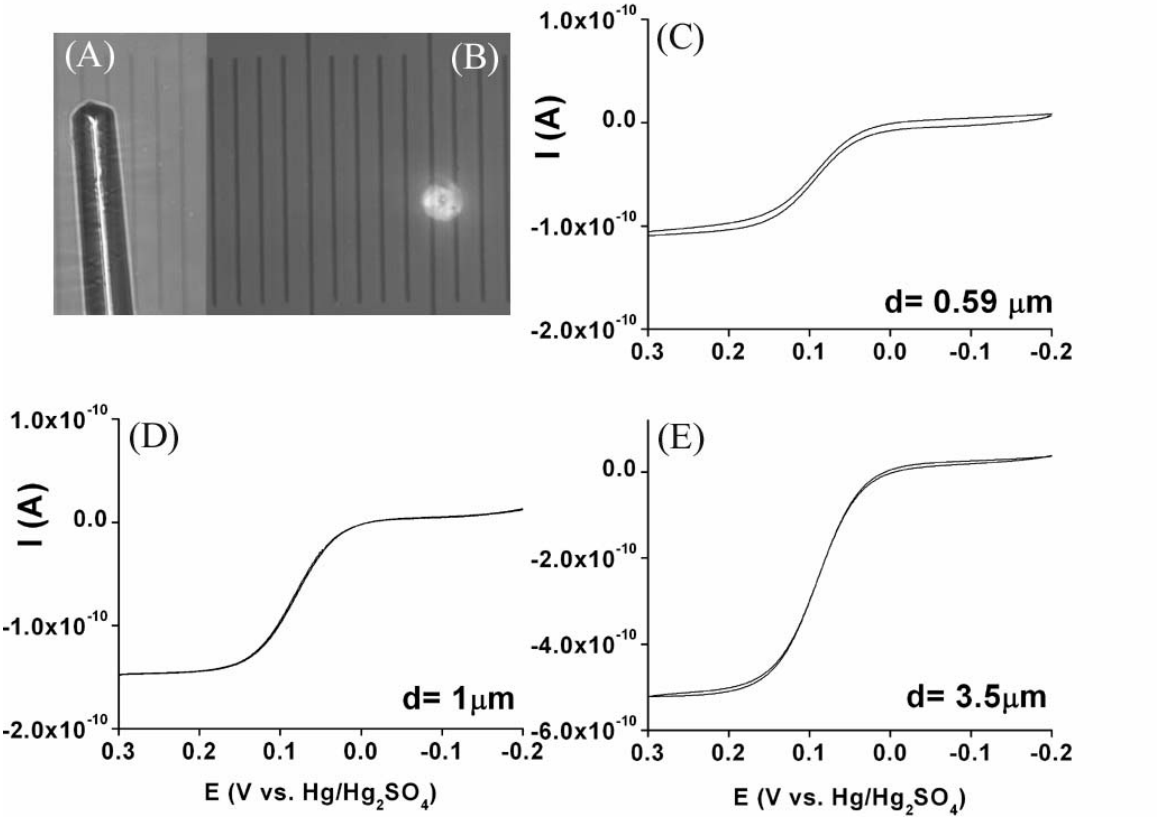

Figure 3.1: The smallest scale division represents 10 μm. (A) Side view of a sharpened laser pulled Pt UME. (B) Top view of an exposed and polished laser pulled Pt UME. (C), (D), (E) Voltammograms of 0.59, 1 and 3.5 μm, respectively, Pt diameter laser pulled UME in 1 mM ferrocene methanol solution in 0.1 M KCl electrolyte. The potential was measured versus a Hg/Hg_2SO_4 reference electrode and a 0.5 mm Pt wire was used as an auxiliary electrode. Argon was bubbled through the solution prior to the experiments.

A 0.5 mm Pt wire (Goodfellow, Cambridge, UK) and Hg/Hg_2SO_4 (Radiometer, Copenhagen, Denmark) electrode (SMSE) were used as counter and reference electrodes, respectively, in the bulk yeast experiments while in the aggregate experiments a Ag/AgCl coil reference electrode was used.

ELECTROCHEMISTRY

A CHI model 900 scanning electrochemical microscope (CH Instruments, Austin, TX) was used to control the tip potentials, obtain the approach curves and monitor the tip to substrate distance.

The electrochemical behavior of synthesized thiodione, the spontaneous reaction between menadione and reduced GSH and the bulk yeast cell experiment were monitored by cyclic voltammetry and used both conventional 25 μm and laser pulled Pt electrodes. The particular experimental parameters are given in the figure captions. The progression of the in situ reaction and the absorbance of the synthesized compound were confirmed by UV-Vis spectroscopy (Milton-Roy Spectronic 3000 array).

To perform the experiments on the immobilized yeast cell aggregates, the SECM head was placed on the stage of an inverted microscope (Eclipse TE300 Nikon Inverted Microscope, Melville, NY) to facilitate the tip positioning over the cells (Figure 2). The tip was first positioned in air over the yeast aggregates using the piezoelectric drivers of the SECM. The quartz tips are very flexible and do not break upon contact with the glass surface. The electrode was therefore approached in air until the tip was visually seen to touch a bare glass region. The tip was then retracted 10 μm away from the sample and positioned over an aggregate optically. The tip and fiber optic were held in the middle of a Ag/AgCl reference coil so that a 50 μL drop of menadione solution could be supported and would just contact the sample surface. These experiments were performed in a two

electrode setup since the currents are small when UMEs are used. The fiber optic was used to illuminate the sample and reduce the shadowing effect of the tip holder. Once positioned, a small drop of buffer was placed in the reference coil and a voltammogram was recorded. The drop was then aspirated out and replaced by a 50 µL drop of degassed menadione (0.1 mM). The cyclic voltammetry was immediately started. Cyclic voltammetry as a means of monitoring the cell processes was preferred to amperometry because both menadione uptake and thiodione export results could be obtained independently at different potentials.

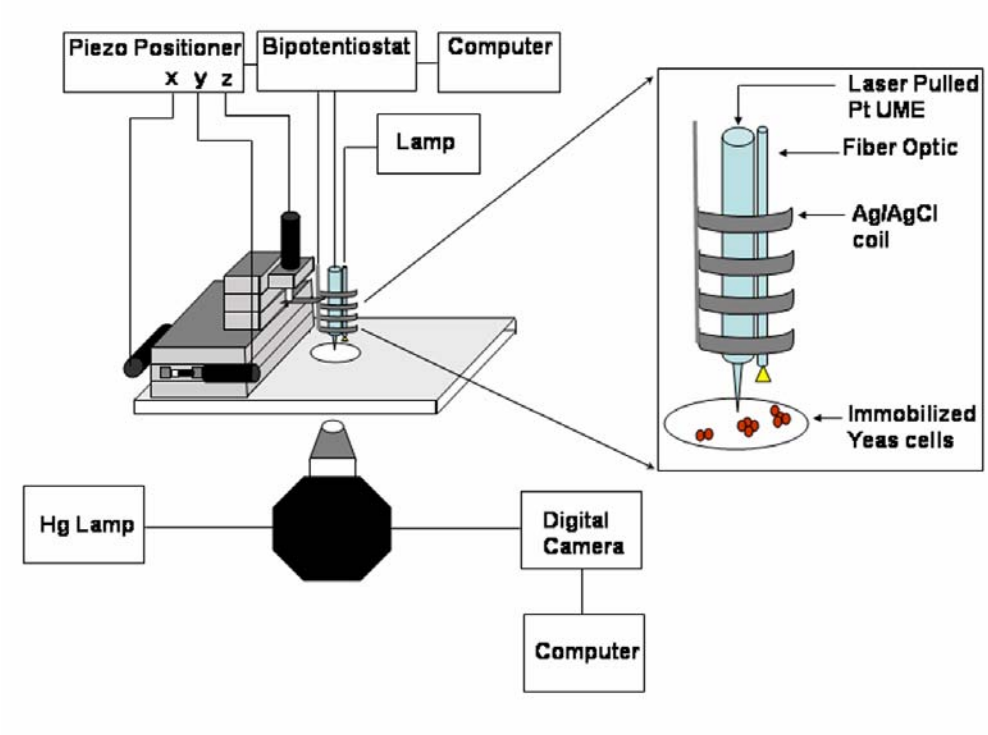

Figure 3.2: Experimental setup for the electrochemical detection of the export of thiodione from immobilized yeast aggregates using laser pulled Pt UMEs.

Results and Discussion

THIODIONE ELECTROCHEMISTRY

The voltammograms of menadione, reduced GSH and synthesized thiodione are presented in Figure 3A. The reduced GSH does not have any appreciable electrochemistry at Pt under these conditions whereas the menadione and thiodione both show a two-electron reduction of the quinone moiety at about –0.7 V vs. SMSE. The steady-state current for the thiodione is significantly smaller than that of the menadione at the same concentration because it is larger and has a smaller diffusion coefficient, 4×10^{-6} cm^2/s, vs. 8×10^{-6} cm^2/s for menadione. The thiodione reduction $E_{1/2}$ is about 15 mV more negative than that of menadione. This spacing is insufficient for clear differentiation between the two compounds using cyclic voltammetry. These results agree with previous studies that reported similar decreases in $E_{1/2}$ for thiodione versus menadione as measured by HPLC with electrochemical detection.[16]

The thiodione conjugate also shows an irreversible oxidation wave at about 0.1 V vs. SMSE (Figure 3B). In this potential region, neither menadione nor GSH give any electrochemical response. This allows one to analyze simultaneously for the conjugate and the combined menadione and thiodione by cyclic voltammetry (CV) during the spontaneous reaction of menadione and reduced GSH via the nucleophilic addition of the glutathionyl at the 3- position of the 2-methyl-1,4-naphthoquinone ring. Upon mixing equal molar amounts of menadione and reduced GSH, the oxidation wave increases with time until it levels off to a limiting current upon completion. Using the synthesized compound, the steady-state current was shown to be proportional to the concentration (Figure 3C).

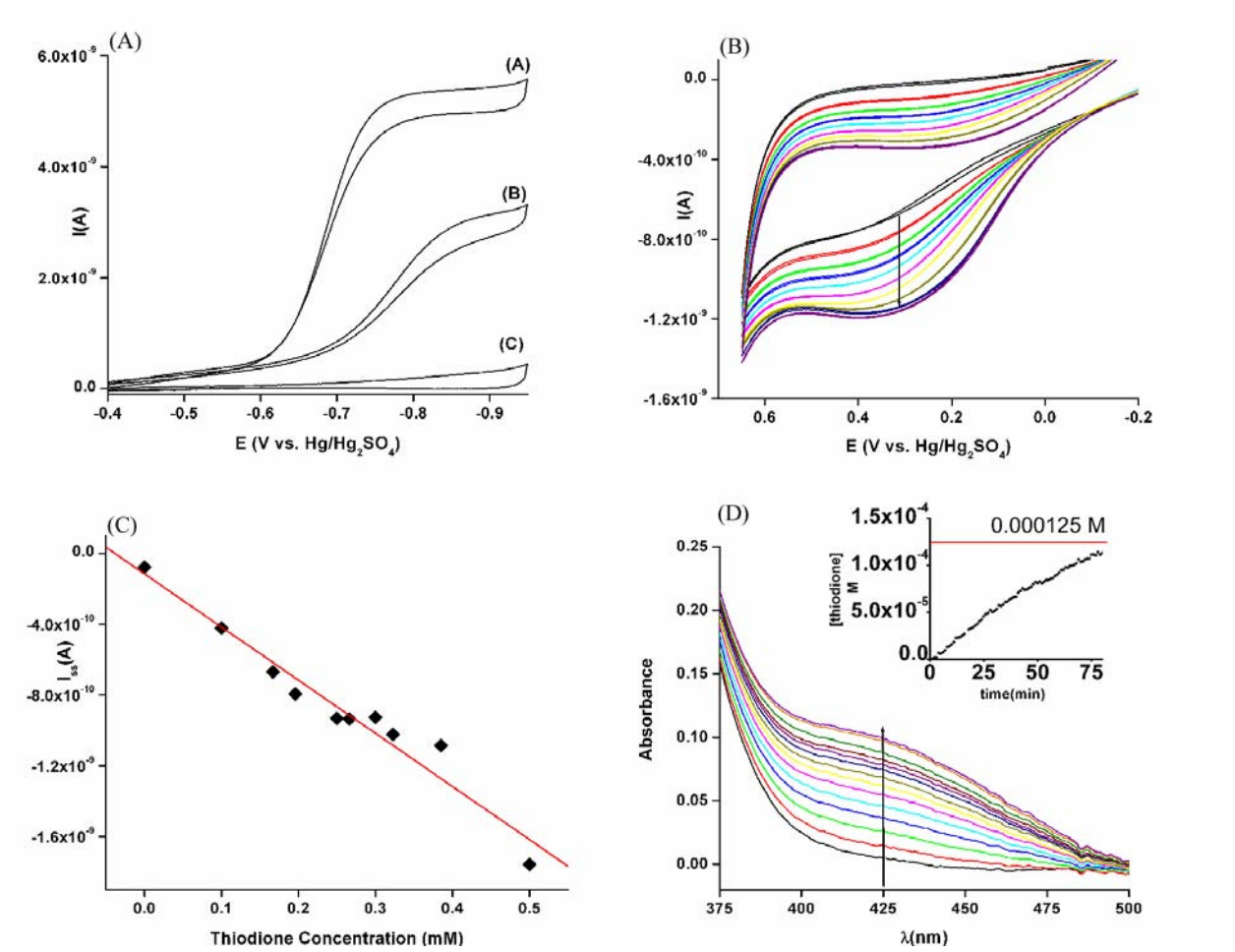

Figure 3.3: (A) Voltammetric response of (A) 0.5 mM menadione, (B) 0.5 mM synthesized thiodione and (C) 0.5 mM reduced GSH. (B) Oxidation wave for the formation of thiodione with time. Equal molar amounts of menadione (0.25 mM) and reduced GSH (0.25 mM) spontaneously react to form thiodione. The limiting current of the oxidation wave becomes larger with time until the reaction is complete. (C) Calibration curve for the synthesized thiodione; oxidation current vs. concentration of thiodione. The responses (A,B,C) were obtained in PBS pH=7, the potential was measured with respect to Hg/Hg_2SO_4 and the scan rate was 50 mV/s. Argon was bubbled through all solutions for 30 min and a 0.5 mm Pt auxiliary electrode was used. (D) Appearance of a broad shoulder at 425 nm during thiodione formation. Equimolar amounts of menadione (0.125mM) and reduced GSH (0.125mM) in PBS pH=7 electrolyte spontaneously reacted to form thiodione. As thiodione is formed, the absorbance at 425 nm increased. Inset, the calculated concentration of thiodione increase with time.

The mechanism of this oxidation has yet to be elucidated but is probably an irreversible oxidation of the sulfide to the sulfoxide, based on previous reports of the electrochemistry of similar sulfur containing compounds.[17] From H-NMR data (both in water and dimethyl sulfoxide), the electrochemistry at large electrodes (data not shown) and previously reported studies,[18] it does appear that the menadione glutathione conjugate remains in the oxidized form following the conjugation reaction.

The formation of thiodione was also monitored by UV-Vis spectrophotometry of the solution at different times during the conjugation reaction and confirms the reported growth of a broad shoulder at 425 nm (Figure 3D).[11] The concentration of thiodione increased with time until completion and the final concentration observed was very close to 0.125 mM, the expected yield calculated from the initial concentrations (Figure 3D inset). The spontaneous reaction between menadione and reduced GSH is slow with a half life of the reaction, $t_{1/2}$, of 36 min. This long reaction time supports the idea that in cells, the conjugation is enzyme assisted in organisms, consistent with studies showing that GSTs catalyze the formation of GS-X in Saccharomyces Cerevisiae.[9,19]

BULK YEAST CELL EXPERIMENTS

About 10^9 cells in 2 mL of 0.5 mM menadione solution were used to detect the export of thiodione from yeast cells. Menadione readily diffuses into the cells where it conjugates with intracellular GSH and is either exported or sequestered via the yeast orthologue of the MRP pump in the extracellular medium or in the vacuole respectively.[4,19,20,21,22] Export of thiodione to the extracellular medium can be detected with a 25 μm Pt electrode immersed in the solution.

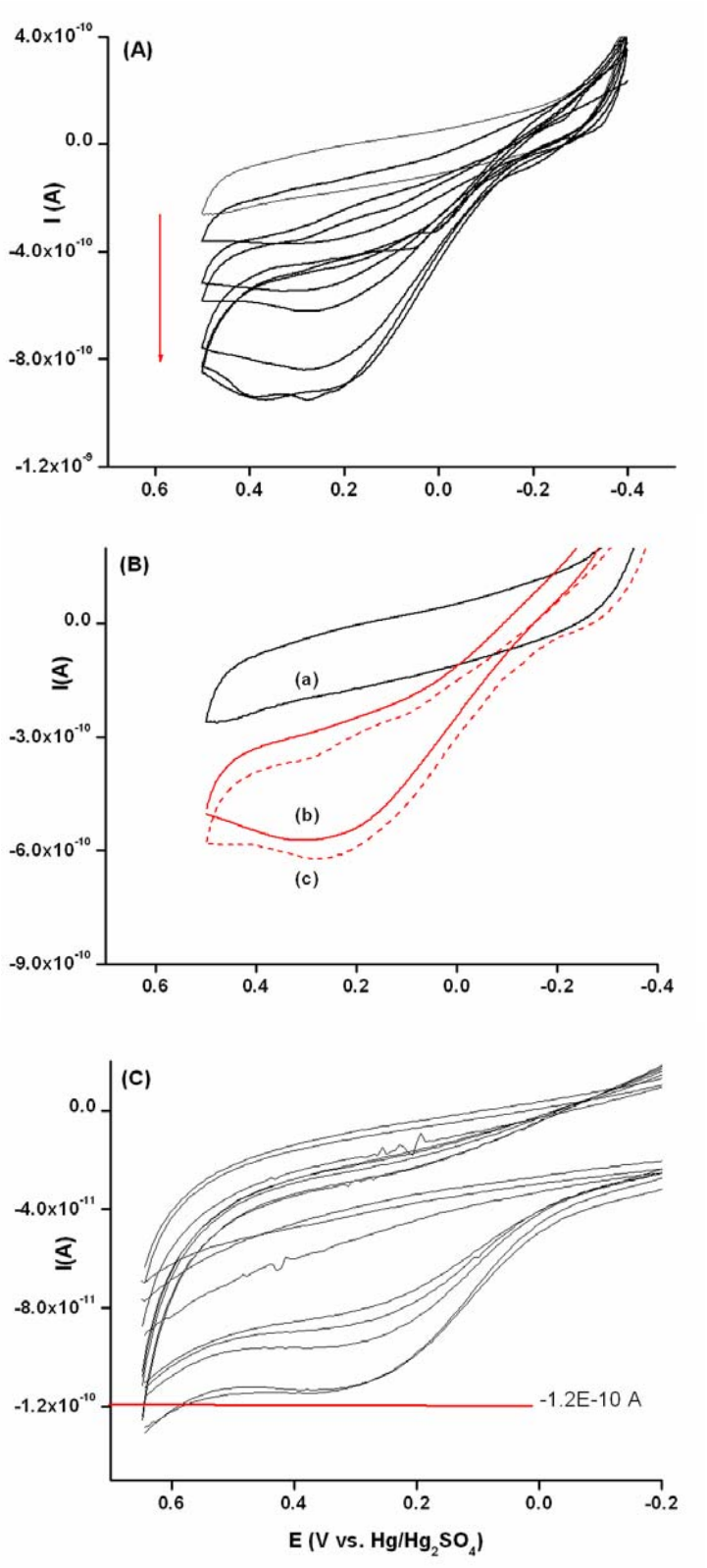
(A)
4.0x10^-10
0.0
I (A)
-4.0x10^-10
-8.0x10^-10
-1.2x10^-9
0.6
0.4
0.2
0.0
-0.2
-0.4
(B)
0.0
I(A)
-3.0x10^-10
-6.0x10^-10
-9.0x10^-10
(a)
(b)
(c)
(C)
-4.0x10^-11
-8.0x10^-11
-1.2x10^-10
-1.2E-10 A
E (V vs. Hg/Hg2SO4)

Figure 3.4: (A) Electrochemical detection of thiodione exported from bulk DAY4 yeast cells at a 25 μm Pt electrode. Approximately 10^9 cells were treated with 0.5 mM menadione in PBS pH=7 electrolyte. The potential was cycled between -0.95 and 0.5 V at 10 mV/s. The wave height increased with time until it reached a steady-state value. (B) Comparison of the oxidation response at a 25 μm Pt electrode for PBS pH=7 buffer (a) to that of the synthesized thiodione (b) and that recorded from the bulk DAY4 yeast cells. (C) Electrochemical detection of the formation of thiodione at a 4 μm Pt UME from the spontaneous reaction of menadione (0.25 mM) and reduced GSH (0.25 mM) in PBS pH=7.4 solution. The red line represents the expected steady-state current value for 100% completion reaction. The potential was cycled between -0.95 and 0.5 V at 50 mV/s. All potentials (A,B,C) were measured with respect to a Hg/Hg_2SO_4 electrode, and a 0.5 mm Pt auxiliary electrode was used. All solutions were degassed with Ar for 30 min.

The voltammogram shows the growth of the anodic thiodione wave with time at the same potential as that seen in the thiodione synthesis experiment (Figure 4A and B). This confirms the electrochemical detection of the conjugate exported from yeast cells as a result of menadione imposed oxidative stress. Similar bulk cell experiments and the in-situ reaction of menadione and GSH were also carried out with smaller laser pulled 4 μm tips. As seen in Figure 4C, the limiting current obtained upon completion of the reaction is almost identical to that calculated from the initial concentrations of reagents. To obtain good quantitative results with the small UME, the solution had to be degassed and a large potential sweep was required. The large potential sweep was useful in desorbing material from the electrode surface and insured good quantitative results. This was also needed to measure the menadione signal in later experiments.

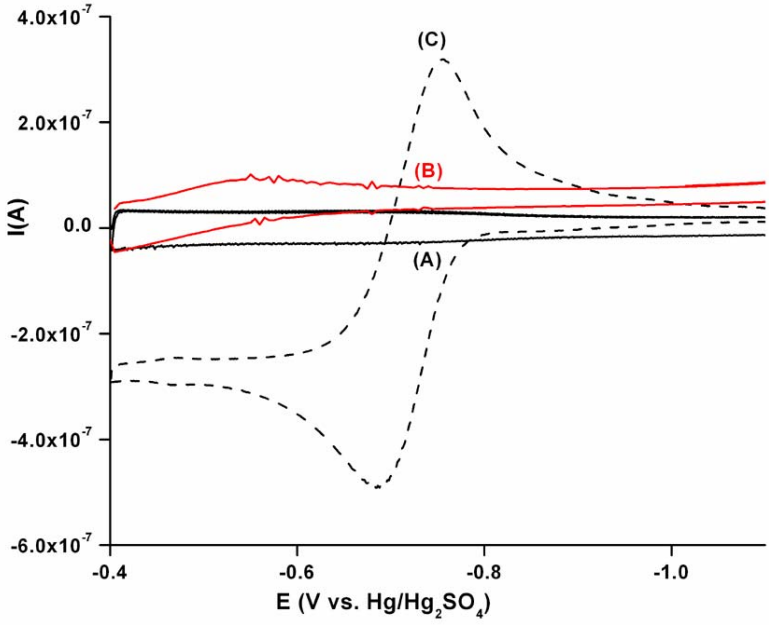

Figure 3.5: Electrochemical detection of reduced GSH at a HMDE (area, A= 0.0139 ± 0.0003 cm^2). Voltammograms of the HMDE for (A) PBS pH=6.97 electrolyte (B) over DAY4 yeast cells left soaking in the PBS for 1 h in a 2 mL volume and (C) in a 0.5 mM reduced GSH solution. The response was obtained between -1.8 and -0.4 V at 50 mV/s. The solutions were previously bubbled with Ar for 30 min. The potentials are reported versus Hg/Hg_2SO_4 electrode and a 0.5 mm Pt wire was used as an auxiliary electrode.

Studies have suggested that GSH itself might be released from cells via the ATP-dependent low affinity transport YCF1 transporter.[20] The amounts of extracellular GSH, used as a signaling molecule, in this instance, is reported as 0.2% of the intracellular concentration of reduced GSH that is normally between 1-10 mM. Any appreciable amounts of reduced GSH exported during the present measurements would spontaneously react with the extracellular menadione and contaminate the response observed. Using a hanging mercury drop electrode (HMDE) and mercury hemispherical electrodes,[25] we repeated the bulk yeast cell experiments in the absence of extracellular

menadione. GSH alone in a PBS solution gives a well-defined quasi-reversible oxidation signal at low concentrations (Figure 5). At higher concentrations, adsorption processes dominate and alter the response.[26] In presence of bulk cells neither the HMDE nor the hemispherical mercury UMEs were able to detect any significant amount of reduced GSH coming from the cell over a time period of hours. This lack of detection was not due to electrode fouling, since at the end of these experiments an aliquot of known GSH concentration was added and a good electrochemical response was observed. If there is any GSH exported, the amounts are sufficiently small that they do not significantly affect the detection of the export of the conjugate.

YEAST CELL AGGREGATE EXPERIMENT

Under physiological conditions, Saccharomyces Cerevisiae cells have a negatively charged cell surface.[27] The yeast cell surface macromolecules, like mannoproteins and glucan, have phosphodiesters; amino and carboxyl groups that regulate the charge of the cell to aid in adhesion processes.[28] Yeast cells can therefore be immobilized on glass supports that have been pretreated with poly-l-lysine. The immobilized cells remain alive for several hours as confirmed by fluorescence studies performed with FUN1 viability dye (Figure 6A,B) which identified the proper dose of menadione (0.1 mM) to be used and documented the effect of the microscope Hg lamp exposure on the cell viability.

The thiodione export from 100 cells is presented in Figure 6C, D. As can be seen at 0.35 V, the thiodione signal increased and then leveled off. If significant evaporation of the solution were taking place, the signal would not have leveled off but would have kept increasing.

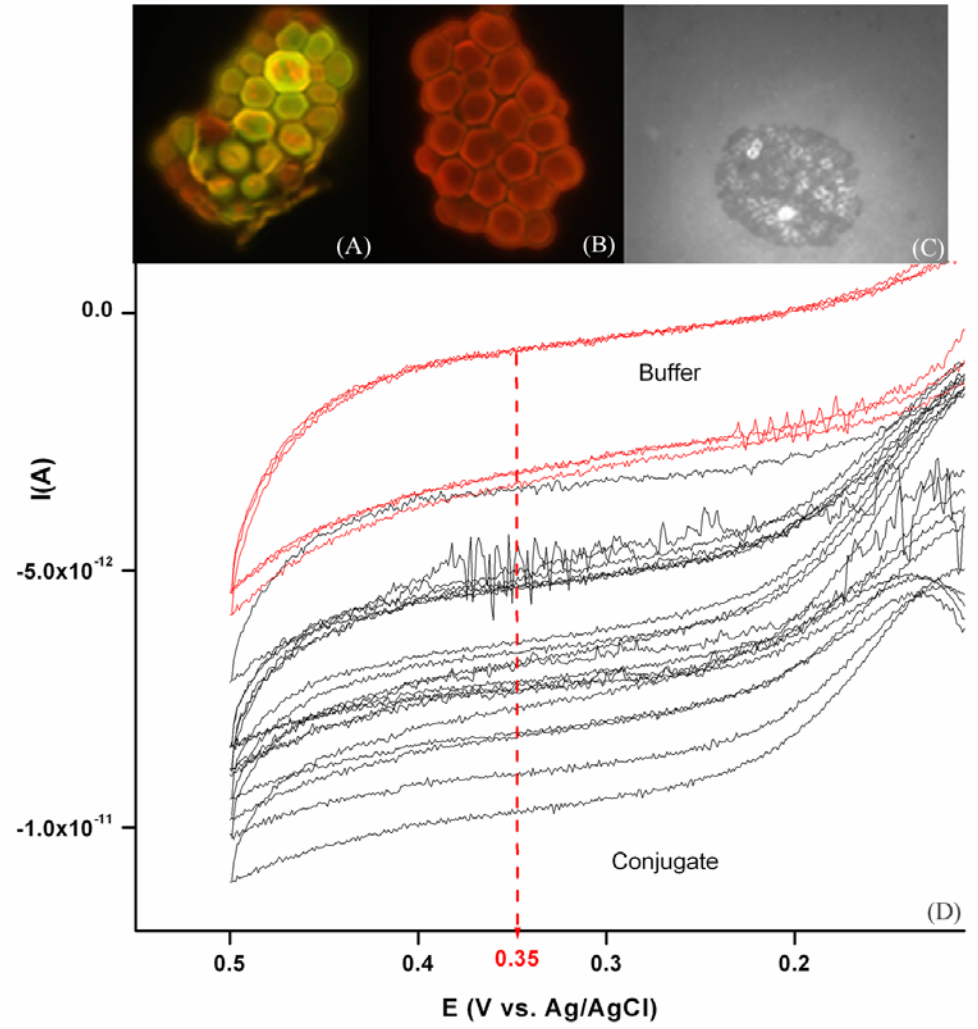

Figure 3.6: (A) Positive control of living immobilized DAY4 yeast cells on glass. The cells were treated with 10 mM FUN1 dye for 1 h incubation time. The living cells metabolize the dye, to produce diffuse green fluorescence in the cytosol and red cylindrical features. (B) Negative control of living immobilized DAY4 yeast cells on glass. The immobilized cells were incubated in the UV reactor for 1 h. The dead cells do not metabolize the dye and produce diffuse red fluorescence with no features. (C) Optical micrograph of the 4 µm Pt wire from the tip (bright spot) over the immobilized aggregate of cells prior to the start of the collection experiment. The tip was10 µm away from the glass surface. (D) Collection of exported thiodione from the immobilized aggregate of DAY4 yeast cells following the imposition of oxidative stress by 50 µL of 0.1 mM menadione. The response was collected between -0.5 to 0.5 V at a 20 mV/s. The potential was recorded with respect to a Ag/AgCl electrode coil in a two electrode configuration.

Similarities between these results and that of the bulk cell experiments suggest that the immobilization process does not significantly hinder the export dynamics. Figure 6C shows the simultaneous optical micrograph of the 4 μm tip over the yeast cell aggregate. The current at 0.35 V was measured and plotted versus time in Figure 7C. The general behavior of conjugate export is consistent with the behavior observed in other studies that looked at efflux of thiodione from rat platelet-rich plasma using a HPLC-UV-Vis detection scheme.[7]

THEORETICAL MODEL

A theoretical model (Figure 7a) was used to identify the slow rate-determining process of the experiment presented in Figure 6. The concentration profile of menadione with time can be monitored at -0.5 V vs. Ag/AgCl. The steady-state current,

$$I_{ss} = 4nFDC_o a \qquad (1)$$

where I_{ss} is the steady-state current, n is the number of electrons, F is the Faraday constant, D is the diffusion coefficient, a is the radius of the Pt disk, and C_0 is the concentration of electroactive species, can be used to obtain the concentration of menadione at the tip with time (Figure 7b). The concentration of menadione follows a first order exponential decay. An apparent first order rate constant of 5×10^{-3} s^{-1} for the uptake of menadione is obtained. The response at long times does not go to zero because of the added contribution of the conjugate export as shown in Figure 3A(B). The contribution of the conjugate, because of the much lower concentration exported, does not significantly affect the menadione signal. This value is a first approximation of the rate of uptake of menadione. If this is the slow dominant process, the value extracted

from the detection of thiodione should be consistent with the one extracted independently from the menadione signal.

Inside the cell, the menadione (M_i) is rapidly conjugated to reduced glutathione (G) and is converted to thiodione (MG_i) via the action of GSTs.[9] Similar studies based on rat hepatocytes also confirm that the formation of the conjugate, once menadione is inside the cell, was rapid as opposed to the slow spontaneous solution reaction between menadione and reduced GSH that has a 36 min half life.[29] Also, platelet-rich plasma studies in rats showed that as much menadione is consumed by conjugation as is taken up by the cells using HPLC with absorbance measurements.[7]

Once conjugated, thiodione is rapidly exported into the extracellular medium (MG_o) at an assumed first order rate (k_i) using the GS-X pump. Any vacuolar sequestration is neglected since it would only affect the magnitude of the response and not its shape. An expression for the concentration profile of MG_o with time can be derived. The particulars of the model are presented in a diagram, Figure 7a. The electrode is positioned 10 μm away from the substrate. Initially a solution of menadione (M_o) is added to impose oxidative stress to the cells. Menadione readily diffuses into the cells at a rate that is assumed to be of the first order (k_o). Inside the cell, the menadione (M_i) quickly conjugates to reduced glutathione (G) and is converted to thiodione (MG_i). Once conjugated, thiodione is rapidly exported out into the extracellular media (MG_o) at an assumed first order rate (k_i) using the GS-X pump. The vacuolar sequestration is neglected since it would only affect the magnitude of the response and not its shape.

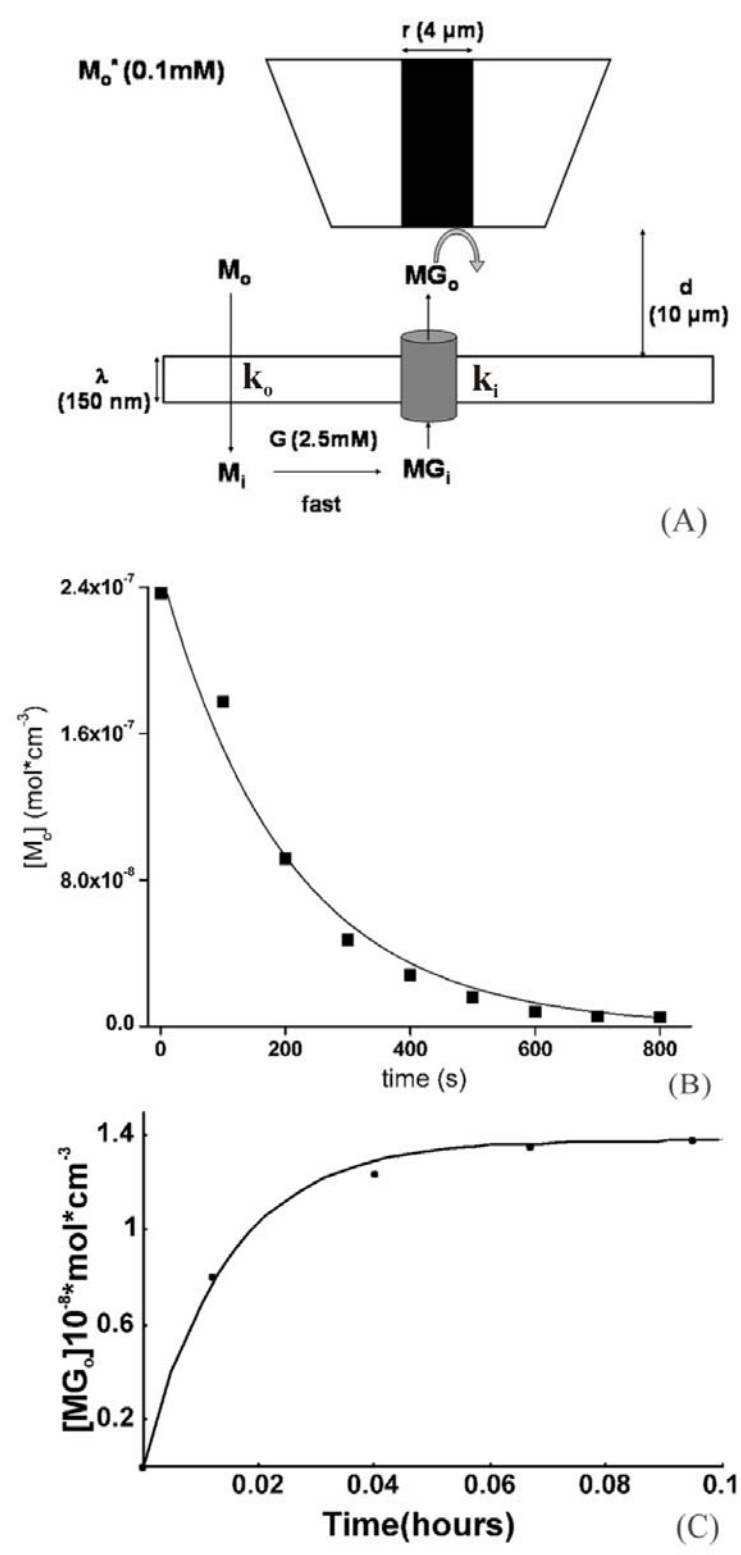
r (4 µm)
M_o^* (0.1mM)
M_o
MG_o
d
(10 µm)
λ
(150 nm)
k_o
k_i
G (2.5mM)
M_i
MG_i
fast
(A)
2.4x10^{-7}
1.6x10^{-7}
8.0x10^{-8}
0.0
[M_c] (mol*cm^{-3})
0
200
400
600
800
time (s)
(B)
1.4
1
0.6
0.2
[MG_o]10^{-8}*mol*cm^{-3}
0.02
0.04
0.06
0.08
0.1
Time(hours)
(C)

Figure 3.7: (A) Schematic representation of the theoretical model used to treat the immobilized aggregate collection experiments. The model was applied to a 4 μm Pt UME, 10 μm away from the glass surface and in presence of 0.1 mM bulk concentration of menadione (M_o*). The menadione (M_o) diffuses through the cell wall and membrane with time at the assumed first order rate k_i (s^{-1}). Once inside, the menadione (M_i) rapidly conjugates with intracellular reduced glutathione (G =2.5 mM). The intracellular thiodione (MG_i) is then pumped out of the cell via the GS-X analog pump at an assumed first order rate k_o (s^{-1}). The expelled thiodione (MG_o) is then detected at the UME with time. The diffusion time from the cells to the tip is neglected. (B) Uptake of menadione with time. The concentration was calculated from the menadione current at -0.5 V vs. Ag/AgCl. This is a two electron process at a 2 μm radius Pt UME and a diffusion coefficient of 4 x 10^{-6} cm^2/s was used. An apparent rate of uptake of menadione of 5 (±0.6) x 10^{-3} s^{-1} was obtained.(C) Fit of the appearance of menadione with time for the immobilized aggregate experiments. The concentration was obtained from the steady-state current at 0.35 V vs. Ag/AgCl and used a diffusion coefficient of 8 x 10^{-6} cm^2/s. The concentration profiles with time were fit to eq. 7. From the fit, the apparent rate of uptake of menadione is in the range 0.6 x 10^{-3} to 30 x 10^{-3} s^{-1}. The uptake of menadione is the rate-determining step in this experiment and the rate of export through the pump was too fast to be measured.

An expression for the concentration profile of MG_o with time can be derived:

$$d[MG_o]/dt = k_i[MG_i] \quad (2)$$

$$d[MG_i]/dt = k_o[M_o] - k_i[MG_i] \quad (3)$$

$$d[M_o]/dt = -k_o[M_o] \quad (4)$$

From Figure 7b in the article, we know experimentally that $M_o = Ce^{-k_o t}$ such that

$$d[MG_i]/dt = k_o Ce^{-k_o t} - k_i[MG_i] \quad (5)$$

For $[MG_i]_{t=0} = 0$ as initial condition, the concentration of thiodione inside the cell with time is:

$$[MG_i] = \frac{e^{-k_i t}\left(\frac{k_i k_o C}{-k_i + k_o} - \frac{k_o{}^2 C}{-k_i + k_o} + k_o C e^{(k_i - k_o)t}\right)}{k_o - k_i} \qquad (6)$$

Substituting eq. (6) in eq. (2) and solving the differential equation using $[MG_o]_{t=0} = 0$ as initial condition,

$$[MG_o] = C + \frac{C}{k_i - k_o}\left(k_o e^{-k_i t} - kie^{-k_o t}\right) \qquad (7)$$

where C is a concentration term related to how much menadione is taken up, k_o is the assumed first order rate constant for the export of thiodione across the pump, k_i first order rate constant for the diffusional uptake of menadione and t is the time. Equation (6) and (7) were solved using Mathematica software.

The profiles fitted to eq. 2 yield values for the uptake of menadione in the range of 0.6 x 10^{-3} s^{-1} to 30 x 10^{-3} s^{-1}. The large range occurs because of the small number of points collected in the rise time of the signal. Nevertheless, this range is close to that found for the uptake of menadione (5 (±0.6) x 10^{-3} s^{-1}) and confirms that the uptake of menadione is the slow rate-determining process in this experiment. This means that menadione slowly diffuses into the cell and that is followed by rapid conjugation with reduced glutathione which is rapidly pumped out of the cell. No value for k_i could be extracted from the data.

That the uptake of menadione is the slow step is not surprising when one considers that the uptake is a diffusional process, while the export of thiodione is assisted by the GS-X pump. The uptake of menadione cannot be compared to the uptake of menadione by mammalian cells since the yeast cell envelope is thicker and quite different. The composition, organization and porosity of the yeast cell envelopes is a very complex problem that has been studied for many years.[30,31] The cell envelope, that would include the cell wall, slime layer and plasma membrane, has been reported to have a thickness of 70 (± 15),[32] 90,[33,34] and 150[35] nm. All of these are very thick compared to mammalian cells that have a membrane thickness around 10 nm. Furthermore, crossing the envelope from the extracellular to the intracellular medium implies diffusing through stratified layers of densely packed glycosylated mannoproteins that are linked by β1,6 glucan to the inner wall composed mainly of a β1,3 glucan-chitin complex and across the plasma membrane. Finally, the porosity of the cells is not fixed and varies with many different parameters, such as the environmental conditions and cell age.[36] By performing similar measurements on mammalian cells that would allow, perhaps, a less hindered transport across the membrane, it may be possible to quantify the rate of export of thiodione across the GS-X pump. Also, in these larger systems, imaging of the export process at the cellular level would be possible.

By comparing Figure 7b and 7c, we find that the concentration of conjugate exported is 42% lower than the initial concentration of menadione taken up by the cells. Yeast cells can use an internal vacuole as a sequestration zone for toxic compounds.[19,21] Also, Saccharomyces Cerevisiae have the orthologue of MRP that mediates ATP dependent transport of GS-X through the vacuolar membrane.[20] A fraction of the formed conjugate could thus be sequestered in the vacuoles and decrease the overall concentration available for export. Bulk experiments with vacuolar deficient DAY4[37]

mutants were attempted to see if increase export could be observed. In these experiments, thiodione export was observed (data not shown) but aggregate experiments were not successful due to the small size of these mutants compared to the wild type strain. To improve the model, development of a numerical simulation for biological systems responding to menadione oxidative stress is underway.

Conclusions

Thiodione can be identified and detected electrochemically in a solution of the synthesized compound made by reaction of menadione and reduced GSH. It can also be detected when exported from a bulk yeast cell suspension and from small yeast cell aggregates exposed to menadione. The electrochemical detection of thiodione was corroborated by UV-vis studies. From a theoretical treatment, an apparent first order rate constant range for the uptake of menadione was extracted that identified this process as the slow dominant process. The pumping of thiodione following conjugation is rapid and a rate constant for this process could not be determined. The model used oversimplifies the complexity of this system and efforts are currently underway to develop numerical simulations that would more accurately describe the system.

Ongoing work in this group is now focusing on human liver cells that are larger (20-45 μm diameter) and have a thinner membrane than the yeast cells. Also, imaging of the export process at the cellular level would then be possible.

References

[1] Bard, A. J.; Mirkin, M. V.; Eds.; *Scanning Electrochemical Microscopy,* Marcel Dekker, Inc., New York, **2001.**

[2] Monks, T. J.; Lau, S. S. *Annu. Rev. Pharmacol. Toxicol*. **1998,** *38*, 229.

[3] Reed, D. J.; Meredith, M. J. in *Bioactivation of Foreign Compounds*, M.W. Anders, Ed., Orlando Academic Press, **1985,** 71.

[4] Foyer, C. H.; Theodoulou, F. L.; Delrot, S. *Trends in Plant Sci*. **2001,** *16*, 486.

[5] Keppler, D. *Free Rad. Bio. & Med*. **1999,** *27*, 985.

[6] Sies, H. *Free Rad. Bio. & Med*. **1999,** *27*, 916.

[7] Chung, J.-H.; Seo, D.-C.; Chung, S.-H.; Lee, J.-Y.; Seung, S.-A. *Toxicol. & Appl. Pharm.* **1997,** *142*, 378.

[8] Costa, V.; Moradas-Ferreira, P. *Mol. Asp. of Med*. **2001,** *22*, 217.

[9] Sies, H.; Ketterer, B. in *Glutathione Conjugation. Mechanisms & Biological Significance,* Eds., Academic Press, London, **1988.**

[10] Monks, T. J.; Lau, S. S. *Chem. Res. Toxicol*. **1997,** *10*, 1296.

[11] Zadiński, R.; Fortuniak, A.; Biliński, T.; Grey, M.; Bartosz, G. *Biochem. & Mol. Bio. Int.* **1998,** *44*, 747.

[12] Morrow, C. S.; Smitherman, P.D.; Townsend, A. J. *Biochem. Parmacol*. **1998,** *56,* 1013.

[13] Morrow, C. S.; Smitherman, P. K.; Diah, S. K.; Schneider, E.; Townsend, A. J. *J. Biol. Chem*. **1998,** *273*, 20114.

[14] Nickerson, W. J.; Falcone, G.; Strauss, G. *Biochemistry* **1963,** *2*, 537.

[15] Katemann, B. B.; Schuhmann, W. *Electroanalysis* **2002,** *14*, 22.

[16] Buffington, G. D.; Öllinger, K.; Brunmark, A.; Cadenas, E. *Biochem. J.* **1989,** *257*, 561.

[17] Chambers, J. Q. in *Encyclopedia of Electrochemistry of the Elements XII*, Eds., Bard, A. J.; Lund, H.; Marcel Dekker, Inc., New York, **1978,** 453.

[18] Lau, S. S.; Jones, T. W.; Highet, R. J.; Hill, B. A.; Monks, T. J. *Toxi. & App. Pharm.* **1990,** *104*, 334.

[19] Penninckx, M. *Enzyme and Microbial Technology* **2000,** *26*, 737.

[20] Rebbeor, J. F.; Connolly, G. C.; Dumont, M. E.; Ballatori, N. *J. Bio. Chem*. **1998,** 273, 33449.

[21] Li, Z.-S.; Szczypka, M.; Lu, Y. P.; Thiele, D. J.; Rea, P. A. *J. Bio. Chem*. **1996,** *271*, 6509.

[22] Falcón-Pérez, J. M.; Mazón, M. J.; Molano, J.; Eraso, P. *J. Bio. Chem*. **1999,** *274*, 23584.

[25] Mauzeroll, J.; Hueske, E. A.; Bard, A. J. *Anal. Chem*., **2003,** *75*, 3880.

[26] Jin, W.; Zhao, X.; Xia, L. *Electroanalysis* **2000,** *12*, 858.

[27] Ahimou, F.; Denis, F. A.; Touhami, A.; Dufrêne, Y. F. *Langmuir* **2002,** *18*, 9937.

[28] Eddy, A. A.; Rudin, A. D. *Proc. R. Soc. London, B*. **1958,** *149*, 419.

[29] Di Monte, D.; Ross, D.; Bellomo, G.; Eklöw, L.; Orrenius, S. *Arch. of Biochem. & Biophys.* **1984,** *235*, 334.

[30] Lipke, P. N.; Ovalle, R. *J. Bacteriol*. **1998,** *180*, 3735.

[31] Bacon, J. S. D. in *Yeast Cell Eenvelops: Biochemistry, Biophysics, and Ultrastructures,* Eds., Boca Raton, FL., **1981**, 65.

[32] Srinorakutara, T. *J. Ferment. Bioeng*. **1998,** *86*, 253.

[33] Smith, A. E.; Zhang Z.; Thomas, C. R.; Moxham, K. E.; Middelberg, A. P. J. *PNAS*, **2000,** *97*, 9871.

[34] Smith, A. E.; Moxham, K. E.; Middelberg, A. P. J. *Chem. Eng. Sci*. **2000,** *55*, 2031.

[35] Yamaguchi, M.; Biswas, S. K.; Suzuki, Y.; Furukawa, H.; Takeo, K. *FEMS Microbiology Letters* **2003,** *219*, 17.

[36] De Nobel, J. G.; Klis, F. M.; Munnik, T.; Priem, J.; Van den Ende, H. *Yeast* **1990,** *6*, 483.

[37] Chan, S. Y.; Appling, D. R. *JBC* **2003,** in press.

CHAPTER 4: MENADIONE TOXICITY STUDY ON HEPATOBLASTOMA HEP G2 CELLS USING SCANNING ELECTROCHEMICAL MICROSCOPY

Introduction

The cytotoxicity of menadione on hepatocytes was studied using the tip collection mode of scanning electrochemical microscopy (SECM). Hepatocyte exposure to cytotoxic concentrations of menadione results in an oxidative stress response similar to that of adriamycin®, a widely used chemotherapy agent, that ultimately leads to cell death. The menadione-S-glutathione conjugate (thiodione) is formed during the cellular detoxification process and is expelled from the cell by an ATP-dependent pump. This efflux is directly detected electrochemically and allows for SECM studies of single and groups of live cells.

MENADIONE: A MODEL SYSTEM FOR ADRIAMYCIN®

Menadione has been used in numerous oxidative stress studies because it readily generates reactive oxygen species (ROS) that can damage the cell. The mechanism by which the menadione generates the ROS is assumed to be via the one electron reduction of the quinone to the semiquinone. The semiquinone is autooxidized under aerobic condition back to the quinone. The byproducts of this reaction are ROS such as superoxides, oxygen radical anions and, most damaging, the hydroxyl radical. The cytotoxicity of menadione and adriamycin® (doxorubicin hydrochloride) are related to the formation of such radicals that eventually cause DNA damage that leads to cell death. The cell defends itself against these toxicants. Menadione mimics the toxicity of adriamycin® and its cellular metabolite, thiodione, can easily be detected

electrochemically as discussed in Chapter 3. Similar substitution of adriamycin® by menadione in cytotoxicity studies of the same cell line have previously been reported.[1] In subsequent work, it was also shown that following stepwise increases in menadione exposure, cells developed a resistance to concentrations of menadione that would have been otherwise toxic to them.[2]

RELATIONSHIP BETWEEN MULTIDRUG RESISTANCE AND GLUTATHIONE CONJUGATE TRANSPORT

One of the main problems in chemotherapy treatment is the development of multidrug resistance (MDR). MDR implies that prolonged transient exposure of a drug-sensitive cell to a drug can lead to the development of a resistance to a wide range of structurally distinct drugs. Classically, this is characterized by cross-resistance to four classes of commonly used drugs: anthracyclines, *Vinca* alkaloids, taxanes and epipodophyllotoxins. MDR is, for example, observed in H69AR cells, small cell lung cancer, which displays high levels of resistance to the *Vinca* alkaloids, epipodophyllotoxins, doxorubicin, mitoxantrone and other drugs following repeated transient exposure to doxorubicin.[3] This resistance reduces drug accumulation in tumor cells and increases drug efflux into the extracellular media.

To date, there are only two proteins known to cause such MDR phenotype: P glycoprotein (Pgp) and the multidrug resistance proteins (MRP). Pgp and MRP are distinct members of the ABC superfamily of transporters whose numerous members are responsible for transport across biological membranes of ions, phospholipids, steroids, polysaccharides, amino acids and peptides.[4] Although the structures of the two proteins are similar, there is only 15% amino acid homology between the two and most of this homology is contained in the nucleotide binding domain responsible for the binding and

consumption of ATP required for transport.[5] Detailed review of the structure of the transmembrane protein is available.[3]

MRP overexpression has been shown to accompany MDR in tumor cells of many types.[5,6,7,8,9,10] This is most interesting because MRP members are organic anion transporters that transport anionic drugs, like methotrexate, as well as neutral drugs and compounds that are conjugated to acidic ligands, such as reduced glutathione (GSH), glucuronate and sulfate. These proteins can also facilitate the transport of neutral drugs that are not conjugated to glutathione but co-transported with glutathione.[11] The effect of glutathione on these pumps is still under debate. Some report that transport requires conjugation to the substrate,[12,12] or that GSH might be co-transported with the drugs,[12] or finally, that GSH is an activator of the pump that leads to a structural change.[13] What is clear is that GSH is required for the proper function of the transport pumps. This statement is supported by studies that have shown that simultaneous increases in MRP1 and γ-glutamylcysteine synthetase, the rate limiting enzyme in the GSH biosynthetic pathway, is observed in tumor cells.[14,15] Studies that used buthionine sulphoximide (BSO), an irreversible inhibitor of γ-glutamylcysteine synthetase, have shown that the MDR can be reversed and allow for some renewed drug accumulation.[16]

The wide substrate selectivity of the MRP members is in line with the idea that these pumps are involved in the detoxification and development of MRD to a wide variety of xenobiotics and drugs. This has lead to considerable study of these systems and hence a varied nomenclature is used to describe the same system as tabulated below:

TABLE 4.1: The human multidrug resistance protein (MRP) family and other reported nomenclature for individual members.

MRP Members	Other Reported Nomenclature*
MRP1	ABCC1, MRP & GS-X PUMP
MRP2	ABCC2, cMOAT, cMRP & GS-X PUMP
MRP3	ABCC3, MOAT-D & cMOAT-2
MRP4	ABCC4 & MOAT-B
MRP5	ABCC5, MOAT-C & pABC11
MRP6	ABCC6, MOAT-E, MLP-1 & ARA
MRP7	ABCC10

This table is adapted from a recent review.[17] The ABCC refers to the C group of the ABC (adenosine triphosphate-binding cassette) transporter nomenclature originating by the work of Allikmets et al.;[18] MOAT stands for multispecific organic anion transporter and the c implies canalicular localization;[19] pABC11 comes from McAleer et al.;[20] ARA stands for anthracycline resistant associated;[21] The GS-X stands for the glutathione-S-conjugate pump and was not in the original reported table.

The glutathione-S-conjugate (GS-X) pump description is elusive and has always been presented in terms of a third step in the xenobiotic detoxification process of cells while the MRP in terms of observed MDR phenotype. Clearly, the two systems are interrelated and although it did not figure into the originally reported table, it is known that MRP1 and MRP2 are two of the GS-X pumps.[12,22,23]

STUDIED SYSTEM: HEPATOBLASTOMA HEP G2 CELL LINE

In hepatocytes, there are three members of the MRP present: MRP1-3. Much debate has gone on about the function of each member and its localization in the membrane but no one study is unequivocal. Considering the detoxification pathway used in the menadione imposed oxidative stress, one or more of these transporter proteins probably will be used for expulsion of thiodione. Although menadione is transported into

the cell through the membrane by passive diffusion, the thiodione is too hydrophilic to be transported by passive diffusion and requires the use of an ATP-dependent pump. The challenge of this work will be to see if anything can be said that is biologically relevant to these transport proteins based on the SECM results.

There are different in vitro systems that could have been chosen. The most complete system is the isolated perfused liver but the complications, time constraints for the experiment (3-4 h) and restriction in the number of experiments possible on a single liver are limiting. This system would also not be convenient for SECM experiments. Freshly isolated hepatocytes, immortalized cell lines from a malignant source, inside-out plasma membrane vesicles, and precision cut-liver slices are other possible systems that are commonly used in the literature.[19] Care must be taken in inferring biological significance from the conclusions obtained from these model systems and this should be kept in mind here.

In our study, hepatoblastoma Hep G2 cell line was used. These cells are well differentiated such that they retain specific hepatic functions such as albumin and bile acid synthesis.[24,25] In monolayer cultures bile caniculus-like structures, apical vacuoles, can be observed optically and uptake of fluorescent glutathione conjugates into these structures has been reported.[26,27] Since they originate from a malignant source, they express high levels of three of the MRP members including the MRP1 member, whose expression level is usually extremely low in normal hepatocytes.[28,28]

Aside from being a biologically relevant model, Hep G2 cells readily grow and strongly adhere to plastic dishes. They do not require the use of a sticking agent such as poly-l-lysine, used in Chapter 3. Hep G2 cells also have easily observable changes in morphology that are indicative the cell's viability. The cells maintain an irregular shape

while healthy but upon toxic conditions, they lose their shape and their adherence to the bottom of the dish.

OBJECTIVES

The purpose of this work was to study the cytotoxic effects of menadione on hepatocytes. Menadione is a model system of adriamycin®-like toxicity, is directly detectable electrochemically and allows for full cell SECM studies that do not require the use of specific monoclonal fluorescent antibodies or the use of inside-out vesicles.

The benefits of using SECM for biological systems have been outlined in Chapter 3. Here, the SG-TC mode of SECM was used to detect the efflux of thiodione from differentiated and isolated Hep G2 cells. Thiodione is actively exported out of the cells by a glutathione-S-conjugate pump following the application of oxidative stress by menadione on the hepatocytes. The location of the efflux of thiodione from the cells could be imaged by SECM and time profiles of the export can also be obtained. We could detect an efflux of thiodione from both isolated and differentiated cells following exposure to a cytotoxic concentration of menadione. This concentration was determined via a neutral red viability assay.

Materials and Methods

CHEMICALS AND SOLUTIONS

Menadione (Aldrich) was recrystallized from ethanol prior to use. 1 mM ferrocene methanol (Aldrich) in 0.1 M KCl was used to characterize the electrochemical behavior of the electrodes prior to experiments. All solutions were kept in glass containers previously washed overnight in saturated NaOH in EtOH, rinsed in water and

air dried. The supporting electrolyte used in cell experiments was a 0.1 M KCl solution buffered with a 1:1 molar ratio of NaH_2PO_4/Na_2HPO_4 of total concentration 0.01 M at pH 7 (Mallinckrodt AR, Paris, KY). This buffer was sterilized in the UV reactor (Southern New England UV cie., Hamden, CT) for an hour and prior to all experiments. All solutions were prepared with Milli-Q (Millipore Corp., Bedford, MA) reagent water, and degassed with Ar for 30 min prior to experiments. The washing buffer solution and menadione solution were always warmed to 37.5°C in a water bath prior to any contact with the cells.

CELL GROWTH AND SAMPLE PREPARATION

The Hep G2 liver cells (ATTC, Manassas, VA) were grown in Eagle's Minimum Essential Medium (ATTC, Manassas, VA) modified to contain: 0.1 mM sodium pyruvate, 0.1 mM non-essential amino acids and 1.5 g/L of sodium bicarbonate. The medium was supplemented by 10% fetal bovine serum (Atlanta Biology) and grown at 37.5°C in a water jacket incubator (VWR Int., model 2310, Cornelius, OR) at 5% CO_2. The growth media was changed biweekly. The cells were grown until they were above 75% confluency and were then used in the SECM experiments. The growth medium was removed and replaced by a simple PBS buffer pH= 7.4 at 37.5°C.

NEUTRAL RED CYTOTOXICITY ASSAY

This assay is a cell viability test based on the uptake and binding of a water soluble weakly cationic dye. Neutral red, 3-amino-7-dimethylamino-2-methyl-phenazine hydrochloride, (NR) yields a deep red color at slightly acidic pH. A detailed description of this viability assay has been reported elsewhere.[29,30] NR readily diffuses through the

plasma membrane and concentrates in the lyposomes where it binds electrostatically with the anionic sites. Toxic compounds that alter the cell surface or disturb the lysosome membrane, reduce or prevent the uptake of NR by the lyposomes. Toxicity of a compound results in a decrease in NR binding to the lyposome matrix. This decreases the absorbance of a well with respect to the control well and measures the overall loss of viability of the studied cells. In this work, the assay was mainly used to identify a concentration of menadione that is toxic to the Hep G2 cells over a reasonable time frame such that the SECM experiments can be performed.

Assay solutions: A stock solution of NR (8.7 mM) is prepared in nanopure water. The solution is filter sterilized, wrapped in foil and stored in the refrigerator. On the morning of the assay, the stock solution is diluted fifty fold in Dulbecco's Modified Eagle's Medium (DMEM). The solution is wrapped in foil and kept in the CO_2 incubator at 37.5°C. A washing-fixation solution must also be made and contains 1% formaldehyde, 1% $CaCl_2$ in nanopure water. The extraction solution contains 1% glacial acetic acid in 50% ethanol solution.

Protocol: Monolayer cultured Hep G2 cells cultured in 24-well tissue culture plates are exposed to different concentrations of menadiones such that three replicates of each concentration are obtained. Each well is treated with the known concentration of menadione dissolved in 1 mL of DMEM. The cells are then left in the water jacket incubator (37.5°C, 5% CO_2) for one hour. After 30 min, optical inspection is made to insure that the dose is not so elevated as to have killed off the cells. Changes in morphology, such as the loss of irregular shape of the cells or the loss of adhesion to the Petri dish, are all indications that the dose used is too high.

At the end of menadione incubation, the 24-well plate is turned over onto absorbent paper and 2 mL of 37.5°C DMEM is added to each well to wash the cells. The 24-well plate is then emptied and blotted. 1 mL of NR stock solution (37.5°C) is added from the upper row to the bottom row. The plates are then incubated (37.5°C, 5% CO_2) for 1 h after which the NR solution is removed by turning and blotting. The cells are washed with 1 mL of the washing solution to remove the excess NR solution. This step must not take more than 25 s. The solution is then stirred for 20 s and the contents of the wells are turned and blotted on absorbent paper. Finally, 1 mL of the extraction solution is added to each well using an Ependorf pipette. The plate is wrapped in foil and incubated at room temperature for 15 min. After 3 repetitive pipetting of each well to insure thorough mixing of the extraction solution in the wells, the content of the wells is transferred to a 1 mL plastic cuvette. The control reference is the extraction solvent. The absorbance of all wells, including the control well, is taken at 540 nm. The cell viability is then expressed as the percent ratio of the absorbance of the wells to that of the control well that had a zero menadione concentration. This assay was performed for 5, 10, 20, 40 and 80 μM menadione for cells having confluencies between 75 to 100%. Viability is expressed as the percentage of the absorbance at 540 nm from the non-treated cells and is averaged over the number of replicates made.

ELECTRODE FABRICATION

Ultramicroelectrodes (UMEs) (10 μm Pt) were used in the experiments. A detailed description of their fabrication and behavior are described elsewhere.[31] 0.5 mm Pt wire (Goodfellow, Cambridge, UK) and Hg/Hg_2SO_4 (Radiometer, Copenhagen, Denmark) electrodes were used as counter and reference electrodes, respectively.

ELECTROCHEMISTRY

A CHI model 900 scanning electrochemical microscope (CH Instruments, Austin, TX) was used to control the tip potentials, obtain the approach curves and monitor the tip to substrate distance.

SECM CYCLIC VOLTAMMETRY EXPERIMENTS

To perform the experiments on the immobilized cells, the SECM head had to be combined with an inverted microscope (Eclipse TE300 Nikon Inverted Microscope, Melville, NY) to facilitate the tip positioning over the cells (Figure 1). The tip was first positioned in air over the PBS moist cells using the piezo-electric drivers of the SECM. These experiments were performed in a three electrode setup. A side home-built halogen lamp source was necessary to reduce the shadowing effect of the tip holder and to help observe the Hep G2 cells. Once positioned, 1 mL of degassed menadione (80 μM) at 37.5°C solution is added. The cyclic voltammetry (CV) at the tip is then immediately started with a time delay of less than 5 s. The particular applied potential regime, scan rate solutions accompany the figures themselves. At the end of the CV experiment, an insulating approach curve was recorded using the menadione reduction as the redox couple to evaluate the true tip to substrate distance.

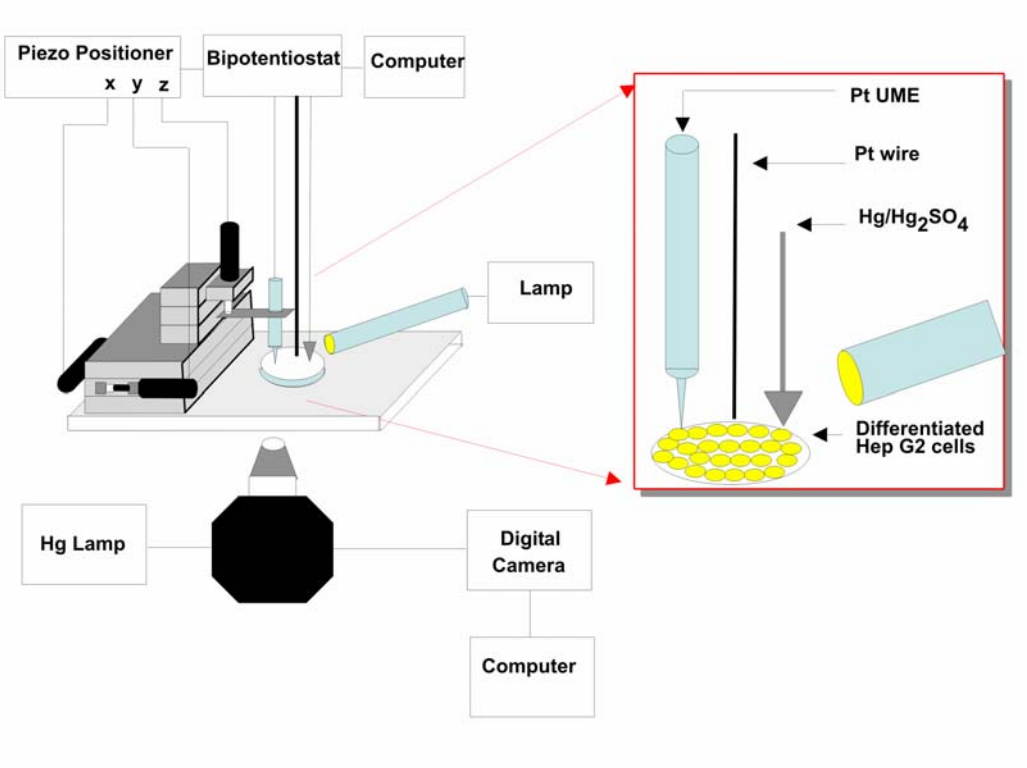

Figure 4.1: Experimental setup used in the SECM measurements of human liver cells. The SECM head is attached to the inverted microscope. The top illumination column could not be used and a side lamp was added to the setup to assist in the acquisition of clear optical images of the liver cells.

SECM IMAGING EXPERIMENTS

For the SECM imaging experiments, the cells were put in contact with the menadione solution and then the tip was approached to the dish using menadione reduction as a redox reaction at the tip. Once within a diameter distance of the substrate, the tip was moved over in a region where live isolated cells were present. The approach and positioning of the tip prior to the acquisition of the image usually required 10 minutes. Since the images were acquired in the constant height mode, the tip was never approached much closer than 5 μm since this usually led to a removal of the adhered cells by the tip upon scanning. A SECM image of the export of the conjugate was then

recorded with an x-y scan over several hundred microns by poising the tip at the thiodione oxidation potential. All imaging experiments were performed within the 1 h time limit as indicated by the cytotoxicity experiments.

Results and Discussion

CYTOTOXICITY EXPERIMENTS

Figure 2A, shows effect of menadione concentration for a 30 min exposure on the Hep G2 cell viability. These measurements were performed several times on cells 75% confluent or more. The dose response appears linear and has an intercept (100.014 ± 0.007) almost identical to the expected 100% viability at zero menadione concentration. The slope of the dose response is measured as -0.272 ±0.006% viability/μM of menadione and presents good linearity (R^2=0.9991). These results are in line with other cytotoxicity studies on Hep G2 cells with menadione that reported a concentration dependent decrease in cell viability based on Tryptan Blue exclusion.[1]

For the purposes of our experiments, 80 μM menadione was used such that a detectable signal can be measured from the cells. As seen in Figure 2B, the experiments have to be performed within one hour or less to maintain cell viability. It was also possible to observe morphological changes in cells as they died. The cells lost their irregular shape and became round and no longer adhered to the bottom of the Petri dish.

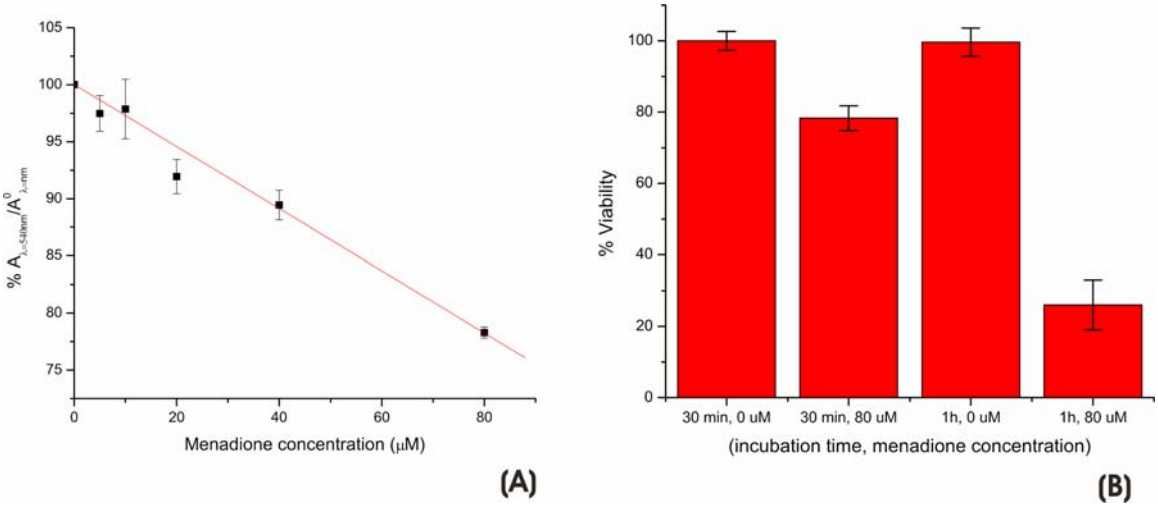

Figure 4.2: Neutral Red assay results for cells of 75% or more confluency. (A) Viability of Hep G2 cells with varying menadione concentration applied to the cells for a 30 min incubation time. The values represent three independent measurements where three replicates of each concentration studied were taken. (B) Histogram of the effect of exposure time of 80 μM menadione on the viability of the Hep G2 cells. The values are representative of three replicates.

COLLECTION EXPERIMENTS ON DIFFERENTIATED CELLS

Menadione readily diffuses into the Hep G2 cells upon addition of 80 μM of menadione to the extracellular media. This purely diffusional menadione transport has been reported for many different cell types, such as yeast,[32] human breast cells[33] and rhodobacter sphaeroides,[34] and can be attributed to the ambiphilic nature of menadione. Menadione is hydrophilic enough to be soluble in water and has sufficient hydrophobic character to be soluble in the plasma membrane without the help of any transport protein or pumps. This ambiphilic character is the reason why quinones are so toxic to cells that cannot prevent their uptake. Some of the most widely prescribed chemotherapeutic drugs for a wide range of malignancies such as adriamycin® and daunorubicin are anthraquinones that capitalize on this easy transport into cells.[35]

Once inside the cell, menadione retains the ability to redox cycle and therefore generates ROS that can damage the cell. As discussed in the previous chapter, intracellular glutathione binds to menadione via nucleophilic addition and forms a stable conjugate. The loss of viability of Hep G2 cells from the exposure to menadione is always preceded by a rapid depletion of intracellular GSH.[1] This decrease in intracellular GSH occurs because of the conjugation of GSH to menadione and also from the oxidation of the GSH to the disulfide dimer (GSSG) from the products of the oxidative stress.[36]

Thiodione is more hydrophilic than menadione and can no longer simply diffuse through the plasma membrane. Good experimental evidence to support this is the lack of uptake of the conjugate by rat platelets.[37] Thiodione is very stable and also redox cycles to form ROS and therefore must be actively removed from the intracellular space via glutathione-S conjugate pump. Once expelled into the extracellular space, thiodione diffuses to a probe electrode 300 μm away from the cells and poised at the oxidation potential for the conjugate. The 10 μm Pt probe electrode detects the exported thiodione using CV and records an increasingly anodic steady-state wave with time (Figure 3A). The time profile of this increasing anodic current is shown in Figure 3B.

Because this experiment is detecting a growing concentration profile, it is very sensitive to any small convection events that disrupt the profile. Such an event was seen during the experiment as shown by the black square results in Figure 3B. This was corrected by eliminating the point at 560 s and translating the remainder of the points upwards as seen in the red tracing. These types of experiments are considered as transient experiments and contain all the kinetic information for the export of the conjugate via the pump. Efforts are presently underway to model these transient responses using numerical simulation to extract the apparent rate of export of thiodione across the pump.

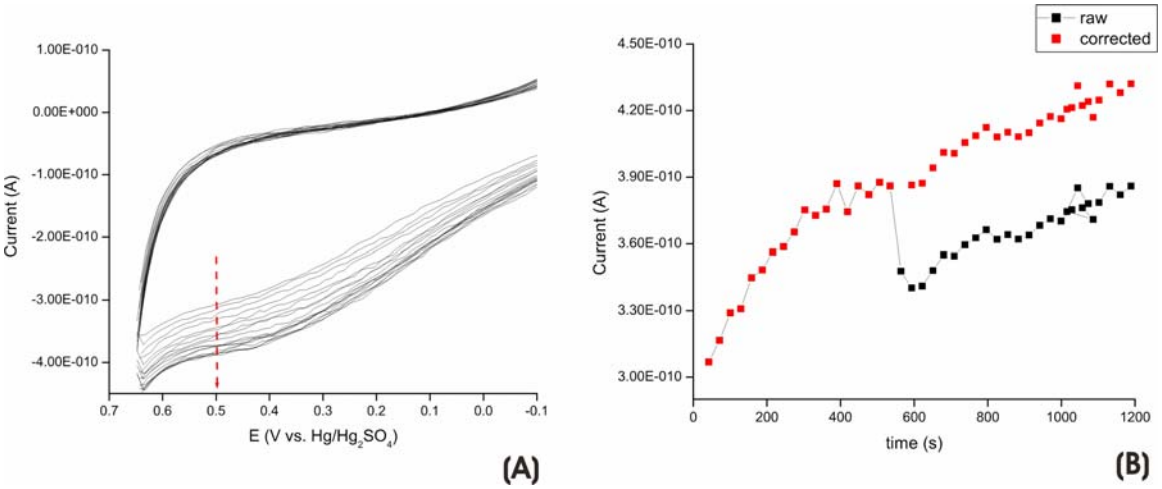

Figure 4.3: Electrochemical detection of thiodione from differentiated Hep G2 cells. (A) Voltammogram of thiodione detection with time. The potential was scanned from -0.8 to 0.65 V vs. Hg/Hg_2SO_4 at a scan rate of 100 mV/s in degassed 37.5°C PBS buffer. The signal was recorded at a 10 µm Pt UME. (B) The steady-state current of the voltammogram in A plotted versus the calculated time. The tip to substrate distance in this measurement was large and can be assumed to be representative of a bulk solution measurement.

SINGLE CELL IMAGING OF THIODIONE EXPORT

Isolated cells, although not fully expressing their differentiating character, do export thiodione following incubation in 80 µM of menadione. To image this process, the probe electrode must be brought in close proximity to the cells using conventional insulating approach curve experiments (Figure 4). Following the addition of menadione to the cells, the 10 µm Pt UME was poised at menadione reduction potential and approached to the surface. As the tip approached, the hemispherical diffusion of menadione is progressively blocked by the bottom of the dish and causes a decrease in the observed steady-state current. The approach curve corresponds to a pure insulating behavior and agrees well to the insulating approach curve theory:

$$I_T(L) = 1/[A + B/L + Cexp(D/L)] + E * L/(F+L) \quad (1)$$

where for a tip RG=2: A= 0.784; B=0.878; C=0.425; D=-1.744; E=0.164 and F=0.199. Parameters A-F are extracted from curve fitting the numerically simulated curves for a pure insulating feedback SECM behavior.[38] $I_T(L)$ is a normalized current as expressed by the ratio of the tip current to that of the steady-state current when the tip is far from the surface and L is the normalized distance as expressed by the ratio of the tip to substrate distance to the radius of the metal disk.

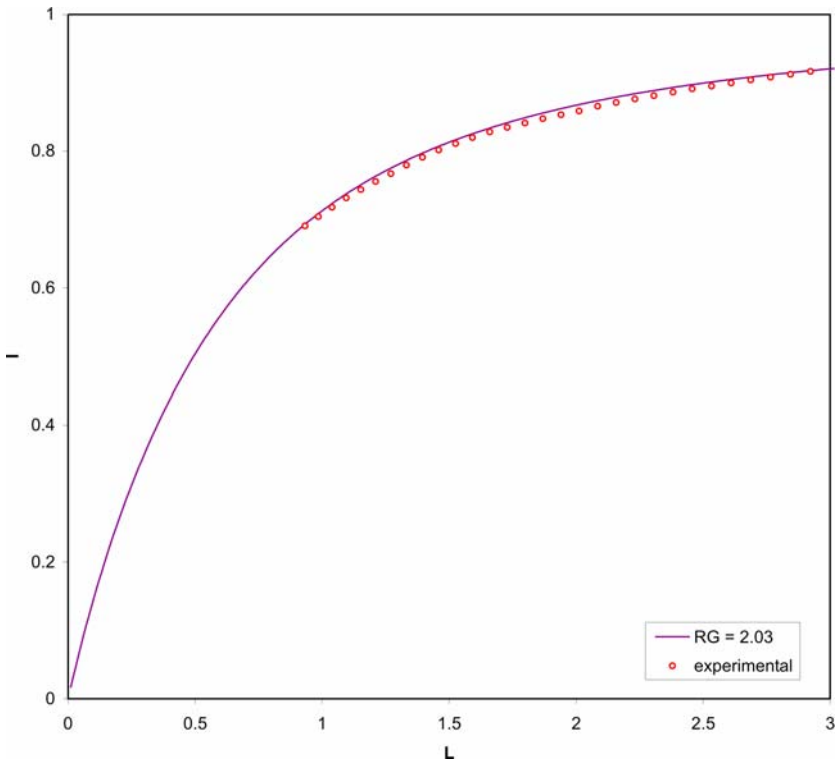

Figure 4.4: Insulating SECM approach curve to the Petri dish using menadione reduction as redox species. The theoretical behavior for a totally insulating approach curve for a 10 µm Pt UME with an RG of 2 is represented by the solid line. The experimental points follow the theory and predict that the electrode was placed 4.3 µm from the substrate.

The tip was approached until it was within a distance comparable to the tip diameter (L=1) as seen in Figure 4. It is not advisable to approach the tip further towards the Petri because of the important topography of the substrate. A closer approach usually results in the removal of the adhered cells from the bottom of the dish upon scanning. This is easily visualized through the inverted microscope. Since the SECM head is fixed to the translation stage of the inverted microscope, it is not possible to correct for tilting of the substrate and so crashing of the electrode on the substrate while imaging is more likely in this setup.

To acquire the SECM collection image, the UME was poised at the potential for thiodione oxidation and scanned in the x-y plane over several hundreds microns. As the tip was scanned at constant height over the cells, the collection current was recorded. From Figure 5A, higher current (yellow) is recorded over the liver cells, while lower currents (green) are measured over the dish. As the tip is recording the SECM image, a simultaneous optical image using the inverted microscope's camera was taken (Figure 5B). The dark disk observed in the middle of the optical micrograph is the 10 μm Pt electrode and several agglomerated human liver cells can be observed. When the optical micrograph is superimposed onto the SECM image, good agreement is observed between the location of the cells and the regions of high thiodione efflux. The cells on the right hand side do not efflux as much as the other cells but they do have a collection current higher than the background current. Similar SECM images can also be recorded on single human liver cells and good correlation is also observed between the cell position and high current domains (Figure 6).

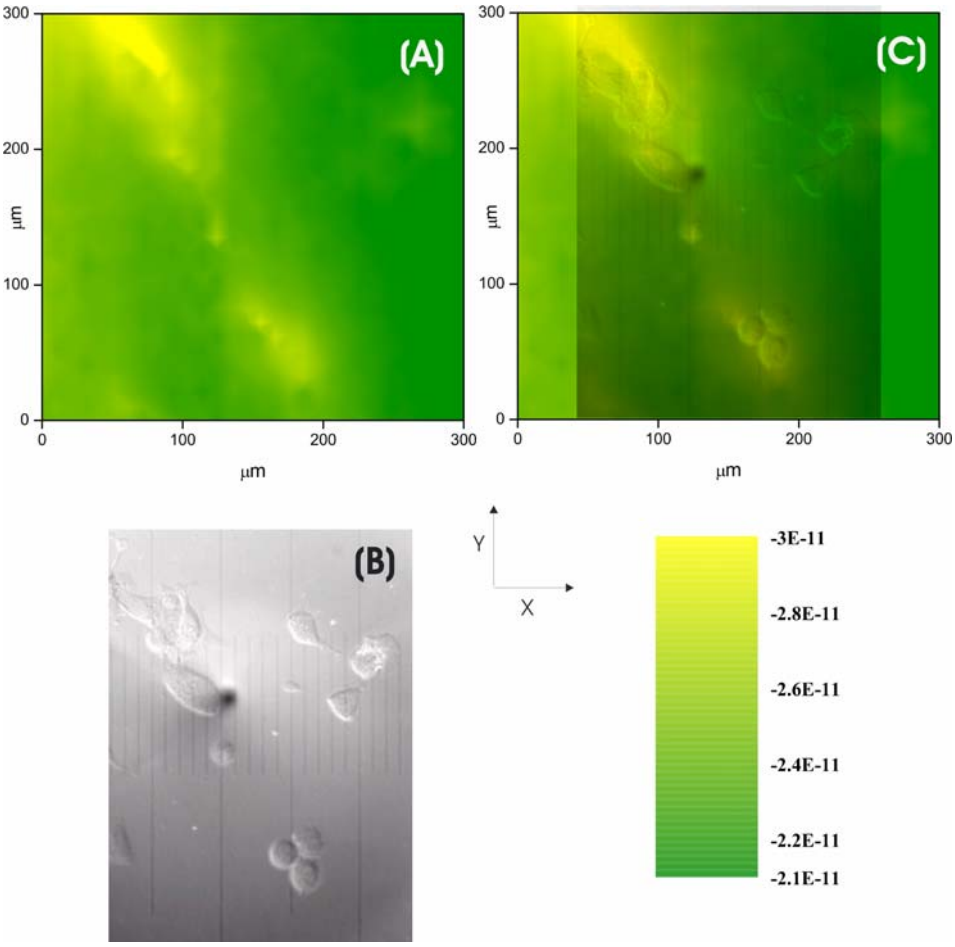

Figure 4.5: SECM imaging of the export of thiodione from Hep G2 cells as detected by a 10 µm Pt UME with an RG of 2. (A) SECM image of Hep G2 cells. The tip potential was held at 0.55 V vs. Hg/Hg_2SO_4 and scanned at 300 µm/s over an area of 300 x 300 µm in the positive x direction. It took 5 min to acquire this image. A 2 s quiet time was applied. (B) Simultaneous optical micrograph of the Hep G2 cells being imaged. The black spot on the micrograph is the Pt UME. One large division corresponds to 50 µm. (C) Superimposed transparent optical micrograph on the SECM image. This image was acquired following 15 min of incubation in the 80 µm menadione solution.

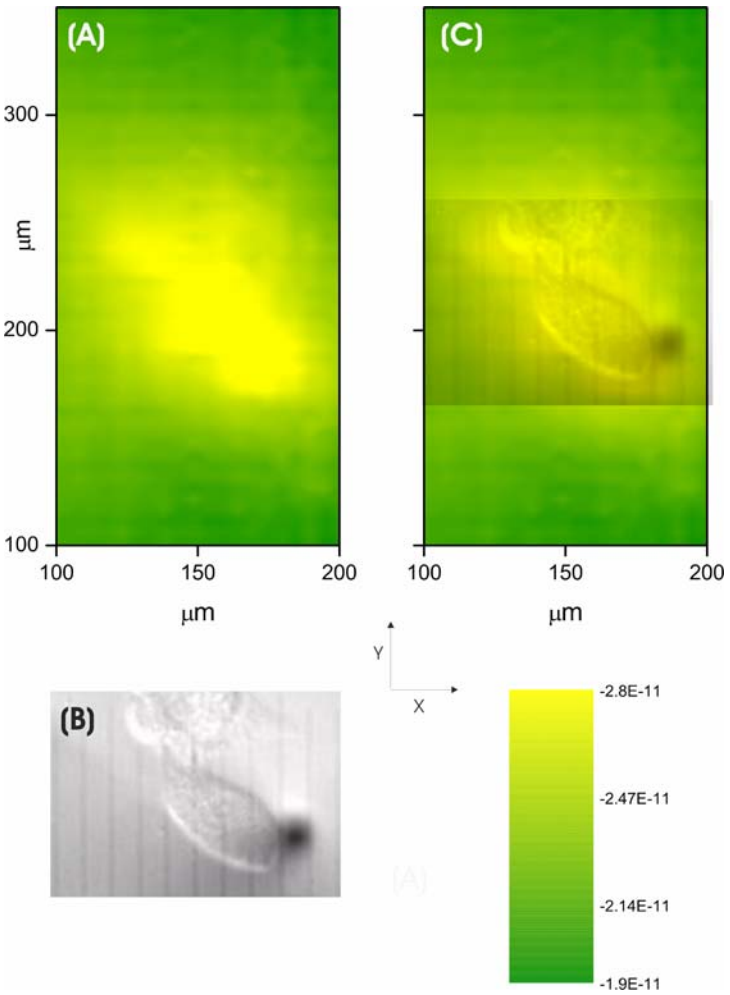

Figure 4.6: SECM imaging of the export of thiodione from two neighboring human liver cells as detected using a 10 µm Pt UME with an RG of 2. (A) SECM image of Hep G2 cells. The tip potential was held at 0.55 V vs. Hg/Hg_2SO_4 and scanned at 150 µm/s over an area of 400 x 200 µm in the positive x direction. The total time to acquire the image was 17 min. A 2 s quiet time was applied. (B) Simultaneous optical micrograph of the Hep G2 cells being imaged. The black disk on the micrograph is the Pt UME. One division corresponds to 10 µm. (C) Superimposed transparent optical micrograph on the SECM image. This image was acquired following 26 min of incubation in the 80 µm menadione solution.

TIME PROFILE OF THIODIONE EXPORT FROM SINGLE HUMAN LIVER CELLS

As indicated in Figure 2B, 80 μM menadione is toxic to Hep G2 cells within 1 h and progressively kills more cells with increasing menadione concentration and time. It is also possible to observe toxicity effects of menadione on single liver cells by taking successive images of the conjugate export with time (Figure 7). The images were acquired rapidly (150 μm/s) so that the time frame allows us to see this profile. It took, on average, 7 min to acquire each image. Slower scan rates might allow for better resolution of the cell, but might be so slow that conjugate efflux changes significantly from the beginning to the end of the image. As seen in Figure 7A-D, the single cell reduces it's export of conjugate with time. These images were taken on the same cell, at different menadione incubation times and for the same tip to substrate distance. The cell's position in the image varies because of a small hysterisis of the piezoelectric inchworms. Since this image sequence was repeated several times and over large areas (around 250 x 400 μm) the hysterisis becomes an important factor in the positioning of the electrode. This is when having the SECM fixed on the inverted microscope becomes advantageous, since optical inspection of the tip positioning following each image allows us to roughly correct for this hysterisis.

Optical micrographs (Figures 7 E-F) of the tip scanning over the cell were simultaneously acquired during SECM imaging. From Figures 7 E and F, it is clear that the only feature that could produce the high current region seen in Figures 7A-D is this isolated single human liver cell. Superposition of the scaled optical micrograph onto the scaled SECM collection image reveals a good agreement (Figures 7 G-J).

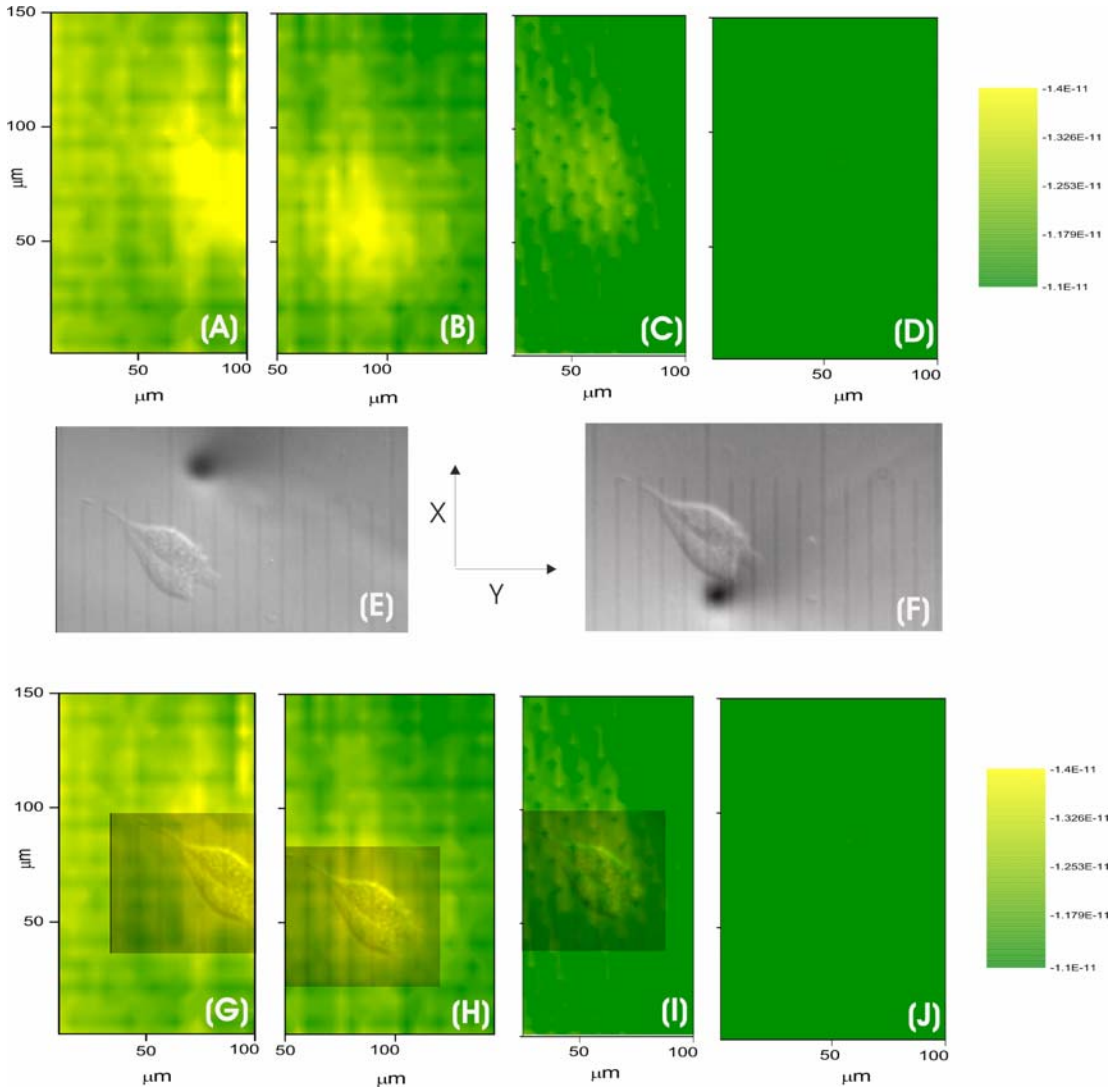

Figure 4.7: Time dependent profile of the export of thiodione from a single human liver cell as detected by SECM imaging. (A-D) SECM image of Hep G2 cell. The tip potential was held at 0.55 V vs. Hg/Hg_2SO_4 and scanned at 150 µm/s in the positive x direction. A 2 s quiet time was applied. (E, F) Simultaneous optical micrograph of the Hep G2 cell being imaged. The black spot on the micrograph is the Pt UME. From (E) and (F) it is clear that the tip is being scanned over this single cell. One division corresponds to 10 µm. (G-J) Superimposed transparent optical micrograph on the SECM image. These images were acquired following 43 min of incubation in the 80 µm menadione solution. All images were formatted such that the same scale is being used for all.

The time at which the SECM images were acquired varies. Cells like the ones imaged in Figures 5 and 6 were only incubated in 80 μM menadione solution for 20 and 26 min, respectively. The currents measured above the imaged cell are comparable for a same tip to substrate distance.

TABLE 4.2**:** List of incubation times in 80 μM menadione for all liver cell figures displayed.

Figures	Incubation time in 80 μM menadione (min)
5	20
6	26
7A	46
7B	49
7C	56
7D	63

The single cell images in Figure 7 were taken after a considerable amount of exposure time. The highest current measured over the cells is now half of what it was after 20 min exposure again for a same tip to substrate distance. Of course, such differences could occur because of differences in cell topography, but the incubation time was found to be the dominant factor. In Figure 7D, the efflux is below the detectable limit and based on the 63 min incubation time reported in Figure 2, the SECM profile seems to agree with the cytotoxicity results. Although this does not unequivocally confirm that the observed cell is dead, it seems possible that the lack of export as measured by SECM is

indicative of cell death. This is based on the similarity between the measured NR assay time line and that observed from the SECM measurement in Figure 7 and Table 1. The NR assay is a multi-step essay while the SECM detection is direct single measurement and it might be worthwhile to investigate its potential as an assay in cytotoxicity experiments.

BIOLOGICAL RELEVANCE

The present results have some limited biological relevance based on the fact that we can measure thiodione efflux from both the isolated and monolayer differentiated cells. As mentioned in the introduction, studies of MDR of tumor cells have revealed that two proteins, Pgp and MRP are responsible for the resistance of tumor cells to chemotherapeutic drugs. In the case of hepatocytes, there are to date three known members of the MRP family that have been identified, localized to different domains of the cells and functional characterization is underway namely in S. P. C. Cole's group in Canada. Although some debate each individual's role is still unresolved, immunofluorescence of monoclonal antibodies that were raised on the unconserved parts of the individual members and Western Blot of selected membranes of hepatocytes have revealed that MRP1-3 are found in Hep G2 cells.[39] MRP1 is localized on the lateral membrane of adjacent cells and not expressed in isolated cells.[25,30] MRP2 is expressed in the canicular membrane where it would be responsible for the transport of organic anion transport from cell to bile.[30] MRP2 is present in the plasma membrane of isolated cells, but is eventually internalized into intracellular vacuoles or apical vacuoles observed in between adjacent Hep G2 cells.[40] MRP3 is localized on the basolateral membrane[41] and would transport species from the cell to the blood under conditions where the MRP2

member is impaired, such as in the case of Dubin-Johnson disease or in TR^- rat strain were MRP2 expression is very low.[25]

It is known that the MRP1 and MRP2 have a high homology and substrate specificity. The SECM results agree with this and show that the members transporting thiodione have a similar qualitative selectivity for this substrate since both isolated and differentiated cells export thiodione. This is not surprising when one considers the similarities in drug selectivity that exists between these two members. Cells over-expressing MRP1 or MRP2 have observed MDR phenotype for vincristine, doxorubicin, epotoside and epirubicin.[12] The main difference between the resistance profile of the two members is that MRP2 induces Cisplatin resistance and this has not been seen in cells over-expressing MRP1.

Based on immunofluorescence studies, it has been suggested that MRP1 and MRP2 expression is cell-cycle dependent and that their regulation would be reciprocal.[30,42] In isolated cells, MRP1 expression would be low, where as MRP2 would be significantly expressed. In differentiated cells, MRP1 expression in the lateral touching regions becomes more important and MRP2 expression shifts to intracellular vesicles or to the membrane of the apical vacuoles that simulate bile ducts. Since a thiodione efflux is detected for both the isolated and the differentiated cells, it appears that at least two different members of the MRP family are active during the detoxification process recorded by SECM.

This interpretation agrees with recent work, but also confirms the hypothesis of the reported work that the menadione imposed oxidative stress on hepatocyte results in the efflux of the stable thiodione conjugate.[42] The isolation of MRP1 from MRP2 relied on the use of the mutant TR^- rat that does not express MRP2. It was, therefore, only concluded that the transport was assisted by the MRP1 member. Although it might be

lower, the use of selective inhibitors of MRP2 and MRP1 could be used in a similar SECM study to allow for the detection of the selective thiodione efflux of each member. In combination with the action of the already developed monoclonal antibodies for theses specific members, we might be able to provide further evidence for the substrate selectivity, localization of the members with time and change in expression of the pumps as they enter the differentiated state.

At present, none of the inhibitors developed are strictly selective for either member and cross-effects are observed.[12] Studied inhibitors have either been designed to act on the substrate rather than the pump or have been focusing on preventing MRP synthesis using anti-sense oligonucleotides. These two approaches have respectively lacked selectivity or resulted in partial inhibition of the pumps. Nevertheless, this is a relatively new protein system, considerable work is still required in inhibitor development, in structural and functional characterization of the members and in the evaluation of the importance of the transport drugs in actual cancer patients. It has to be said that 27 years after its discovery, there is still no consensus about the contribution of Pgp in the development of MDR in cancer patients. In the case of MRP discovered 11 years ago, it is not surprising that its clinical impact is still elusive.

Conclusions

Menadione causes a concentration dependent decrease in Hep G2 cell viability as measured by the neutral red viability essay. The SECM experiments had to be performed within 1 h for 80 μm menadione dose. Such results are supported by similar cytotoxicity of menadione on the same cell line using Tryptan Blue exclusion.[1]

Thiodione efflux from differentiated and isolated cells could be detected using a hybrid SECM inverted microscope setup. This is in line with the results presented in Chapter 3.

Images of the efflux process of thiodione from differentiated and isolated cells were obtained following menadione imposed oxidative stress. A qualitative time profile of the efflux of a single cell was recorded and agrees with the cytotoxicity time frame established by the neutral red assay.

The results are biologically relevant in showing the potential of combined information provided by SECM and the future development of more selective inhibitors for the members of the MRP family. All that we can conclude from the results is that the efflux of thiodione is observed for both isolated and differentiated cells. In light of what is known in the literature, it would appear that more than one member of the MRP family is involved in this efflux. This strongly agrees with recent literature and would be confirmed by the use of selective inhibitors for MRP1 and MRP2.

Pursuing this research is important because menadione mimics the toxicity exhibited by adriamycin® and danorubicin, two of the most widely used drugs in the treatments of a variety of cancers. These drugs a limited by MDR of varying malignant cells and, as such, cause considerable harm to the patient by mistargeting and killing healthy cells. Although research on the Pgp and MRP proteins might not affect drug design directly, it might have an impact if selective pump inhibitors are co-administered and reverse the MDR. Our experimental setup is well suited to combine already developed tools such as the fluorescent tagged monoclonal antibodies, the transport fluorescent dyes and the SECM detection scheme of thiodione. This would also eliminate the need for the use of inside-out micelles that are presently used in transport study with the glutathione conjugate fluorescent dyes.

References

[1]Duthie, S. J. ; Grant, M. H. *Biochem. Pharmacol.* **1989**, *38*, 1247.

[2] Chiou, T.-J.; Tzeng, W.-F. *Toxicology* **2000**, *154*, 75.

[3] Hipfner, D. R.; Deeley, R. G.; Cole, S. P. C. *Biochim. Biophys. Acta* **1999**, *1461*, 359.

[4] Higgins, C. F. *Annu. Rev. Cell. Biol.* **1992**, *8*, 67.

[5] Cole, S. P. C.; Sparks, K. E.; Fraser, K.; Loe, D. W.; Grant, C. E.; Wilson, G. M.; Deeley, R. G. *Cancer Research* **1994**, *54*, 5902.

[6] Cole, S. P. C.; Bhardwaj, G.; Gerlach, J. H.; Mackie, J. E.; Grant, C. E.; Almquist, K. C.; Stewart, A. J.; Kurz, E. U.; Duncan, A. M. V.; Deeley, R. G. *Science* **1992**, *258*, 1650.

[7] Grant, C. E.; Valdimarson, G.; Hipfner, D. R.; Almquist, K. C.; Cole, S. P. C.; Deeley, R. G. *Cancer Res.* **1994**, *54*, 357.

[8] Kruh, G. D.; Chan, A.; Myers, K.; Gaughan, K.; Miki, T.; Aaronson, S. A. *Cancer Res.* **1994**, *54*, 1649.

[9] Zaman, G. J. R.; Flens, M. J.; van Leusden, M. R.; de Haas, M.; Mulder, H. S.; Lankelma, J.; Pinedo, H. M.; Scheper, R. J.; Baas, F.; Broxterman, H. J.; Borst, P. *PNAS USA* **1994**, *91*, 8822.

[10] Chang, X.-B.; Hou, Y.-X.; Riordan, J. R. *J. Biol. Chem.* **1997**, *272*, 30962.

[11] Morrow, C. S.; Smitherman, P. K.; Townsend, A. J. *Mol. Carcinogenesis* **2000**, *29*, 170.

[12] Ishikawa, T. *Trends in Biochem. Sci.* **1992**, *17*, 463.

[13] Manciu, L.; Chang, X.-B.; Buyset, F.; Hou, Y.-X.; Gustot, A.; Riordan, J. R.; Ruysschaert, J. M. *J. Biol. Chem.* **2003**, *278*, 3347.

[14] Ishikawa, T.; Bao, J. J.; Yamane, Y.; Akimaru, K.; Frindrich, K.; Wright, C. D. *J. Biol. Chem.* **1996**, *271*, 1481.

[15] Kuo, M. T.; Bao, J.; Furuichi, M.; Yamane, Y.; Gomi, A.; Savaraj, N.; et al. *Biochem. Pharmacol.* **1998**, *55*, 605.

[16] Zaman, G. J. R.; Lankelma, J.; van Tellingen, O.; Beijnens, J.; Dekker, H.; Paulusma, C.; Elferink, R. P. J.; Baas, F.; Borst, P. *PNAS USA* **1995**, *92*, 7690.

[17] Borst, P.; Evers, R.; Kool, M.; Wijnholds, J. *J. Nat. Can. Inst.* **2000**, *92*, 1295.

[18] Allikmets, R.; Gerrard, B.; Hutchinson, A.; Dean, M. *Hum. Mol. Genet.* **1996**, *5*, 1649.

[19] Elferink, R. P. J. O.; Meijer, D. K. F.; Kuipers, F.; Jansen, P. L. M.; Groen, A. K.; Groothuis, G. M. M. *Biochim. Biophys. Acta* **1995**, *1241*, 215.

[20] McAleer, M. A.; Breen, M. A.; White, N. L.; Matthews, N. *J. Biol. Chem.* **1999**, *274*, 23541.

[21] Cole, S. P. C. *J. Natl. Can. Inst.* **1999**, *91*, 888.

[22] Zaman, G. J.; Lankelma, J.; van Tellingen, O.; Beijnen, J.; Dekker, H.; Paulusma, C. *PNAS USA* **1995**, *92*, 7690.

[23] Müller, M.; Roelofsen, H.; Jansen, P. L. M. *Sem. Liver Dis.* **1996**, *16*, 211.

[24] Knowles, B. B.; Howe, C.C.; Aden, D. P. *Science* **1980**, *209*, 497.

[25] Javitt, N. B. *FASEB J* **1990**, *4*, 161.

[26] Roelofsen, H.; Vos, T. A.; Schippers, I. J.; Kuipers, F.; Koning, H.; Moshage, H.; Jansen, P. L. M.; Müller, M. *Gastroenterology* **1997**, *112*, 511.

[27] Sormunen, R.; Eskelinen, S.; Lehto, V. *Lab. Invest.* **1993**, *68*, 652.

[28] Roelofsen, H.; Müller, M.; Jansen, P. L. M. *Yale J. Biol.Med.* **1997**, *70*, 435.

[29] Borenfreund, E.; Puerner, J. A. *J. Tissue Culture Methods* **1985**, *9*, 7.

[30] Babich, H.; Borenfreund, E. *Alternatives to Laboratory Animals (ATLA)* **1990**, *19*, 129.

[31] Bard, A. J.; Mirkin, M. V.; Eds.; *Scanning Electrochemical Microscopy,* Marcel Dekker, Inc., New York, **2001.**

[32] Mauzeroll, J.; Bard, A. J.; **2003,** manuscript in preparation.

[33] Biao, L.; Rotenberg, S. A.; Mirkin, M. V. *PNAS USA* **2000**, *97*, 9855.

[34] Chenxin, C.; Biao, L.; Mirkin, M. V.; Frank, H. A.; Rusling, J. F. *Anal. Chem.* **2002**, *74*, 114.

[35] Arcamone, F. *Med. Res. Rev.* **1984**, *4*, 153.

[36] Di Monte, D.; Ross, D.; Bellomo, G.; Eklow, L.; Orrenius, S. *Arch. Biochem. Biophys.* **1984**, *224*, 334.

[37] Chung, J.-H.; Seo, D.-C.; Chung, S.-H.; Lee, J.-Y.; Seung, S.-A. *Toxicol. App. Pharmaco.* **1997**, *142*, 378.

[38] Shao, Y.; Mirkin, M. V.; *J. Phys. Chem. B* **1998**, *102*, 9915.

[39] König, J.; Nies, A. T.; Cui, Y.; Leier, I.; Keppler, D. *Biochim. Biophys. Acta* **1999**, *1461*, 377.

[40] Wettsein, M.; Noe, B.; Häussinger, D. *Hepatology* **1995**, *22*, 235.

[41] Cantz, T.; Nies, A. T.; Brom, M.; Hofmann, A. F.; Keppler, D. *Am. J. Physiol. Gastrointest. Liver Phys.* **2000**, *278*, G522.

[42] Roelfosen, H.; Hooiveld, G. J. E. J.; Koning, H.; Havinga, R.; Jansen, P. L. M.; Müller, M. *J. Cell Sci.* **1999**, *112*, 1395.

CONCLUSION

Chapter Highlights

In Chapter 1, the effect of electrode geometry on transient current response measured in SG-TC experiments was demonstrated for a Pt disk and Hg hemispherical tip. The transient current behavior was numerically simulated and was in line with the feedback studies. From the simulations, important experimental parameters such as diffusion coefficients were extracted. The main advantages of the mercury tips were the enhancement of potential window in the negative potential region and the protrusion of the hemisphere beyond the glass sheet. The protrusion of the active electrode area allowed for a close approach and actual touching of the metal to the substrate without problems of premature touching of the glass insulator, thus yielding a better estimation of the true zero distance.

In Chapter 2, the Hg tips were used to detect Tl(I) transport across gramicidin half-channels. Comparison of substrate (HMDE) generation – tip collection behavior of the bare amalgamated, DOPC and gramicidin-DOPC modified HMDE confirmed the selective transport of Tl(I) across gramicidin. An apparent heterogeneous rate constant for the transport of Tl(I) from the HMDE into the bulk solution was obtained. This rate constant indicated that their might be asymmetry in the activation barrier of the half channel. To our knowledge, this was the first time that SECM had been used in an amperometric mode to control and monitor ion transport across ion channels.

In Chapter 3, the SECM methodology was applied to a full biological system. Thiodione export was detected from a bulk yeast cell suspension and from small yeast cell aggregates exposed to menadione. From a theoretical treatment, an apparent first order rate constant range for the uptake of menadione was extracted that identified this process as the slow dominant process.

The study of menadione induced oxidative stress was further studied in Chapter 4 on human liver cells. Menadione caused a concentration dependent decrease in Hep G2 cell viability. Thiodione efflux from differentiated and isolated cells could be detected and imaged using a hybrid SECM inverted microscope setup following menadione

imposed oxidative stress. A qualitative time profile of the efflux of a single cell was recorded and agreed with the cytotoxicity time frame established by the neutral red assay.

These results are biologically relevant in showing the potential of combined information provided by SECM and the future development of more selective inhibitors for the members of the MRP family. In light of what is known in the literature, it would appear that more than one member of the MRP family is involved in this efflux.

Dissertation Highlights and Outlook

THEORETICAL TREATMENT OF TRANSIENTS

SG-TC mode of SECM is less often used in experiments because of its inherent transient component. We have shown in Chapters 1-3 that theoretical treatments of SG-TC transients can be accomplished via numerical simulations or experimental specific models that offer analytical approximations. The development of experimental specific models is useful, but inherently simplistic. They often provide enough information to quantify kinetic events but hardly ever fully describe the true state of a system.

The numerical simulation approach is very flexible and can be applied to a wide variety of systems by changing the initial and boundary conditions. This flexibility will be most useful in further study of biological systems that would require specific theoretical modeling. This method is, however, time consuming and not user friendly. Commercially available packages require considerable effort to fully understand the software and methods used. In the case where a personal program is written, the results are not readily accessible by others and require knowledge of programming languages.

Another important issue to address is the fitting procedures used to compare simulated and experimental results. Many SECM fittings rely on manual fits rather than software that uses a non-linear curve fitting algorithm. As the complexity of the system studied increases, there will be a need to develop specialized fitting software. This is a very similar situation that led to the advent of specialized fitting software for the treatment of diffractograms.

ULTRAMICROELECTRODE DESIGN

The UME probe is the key to SECM. As such, the geometry and size of the tip dictate the response and minimal lateral resolution. To have a chance of detecting and imaging the efflux from a single channel, the tip electrode will have to be made on the nm scale. This implies that a reproducible procedure for tip preparation will need to be available. The laser pulled tip preparation presented in Chapter 3 comes close to the nm magnitude. The smallest tip ever made with this protocol was a 30 nm tip as characterized by CV. Tips of 200 μm and smaller have yet to be characterized by normal feedback experiments. The feedback characterization is necessary to properly assess the tip geometry that will affect the SECM response as seen in Chapter 1. For very small electrodes, optical means are not reliable and cannot assess the true tip geometry. In the advent of nanometer size electrode development, proper protocols for geometry characterization will be required.

Smaller UMEs imply smaller recorded currents that might push the present current detection limits. In conventional SECM experiments, this would be remedied by the use of a very high concentration of redox mediator. In the case of biological studies, this option is only valid if the high dose does not impair cellular functions. It is unlikely that such a strategy would be fruitful in the oxidative stress studies present in Chapter 3 and 4. The study of biological systems with nanometer size electrodes will therefore require the development of very sensitive current amplifiers capable of measuring currents in the order of femtoamps.

SECM AND BIOLOGICAL APPLICATIONS

It is clear from the preceding chapters that SECM has great potential for biological studies. It can quantify fast kinetics with a variety of probe electrodes that can be tailored to the needs of individual experiments. The SECM-microscope hybrid setup is particularly well suited for the addition of fluorescent studies. The combination of selective fluorescent tags was discussed in Chapter 4 and would provide complementary information concerning protein localization and sequestration.

This setup is also appealing for screening assays. Because of the ease in positioning, SECM could be scanned over large arrays of cells where each spot would

have a different engineered mutation. Suppose that the mutation altered a transport function that could be monitored by SECM, the scanned tip could provide a measure of the activity of these transport pumps with the different mutations. This could also be useful in drug testing or in the development of selective inhibitors of transport pumps. To image transport activity on larger scales, care would have to be taken that the imaging speed be sufficiently fast to measure all spots at a similar characteristic time. This might require the use of a controlled delivery system that would administer the chemical stress solution at the individual spots.

There are many scenarios where SECM measurements would be useful in biological studies. All these possibilities and the presented dissertation work reinforce the importance of interdisciplinary collaboration. Biological systems are intrinsically complicated and will require the use of a number of simultaneous techniques to achieve any general conclusions. Combining SECM with fluorescent and bioengineering technologies might be a good combination to further the general understanding of transport processes or to develop screening tools.

BIBLIOGRAPHY

Introduction

[1] Bard, A. J.; Mirkin, M. V.; Eds .; *Scanning Electrochemical Microscopy* , Marcel Dekker, Inc.; New York, **2001**, 1-200.

[2] Kueng, A.; Kranz, C.; Lugstein, A.; Bertagnolli, E.; Mizaikoff, B. *Angew. Chem. Int.* **2003**, *42*, 3237.

[3] Horrocks, B. R.; Mirkin, M. V.; Pierce, D. T.; Bard, A. J.; Nagy, G.; Toth, K. *Anal. Chem.* **1993**, *65*, 1213.

[4] Liebetrau, J. M.; Miller, H. M.; Baur, J. E.; Takacs, S. A.; Anupunpisit, V.; Garris, P. A.; Wipf, D. O. *Anal. Chem.* **2003**, *75*, 563.

[5] Yasukawa, T.; Kaya, T.; Matsue, T. *Anal. Chem.* **1999**, *71*, 4637.

[6] Bard, A. J.; Mirkin, M. V.; Eds.; *Scanning Electrochemical Microscopy* , Marcel Dekker, Inc.; New York, **2001**, 445-519.

[7] Pierce, D. T.; Unwin, P. R.; Bard, A. J. *Anal. Chem.* **1992**, *64*, 1795.

[8] Pierce, D. T.; Bard, A. J. *Anal. Chem.* **1993**, *65*, 3598.

[9] Kranz, C.; Wittstock, G.; Wohlschläger, H.; Schuhmann, W. *Electrochim. Acta* **1997**, *42*, 3105.

[10] Wijayawardhana, C. A.; Wittstock, G.; Halsall, H. B.; Heineman, W. R. *Anal. Chem.* **2000**, *72*, 333.

[11] Wittstock, G.; Schuhmann, W. *Anal. Chem.* **1997**, *69*, 5059.

[12] Horrocks, B. R.; Schmidtke, D.; Heller, A.; Bard, A. J. *Anal. Chem.* **1993**, *65*, 3605.

[13] Horrocks, B. R.; Mirkin, M. V.; Pierce, D. T.; Bard, A. J. *Anal. Chem.* **1993**, *65*, 1213.

[14] Horrocks, B. R.; Mirkin, M. V. *J. Chem. Soc. Faraday Trans.* **1998**, *94*, 1115.

[15] Shiku, H.; Takeda, T.; Yamada, H.; Matsue, T.; Uchida, I. *Anal. Chem.* **1995**, *67*, 312.

[16] Berger, C. E. M.; Horrocks, B. R.; Datta, H. K. *J. Endocrin.* **1998**, *158*, 311.

[17] Shiku, H.; Matsue, T.; Uchida, I. *Anal. Chem.* **1996**, *68*, 1276.

[18] Shiku, H.; Hara, Y.; Matsue, T.; Uchida, I. *J. Electroanal. Chem.* **1997**, *438*, 187.

[19] Zaumseil, J.; Wittstock, G.; Bahrs, S.; Steinrücke, P. *Fresenius J. Anal. Chem.* **2000**, *367*, 352.

[20] Wittstock, G.; Yu, K. J.; Halsall, H. B.; Ridgway, T. H.; Heineman, W. R. *Anal. Chem.* **1995**, *67*, 3578.

[21] Antonenko, Y. N.; Pohl, P.; Rosenfeld, E. *Arch. Biochem. Biophys.* **1996**, *333*, 225.

[22] Wang, J.; Song, F.; Zhou, F. *Langmuir* **2002**, *18*, 6653.

[23] Tsionsky, M.; Cardon, Z. G.; Bard, A. J.; Jackson, R. B. *Plant Physiol.* **1997**, *113*, 895.

[24] Berger, C. E. M.; Rathod, H.; Gillespie, J. I.; Horrocks, B. R.; Datta, H. *J. Bone and Min. Res.* **2001**, *16*, 2092.

[25] Nishizawa, M.; Takoh, K.; Matsue, T. *Langmuir* **2002**, *18*, 3645.

[26] Takii, Y.; Takoh, K.; Nishizawa, M.; Matsue, T. *Electrochim. Acta* **2003**, *48*, 3381.

[27] Kaya, T.; Nishizawa, M.; Yasukawa, T.; Nishiguchi, M.; Onouchi, T.; Matsue, T. *Biotech. Bioeng.* **2001**, *76*, 391.

[28] Shiku, H.; Shiraishi, T.; Ohya, H.; Matsue, T.; Abe, H.; Hoshi, H.; Kobayashi, M. *Anal. Chem.* **2001**, *73*, 3751.

[29] Liu, B.; Rotenberg, S. A.; Mirkin, M. V. *PNAS USA* **2000**, *97*, 9855.

[30] Cai, C.; Liu, B.; Mirkin, M. V.; Frank, H. A.; Rusling, J. F. *Anal. Chem.* **2002**, *74*, 114.

[31] Biao, L.; Rotenberg, S. A.; Mirkin, M. V. *Anal. Chem.* **2002**, *74*, 6340.

[32] Feng, W.; Rotenberg, S. A.; Mirkin, M. V. *Anal. Chem.* **2003**, *75*, 4148.

[33] Mauzeroll, J.; Hueske, E. A.; Bard, A. J. *Anal. Chem*. **2003**, *75*, 3880.

[34]Mauzeroll, J.; Buda, M.; Bard, A. J.; Prieto, F.; Rueda, M. *Langmuir* **2002**, *18*, 9453.

[35] Mauzeroll, J.; Bard, A. J. **2003**, manuscript in preparation.

[36] Mauzeroll, J.; Monks, T.; Bard, A. J. **2003**, manuscript in preparation.

Chapter 1

[1]Bard, A. J.; Mirkin, M. V.; Eds, *Scanning Electrochemical Microscopy,* Marcel Dekker, New York, **2001**.

[2] Bard, A. J.; Denuault, G.; Friesner, R. A.; Dornblaser, B. C.; Tuckerman, L. S. *Anal. Chem.* **1991**, *63*, 1282.

[3] Denault, G.; Mirkin, M. V.; Bard, A. J. *J. Electroanal. Chem.* **1991,** *308***,** 27.

[5] Martin, R. D.; Unwin, P .R. *Anal. Chem.* **1998**, *70*, 276.

[6] Rueda, M.; Navarro, I.; Ramirez, G.; Prieto, F.; Prado, C.; Nelson, A. *Langmuir* **1999**, *15*, 3672.

[6] Mauzeroll, J.; Buda, M.; Bard, A. J.; Prieto, F.; Rueda, M. *Langmuir* **2002,** *18*, 9453.

[8] Selzer, Y.; Turyan, I.; Mandler, D. *J. Phys. Chem. B* **1999**, *103*, 1509.

[9] Wu. H. P. *Anal. Chem.* **1994**, *66*, 3151.

[10] Yoshima, Z. *Bull. Chem. Soc. Jpn.* **1981**, *54*, 556.

[11] Wehmeyer, K. R.; Wightman, R. M. *Anal. Chem*. **1985**, *57*, 1989.

[12] Golas, J.; Galus, Z.; Osteryoung, J. *Anal. Chem.* **1987**, *59*, 389.

[13] Wechter, C.; Osteryoung, J. *Anal. Chim. Acta* **1990,** *234*, 275.

[14] Mirkin, M. V.; Fan, F.-R. F.; Bard, A. J. *J. Electroanal. Chem.* **1992**, *328*, 47.

[15] Demaille, C.; Brust, M.; Tionsky, M.; Bard, A. J. *Anal. Chem.* **1997**, *69*, 2323.

[16] Fulian, Q.; Fisher, A. C.; Denuault, G. *J. Phys. Chem. B* **1999**, *103*, 4387.

[17] Fulian, Q.; Fisher, A. C.; Denuault, G. *J. Phys. Chem. B* **1999**, *103*, 4393.

[18] Selzer,Y.; Mandler, D. *Anal. Chem.* **2000**, *72*, 2383.

[18] Zoski, C. G.; Mirkin, M. V. *Anal. Chem*. **2002**, *74*, 1986.

[20] Fan, F.-R. F.; Bard, A. J. *Science* **1995**, *267*, 871.

[21] Fan, F.-R. F.; Bard, A. J. *Science* **1995**, *270*, 1849.

[22] Fan, F.-R. F.; Bard, A. J. *Proc. Natl. Acad. Sci. U.S.A.* **1999**, *96*, 14222.

[23] Gray, N. J.; Unwin, P. R. *Analyst* **2000**, *125*, 889.

[24] Engstrom, R. C.; Weber, M.; Wunder, D. J.; Burgess, R.; Winquist, S. *Anal. Chem.* **1986,** *58*, 844.

[25] Engstrom, R. C.; Meaney, T.; Tople, R.; Wightman, R. M. *Anal. Chem.* **1987**, *59*, 2005.

[26] Engstrom, R. C.; Wightman, R. M.; Kristensen, E. W. *Anal. Chem.* **1988**, *60*, 652.

[27] Kwak, J.; Bard, A. J. *Anal.Chem.* **1989**, *61*, 1221.

[28] Fulian, Q.; Fisher, A. C.; Dennuault, G. *J. Phys. Chem. B* **1999**, *103*, 4393.

[29] Unwin, P. R. *J. Chem. Soc. Faraday Trans.* **1998**, *94*, 3183.

[30] Slevin, C. J.; Umbers, J. A.; Atherton, J. H.; Unwin, P. R. *J. Chem. Soc. Faraday Trans.* **1996**, *92*, 5177.

[31] Penczek, M.; Stojek, Z. *J. Electroanal. Chem.* **1984**, *170*, 99.

[32] Penczek, M.; Stojek, Z. *J.Electroanal. Chem.* **1984**, *181*, 83.

[33] Moorhead, E. D.; Stephens, M. M. *J. Electroanal. Chem.* **1990**, *282*, 1.

[34] Nann, T.; Heinze, J. *Electrochem. Comm.* **1999**, *1*, 289.

[35] Lee, Y.; Amemiya, S.; Bard, A. J. *Anal. Chem.* **2001**, *73*, 2261.

[36] Mirkin, M. V. In *Scanning Electrochemical Microscopy* , Bard, A. J.; Mirkin, M. V.; Eds.; Marcel Dekker, New York, **2001,** Chapter 4.

[37] Shoup, D.; Szabo, A. *J. Electroanal. Chem.* **1982**, *140*, 237.

[38] Aoki, K.; Osteryoung, J. *J. Electroanal. Chem.* **1981**, *122*, 19.

[39] Martin, R. D.; Unwin, P. R. *J. Electroanal. Chem.* **1997**, *439*, 123.

[40] Bard, A. J.; Faulkner, L. R. *Electrochemical Methods* , *1st ed.* , John Wiley & Sons, New York, **1980,** 180.

[41] Sharifer, B.; Hills, G. J. *J. Electroanal. Chem.* **1981**, *130*, 81.

[42] Wightman, R. M.; Wipf, D. O. *Electroanalytical Chemistry*, Bard, A. J.; Ed.; Marcel Dekker, New York, **1989,** *Volume 15*, 267.

[43] Bard, A. J.; Fan, F.-R. F.; Kwak, J.; Lev, O. *Anal. Chem.* **1989**, *61*, 132.

[44] Davis, J. M.; Fan, F .-R. F.; Bard, A. J. *J. Electroanal. Chem. Interfacial Electrochem.* **1987**, *238*, 9.

[45] Kolthoff, M.; Lingane, J. J. *Polarography*, Interscience Publishers, New York, **1952**, 52.

[46] Mauzeroll, J.; Bard, A. J. unpublished experiments.

Chapter 2

[1] Kwak, J.; Bard, A. J. *Anal. Chem*. **1989**, *61*, 1221.

[2] Bard, A. J.; Fan, F.-R. F.; Kwak, J.; Lev, O. *Anal. Chem.* **1989**, *61*, 132.

[3] Davis, J. M.; Fan, F.-R. F.; Bard, A. J. *J. Electroanal. Chem. Interfacial Electrochem.* **1987**, *238*, 9.

[4] Bard, A. J.; Mirkin, M.V.; Eds.; *Scanning Electrochemical Microscopy*, Marcel Dekker Inc., New York, **2001**.

[5] Bard, A. J.; Denuault, G.; Friesner, R. A.; Dornblaser, B. C.; Tuckerman, L. S. *Anal. Chem.* **1991**, *63*, 282.

[6] Martin, R. D.; Unwin, P. R. *Anal. Chem.* **1998**, *70*, 276.

[7] Engstrom, R. C.; Weber, M.; Wunder, D. J.; Burgess, R.; Winquist, S. *Anal. Chem.* **1986,** *58*, 844.

[8] Engstrom, R. C.; Meaney, T.; Tople, R.; Wightman, R. M. *Anal. Chem.* **1987**, *59*, 2005.

[9] Engstrom, R. C.; Wightman, R. M.; Kristensen, E. W. *Anal. Chem.* **1988**, *60*, 652.

[10] Kranz, C.; Wittstock, G.; Wohlschläger, H.; Schuhmann,W. *Electrochim. Acta* **1997**, *42*, 3105.

[11] Wittstock, G.; Schuhmann, W. *Anal. Chem.* **1997**, *69*, 5059.

[12] Scott, E. R.; White, H. S.; Phipps, J. B. *J. Membrane Sci.* **1991,** *58*, 71.

[13] Macpherson, J. V.; Beeston, M. A.; Unwin, P. R.; Hughes, N. P.; Littlewood, D. *J. Chem. Soc. Faraday Trans*. **1995**, *91*, 1407.

[14] Scott, E. R.; Phipps, J. B.; White, H. S. *J. Invest. Derm.* **1995**, *104*, 142.

[15] Amemiya, S.; Bard, A. J. *Anal. Chem.* **2000**, *72*, 4940.

[16] Amemiya, S.; Ding, Z.; Zhou, J.; Bard, A. J. *Electro. Chem.*, **2000**, *483*, 7.

[17] Nelson, A. *Biophys. J.* **2001**, *80*, 2694.

[18] Miller, I. R.; Rishpon, J.; Tenenbaum, A. *Bioelectrochem. Bioenerg.* **1976**, *3*, 528.

[19] Nelson, A.; Auffret, N. *J. Electroanal. Chem.* **1988**, *244*, 99.

[20] Nelson, A.; Leermarkers, F. A. M. *J. Electroanal. Chem.* **1990**, *278*, 73.

[21] Nelson, A.; Bizzotto, D.; *Langmuir* **1999**, *15*, 7031.

[22] Woolley, G. A.; Wallace B. A. *J. Membrane Biol.* **1992**, *129*, 109.

[23] Hladky, S. B.; Haydon, D. A. *Curr. Topics Membr. Transport* **1984**, *21*, 327.

[24] Rueda, M.; Navarro, I.; Prado, C.; Silva, C. *J. Echem. Soc.* **2001**, *4*, E139.

[25] Ketchem, R. R.; Hu, W.; Cross, T. A.; *Science* **1993**, *261*, 1457.

[26] Ketchem, R. R.; Lee, K. C.; Huo, S.; Cross, T. A.; *J. Biomol. NMR* **1996**, *8*, 1.

[27] Mauzeroll, J.; Bard, A. J. in preparation.

[28] Nelson, A.; Benton, A. *J. Electroanal Chem.* **1986**, *202*, 253.

[29] Selzer, Y.; Mandler, D. *Anal. Chem.* **2000**, *72*, 2383.

[30] Arca, M.; Bard, A. J.; Horrocks, B. R.; Richards, T. C.; Treichel, D. A. *Analyst* **1994**, *119*, 719.

[31] Demaille, C.; Brust, M.; Tsionsky, M.; Bard, A. J. *Anal. Chem.* **1997**, *69*, 2323.

[32] Usui, S.; Yamasaki, T.; Simoiizaka, J. *J. Phys. Chem.* **1967**, *71(10)*, 3195.

[33] Mirkin, M.V.; Bard, A. J. *J. Electrochem. Soc.* **1992**, *139*, 3535.

[34] Bard, A. J.; Faulkner, L. R.; *Electrochemical Methods, 1st ed.* , John Wiley & Sons, New York, **1980**, 180.

[35] Bizzotto, D.; Nelson, A. *Langmuir* **1998**, *14*, 6269.

[36] Rueda, M.; Navarro, I.; Ramirez, G.; Prieto, F.; Prado, C.; Nelson, A. *Langmuir* **1999**, *15*, 3672.

[37] Wallace, B. A. *Annu. Rev. Biphys. Chem.* **1990**, *19*, 127.

[38] Killian, J. A.; *Biochim. Biphys. Acta* **1992**, *1113*, 391.

[39] Hu, W.; Lee, K. C.; Cross T. A. *Biochemistry* **1993**, *27*, 7035.

[40] Wallace, B. A. *Adv. Exp. Med. Biol.* **1996**, *398*, 607.

[41] Bard, A. J.; Faulkner, L. R.; *Electrochemical Methods, 2nd ed.* , John Wiley & Sons, New York, **2001**, 192.

[42] Carslaw, H. S.; Jaeger, J. C. *Conduction of Heat in Solids, 2nd ed.*, Clarendon Press, Oxford, **1959.**

[43] Becucci, L.; Moncelli, M. R.; Guidelli, R. *Biophys. J.* **2002**, *82*, 852.

[44] Amatore, C.; Savéant, J. M.; Tessier, D. *J. Elec. Anal.* **1983**, *147*, 39.

Chapter 3

[1] Bard, A. J.; Mirkin, M. V.; Eds.; *Scanning Electrochemical Microscopy,* Marcel Dekker, Inc., New York, **2001.**

[2] Monks, T. J.; Lau, S. S. *Annu. Rev. Pharmacol. Toxicol*. **1998,** *38*, 229.

[3] Reed, D. J.; Meredith, M. J. in *Bioactivation of Foreign Compounds*, M.W. Anders, Ed., Orlando Academic Press, **1985,** 71.

[4] Foyer, C. H.; Theodoulou, F. L.; Delrot, S. *Trends in Plant Sci*. **2001,** *16*, 486.

[5] Keppler, D. *Free Rad. Bio. & Med*. **1999,** *27*, 985.

[6] Sies, H. *Free Rad. Bio. & Med*. **1999,** *27*, 916.

[7] Chung, J .-H.; Seo, D.-C.; Chung, S.-H.; Lee, J.-Y.; Seung, S.-A. *Toxicol. & Appl. Pharm.* **1997,** *142*, 378.

[8] Costa, V.; Moradas-Ferreira, P. *Mol. Asp. of Med*. **2001,** *22*, 217.

[9] Sies, H.; Ketterer, B. in *Glutathione Conjugation. Mechanisms & Biological Significance,* Eds., Academic Press, London, **1988.**

[10] Monks, T. J.; Lau, S. S. *Chem. Res. Toxicol*. **1997,** *10*, 1296.

[11] Zadi_ski, R.; Fortuniak, A.; Bili_ski, T.; Grey, M.; Bartosz, G. () *Biochem. & Mol. Bio. Int.* **1998,** *44*, 747.

[12] Morrow, C. S.; Smitherman, P.D.; Townsend, A. J. *Biochem. Parmacol*. **1998,** *56,* 1013.

[13] Morrow, C. S.; Smitherman, P. K.; Diah, S. K.; Schneider, E.; Townsend, A. J. *J. Biol. Chem*. **1998,** *273*, 20114.

[14] Nickerson, W. J.; Falcone, G.; Strauss, G. *Biochemistry* **1963,** *2*, 537.

[15] Katemann, B. B.; Schuhmann, W. *Electroanalysis* **2002,** *14*, 22.

[16] Buffington, G. D.; Öllinger, K.; Brunmark, A.; Cadenas, E. *Biochem. J* . **1989,** *257*, 561.

[17] Chambers, J. Q. in *Encyclopedia of Electrochemistry of the Elements XII* , Eds., Bard, A. J.; Lund, H.; Marcel Dekker, Inc., New York, **1978,** 453.

[18] Lau, S. S.; Jones, T. W.; Highet, R. J.; Hill, B. A.; Monks, T. J. *Toxi. & App. Pharm.* **1990,** *104*, 334.

[19] Penninckx, M. *Enzyme and Microbial Technology* **2000,** *26*, 737.

[20] Rebbeor, J. F.; Connolly, G. C.; Dumont, M. E.; Ballatori, N. *J. Bio. Chem*. **1998,** 273, 33449.

[21] Li, Z .-S.; Szczypka, M.; Lu, Y. P.; Thiele, D. J.; Rea, P. A. *J. Bio. Chem* . **1996,** *271*, 6509.

[22] Falcón-Pérez, J. M.; Mazón, M. J.; Molano, J.; Eraso, P. *J. Bio. Chem* . **1999,** *274*, 23584.

[23] Mauzeroll, J.; Hueske, E. A.; Bard, A. J. *Anal. Chem*., **2003,** *75*, 3880.

[24] Jin, W.; Zhao, X.; Xia, L. *Electroanalysis* **2000,** *12*, 858.

[25] Ahimou, F.; Denis, F. A.; Touhami, A.; Dufrêne, Y. F. *Langmuir* **2002,** *18*, 9937.

[26] Eddy, A. A.; Rudin, A. D. *Proc. R. Soc. London, B*. **1958,** *149*, 419.

[27] Di Monte, D.; Ross, D.; Bellomo, G.; Eklöw, L.; Orrenius, S. *Arch. of Biochem. & Biophys.* **1984,** *235*, 334.

[28] Lipke, P. N.; Ovalle, R. *J. Bacteriol*. **1998,** *180*, 3735.

[29] Bacon, J. S. D. in *Yeast Cell Eenvelops: Biochemistry, Biophysics, and Ultrastructures,* Eds., Boca Raton, FL., **1981**, 65.

[30] Srinorakutara, T. *J. Ferment. Bioeng*. **1998,** *86*, 253.

[31] Smith, A. E.; Zhang Z.; Thomas, C. R.; Moxham, K. E.; Middelberg, A. P. J. *PNAS*,

2000, *97*, 9871.

32 Smith, A. E.; Moxham, K. E.; Middelberg, A. P. J. *Chem. Eng. Sci*. **2000,** *55*, 2031.

33 Yamaguchi, M.; Biswas, S. K.; Suzuki, Y.; Furukawa, H.; Takeo, K. *FEMS Microbiology Letters* **2003,** *219*, 17.

34 De Nobel, J. G.; Klis, F. M.; Munnik, T.; Priem, J.; Van den Ende, H. *Yeast* **1990,** *6*, 483.

35 Chan, S. Y.; Appling, D. R. *JBC* **2003,** in press.

Chapter 4

1 Duthie, S. J.!; Grant, M. H. *Biochem. Pharmacol.* **1989**, *38*, 1247.

2 Chiou, T.-J.; Tzeng, W.-F. *Toxicology* **2000**, *154*, 75.

3 Hipfner, D. R.; Deeley, R. G.; Cole, S. P. C. *Biochim. Biophys. Acta* **1999**, *1461*, 359.

4 Higgins, C. F. *Annu. Rev. Cell. Biol.* **1992**, *8*, 67.

5 Cole, S. P. C.; Sparks, K. E.; Fraser, K.; Loe, D. W.; Grant, C. E.; Wilson, G. M.; Deeley, R. G. *Cancer Research* **1994**, *54*, 5902.

6 Cole, S. P. C.; Bhardwaj, G.; Gerlach, J. H.; Mackie, J. E.; Grant, C. E.; Almquist, K. C.; Stewart, A. J.; Kurz, E. U.; Duncan, A. M. V.; Deeley, R. G. *Science* **1992**, *258*, 1650.

7 Grant, C. E.; Valdimarson, G.; Hipfner, D. R.; Almquist, K. C.; Cole, S. P. C.; Deeley, R. G. *Cancer Res.* **1994**, *54*, 357.

8 Kruh, G. D.; Chan, A.; Myers, K.; Gaughan, K.; Miki, T.; Aaronson, S. A. *Cancer Res.* **1994**, *54*, 1649.

9 Zaman, G. J. R.; Flens, M. J.; van Leusden, M. R.; de Haas, M.; Mulder, H. S.;

Lankelma, J.; Pinedo, H. M.; Scheper, R. J.; Baas, F.; Broxterman, H. J.; Borst, P. *PNAS USA* **1994**, *91*, 8822.

[10] Chang, X.-B.; Hou, Y.-X.; Riordan, J. R. *J. Biol. Chem.* **1997**, *272*, 30962.

[11] Morrow, C. S.; Smitherman, P. K.; Townsend, A. J. *Mol. Carcinogenesis* **2000**, *29*, 170.

[12] Ishikawa, T. *Trends in Biochem. Sci.* **1992**, *17*, 463.

[13] Manciu, L.; Chang, X.-B.; Buyset, F.; Hou, Y.-X.; Gustot, A.; Riordan, J. R.; Ruysschaert, J. M. *J. Biol. Chem.* **2003**, *278*, 3347.

[14] Ishikawa, T.; Bao, J. J.; Yamane, Y.; Akimaru, K.; Frindrich, K.; Wright, C. D. *J. Biol. Chem.* **1996**, *271*, 1481.

[15] Kuo, M. T.; Bao, J.; Furuichi, M.; Yamane, Y.; Gomi, A.; Savaraj, N.; et al. *Biochem. Pharmacol.* **1998**, *55*, 605.

170

[16] Zaman, G. J. R.; Lankelma, J.; van Tellingen, O.; Beijnens, J.; Dekker, H.; Paulusma, C.; Elferink, R. P. J.; Baas, F.; Borst, P. *PNAS USA* **1995**, *92*, 7690.

[17] Borst, P.; Evers, R.; Kool, M.; Wijnholds, J. *J. Nat. Can. Inst.* **2000**, *92*, 1295.

[18] Allikmets, R.; Gerrard, B.; Hutchinson, A.; Dean, M. *Hum. Mol. Genet.* **1996**, *5*, 1649.

[19] Elferink, R. P. J. O.; Meijer, D. K. F.; Kuipers, F.; Jansen, P. L. M.; Groen, A. K.; Groothuis, G. M. M. *Biochim. Biophys. Acta* **1995**, *1241*, 215.

[20] McAleer, M. A.; Breen, M. A.; White, N. L.; Matthews, N. *J. Biol. Chem.* **1999**, *274*, 23541.

[21] Cole, S. P. C. *J. Natl. Can. Inst.* **1999**, *91*, 888.

[22] Zaman, G. J.; Lankelma, J.; van Tellingen, O.; Beijnen, J.; Dekker, H.; Paulusma, C. *PNAS USA* **1995**, *92*, 7690.

[23] Müller, M.; Roelofsen, H.; Jansen, P. L. M. *Sem. Liver Dis.* **1996**, *16*, 211.

[24] Knowles, B. B.; Howe, C.C.; Aden, D. P. *Science* **1980**, *209*, 497.

[25] Javitt, N. B. *FASEB J* **1990**, *4*, 161.

[26] Roelofsen, H.; Vos, T. A.; Schippers, I. J.; Kuipers, F.; Koning, H.; Moshage, H.; Jansen, P. L. M.; Müller, M. *Gastroenterology* **1997**, *112*, 511.

[27] Sormunen, R.; Eskelinen, S.; Lehto, V. *Lab. Invest.* **1993**, *68*, 652.

[28] Roelofsen, H.; Müller, M.; Jansen, P. L. M. *Yale J. Biol.Med.* **1997**, *70*, 435.

[29] Borenfreund, E.; Puerner, J. A. *J. Tissue Culture Methods* **1985**, *9*, 7.

[30] Babich, H.; Borenfreund, E. *Alternatives to Laboratory Animals (ATLA)* **1990**, *19*, 129.

[31] Bard, A. J.; Mirkin, M. V.; Eds.; *Scanning Electrochemical Microscopy,* Marcel Dekker, Inc., New York, **2001.**

[32] Mauzeroll, J.; Bard, A. J.; **2003,** manuscript in preparation.

[33] Biao, L.; Rotenberg, S. A.; Mirkin, M. V. *PNAS USA* **2000**, *97*, 9855.

[34] Chenxin, C.; Biao, L.; Mirkin, M. V.; Frank, H. A.; Rusling, J. F. *Anal. Chem.* **2002**, *74*, 114.

[35] Arcamone, F. *Med. Res. Rev.* **1984**, *4*, 153.

[36] Di Monte, D.; Ross, D.; Bellomo, G.; Eklow, L.; Orrenius, S. *Arch. Biochem. Biophys.* **1984**, *224*, 334.

[37] Chung, J.-H.; Seo, D.-C.; Chung, S.-H.; Lee, J.-Y.; Seung, S.-A. *Toxicol. App. Pharmaco.* **1997**, *142*, 378.

[38] Shao, Y.; Mirkin, M. V.; *J. Phys. Chem. B* **1998**, *102*, 9915.

[39] König, J.; Nies, A. T.; Cui, Y.; Leier, I.; Keppler, D. *Biochim. Biophys. Acta* **1999**, *1461*, 377.

[40] Wettsein, M.; Noe, B.; Häussinger, D. *Hepatology* **1995**, *22*, 235.

[41] Cantz, T.; Nies, A. T.; Brom, M.; Hofmann, A. F.; Keppler, D. *Am. J. Physiol. Gastrointest. Liver Phys.* **2000**, *278*, G522.

[42] Roelfosen, H.; Hooiveld, G. J. E. J.; Koning, H.; Havinga, R.; Jansen, P. L. M.; Müller, M. *J. Cell Sci.* **1999**, *112*, 1395.

VITA

Janine Mauzeroll was born August 29th 1977 in Buckingham, Québec in Canada. She is the daughter of Guy Mauzeroll and Hélene Carrière Mauzeroll.

She received her early education at "l'École Secondaire St-Joseph" in Hull and attended Brébeuf College for the International Baccalaureate (IB) in sciences. Her undergraduate work in chemistry was done at McGill University (BSc 1999). Her honors thesis work was done under Prof. R.B. Lennox.

In August 1999, she joined Prof. Allen J. Bard's group at the University of Texas at Austin where she is currently finishing her graduate work. She has been awarded the E. Weston summer fellowships from the Electrochemical society (2003) and the University of Texas at Austin Continuing Fellowship (2003-2004).

Her research interests have been in the application of scanning electrochemical microscopy to kinetic studies of channel and cellular transport processes.

Permanent address: 36 Millar, Gatineau, Québec, Canada, J8Y 3N7

This dissertation was typed by Janine Mauzeroll.